Radiative Capture Reactions of Astrophysical Interest

by

Junting Huang

Submitted to the Faculty of the Graduate School
of Texas A&M University-Commerce
in partial fulfilllment of the requirements
for the degree of
MASTER OF SCIENCE

July 2009

Radiative Capture Reactions of Astrophysical Interest

Approved:

_____

Advisor

_____

Dean of the College of Arts & Science

_____

Dean of Graduate Studies and Research

ABSTRACT

Radiative Capture Reactions of Astrophysical Interest

Junting Huang, MS
Texas A&M University-Commerce 2009

Advisor: Carlos Bertulani, PhD

Radiative capture of nucleons at energies of astrophysical interest is one of the most important processes for nucleosynthesis. The nucleon capture can occur either by a compound nucleus reaction or by a direct process. The compound reaction cross sections are usually very small, specially for light nuclei. The direct capture proceeds either via the formation of a single-particle resonance, or a non-resonant capture process. In this thesis I calculate radiative capture cross sections and astrophysical S-factors for nuclei in the mass region $A < 20$ using single-particle states. I carefully discuss the parameter fitting procedure adopted in the simplified two-body treatment of the capture process. Then I produce a detailed list of cases for which the model works well. Useful quantities, such as spectroscopic factors and asymptotic normalization coefficients, are obtained and compared to published data.

A novel effect due to non-inertial motion in reactions occurring in stars, and elsewhere is also discussed. I demonstrate that non-inertial effects due to large accelerations present in collision reactions will appreciably modify the excitation processes in nuclear and atomic collisions. Applying Einstein's equivalence principle, I also explore the magnitude of the corrections induced by strong gravitational fields on nuclear reactions in massive and/or compact stars.

Acknowledgements

First I would like to thank my advisor, Prof. Carlos Bertulani, for his guidance during my research and study at Texas A&M University-Commerce. he was always accessible and willing to help his students with their research, and one could not wish for a friendlier supervisor.

Many thanks go in particular to Prof. Bao-An Li as one of my instructors and committee members. Also, without his financial help, I would not be able to start my graduate study in Commerce.

I gratefully thank Prof. Anil Chourasia and Prof. Rogers, for their valuable lectures. From there I solidified my knowledge in physics and learnt many useful pratical skills.

It is a pleasure to pay tribute also to Dr. Plamen Krastev and Dr. Arturo Samana, for the meaningful discussion and advice.

My parents deserve special mention for their inseparable support. My father, Jinxin Huang, in the first place gave me an exploring character. My mother, Fen Deng, is the one who raised me with her caring. Yuping, thanks for being a supportive brother.

Finally, I would like to thank everybody who was important to the successful realization of thesis, as well as expressing my apology that I could not mention personally one by one.

Contents

List of Tables

List of Figures

Chapter 1

Introduction to Nuclear Astrophysics

1.1   Stellar evolution: hydrogen and CNO cycles

The energy production in the stars is a well known process. The initial energy which ignites the process arises from the gravitational contraction of a mass of gas. The contraction increases the pressure, temperature, and density, at the center of the star until values able to start the thermonuclear reactions, initiating the star lifetime. The energy liberated in these reactions yield a pressure in the plasma, which opposes compression due to gravitation. Thus, an equilibrium is reached for the energy which is produced, the energy which is liberated by radiation, the temperature, and the pressure.

The Sun is a star in its initial phase of evolution. The temperature in its surface is 6000° C, while in its interior the temperature reaches 1.5×10^7 K, with a pressure given by 6×10^{11} atm and density 150 g/cm^3. The present mass of the Sun is $M_\odot = 2 \times 10^{33}$ g and its main composition is hydrogen (70%), helium (29%) and less than 1% of more heavy elements, like carbon, oxygen, etc.

What are the nuclear processes which originate the huge thermonuclear energy of the Sun, and that has last 4.6×10^9 years (the assumed age of the Sun)? It cannot be the simple fusion of two protons, or of α-particles, or even the fusion of protons with α-particles, since neither $^2_2$He, $^8_4$Be, or $^5_3$Li, are stable. The only possibility is the proton-proton fusion in the form

$$\mathrm{p} + \mathrm{p} \longrightarrow \mathrm{d} + \mathrm{e}^+ + \nu_e, \tag{1.1}$$

which occurs via the β-decay, i.e., due to the weak-interaction. The cross section for this reaction for protons of energy around 1 MeV is very small, of the order of 10^{-23} b. The average lifetime of protons in the Sun due to the transformation to deuterons by means of eq. (1.1) is about 10^{10} y. This explains why the energy radiated from the Sun is approximately constant in time, and not an explosive process.

The deuteron produced in the above reaction is consumed almost immediately in the process

$$\mathrm{d} + \mathrm{p} \longrightarrow \quad ^3_2\mathrm{He} + \gamma. \tag{1.2}$$

p(p,e$^+\nu$)d

d(p,γ)^{3}He

86%   14%

^{3}He(^{3}He,2p)^{4}He ^{3}He(α,γ)^{7}Be

14%   0.02%

Be(e$^-$,ν)^{7}Li ^{7}Be(p,γ)^{8}B

^{7}Li(p,α)^{4}He ^{8}B(e$^+\nu$)^{8}Be

^{8}Be(α)^{4}He

Chain I   Chain II   Chain III
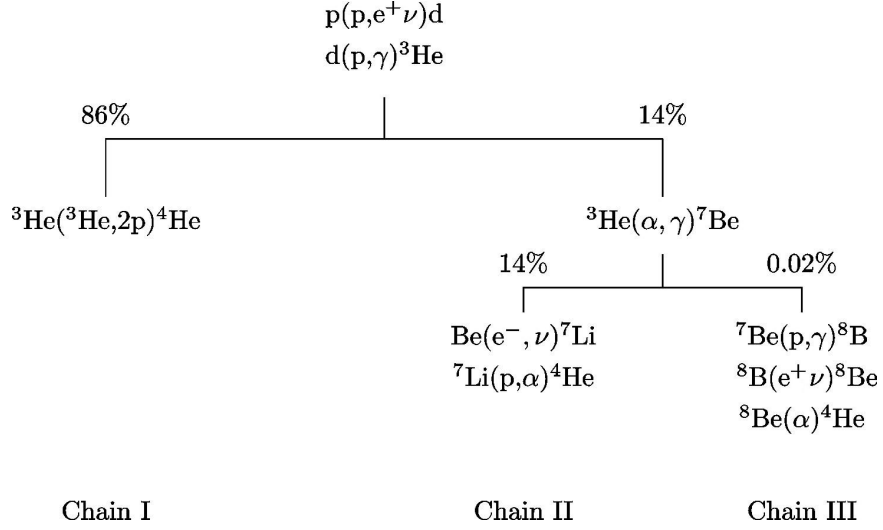
Figure 1.1: The p-p chain reaction (p-p cycle). The percentage for the several branches are calculated in the center of the Sun [1].

The resulting $^3_2$He reacts by means of

$$^3_2\text{He} + \quad ^3_2\text{He} \longrightarrow \quad ^4_2\text{He} + 2\text{p}, \tag{1.3}$$
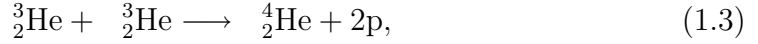
which produces the stable nucleus $^4_2$He with a great energy gain, or by means of the reaction

$$^3_2\text{He} + \quad ^4_2\text{He} \longrightarrow \quad ^7_4\text{Be} + \gamma. \tag{1.4}$$

In the second case, a chain reaction follows as

$$^7_4\text{Be} + \quad \text{e}^- \longrightarrow \quad ^7_3\text{Li} + \nu_e, \qquad ^7_3\text{Li} + \quad \text{p} \longrightarrow 2\left(^4_2\text{He}\right), \tag{1.5}$$

or

$$^7_4\text{Be} + \quad \text{p} \longrightarrow \quad ^8_5\text{B} + \gamma, \qquad ^8_5\text{B} \longrightarrow \quad 2\left(^4_2\text{He}\right) + \text{e}^+ + \nu_e. \tag{1.6}$$
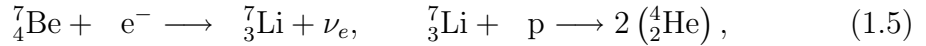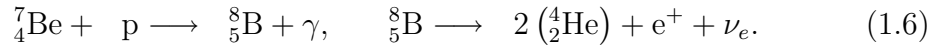
The chain reaction (1.1)-(1.6) is called the *hydrogen cycle.* The result of this cycle is the transformation of four protons in an α-particle, with an energy gain of 26.7 MeV, about 20% of which are carried away by the neutrinos (see fig. 1.1).

If the gas which gives birth to the star contains heavier elements, another cycle can occur; the *carbon cycle*, or *CNO cycle*. In this cycle the carbon, oxygen, and nitrogen nuclei are catalyzers of nuclear processes, with the end product also in the form 4p$\longrightarrow$ $^4_2$He. fig. 1.2 describes the CNO cycle. Due to the larger Coulomb repulsion between the carbon nuclei, it occurs at higher temperatures (larger relative energy between the participant nuclei), up to 1.4×10^7 K. In the Sun the hydrogen cycle prevails. But, in stars with larger temperatures the CNO cycle is more important. Fig. 1.3 compares the energy production in stars for the hydrogen and for the CNO cycle as a function of the temperature at their center. For the Sun temperature, $T_\odot$, we see that the pp cycle is more efficient.

After the protons are transformed into helium at the center of a star like our Sun, the fusion reactions start to consume protons at the surface of the star. At
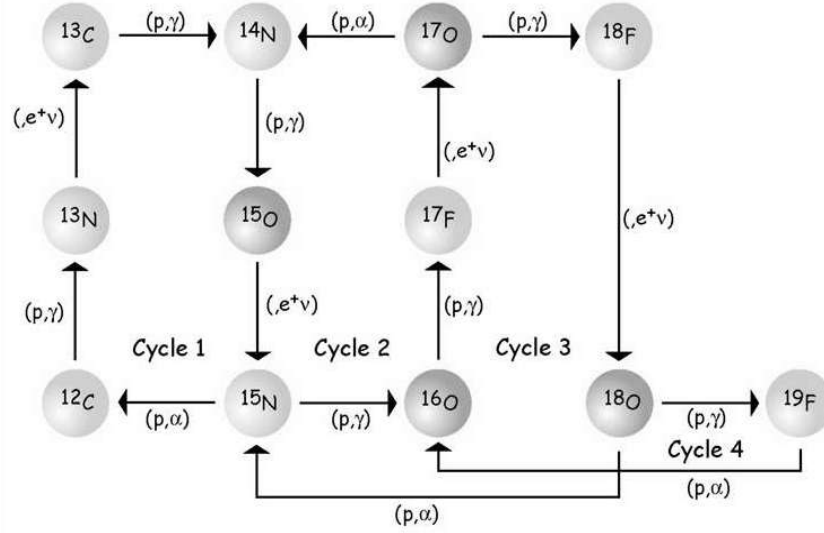
Figure 1.2: The CNO cycle.

this stage the star starts to become a *red giant.* The energy generated by fusion increases the temperature and expands the surface of the star. The star luminosity increases. The red giant contracts again after the hydrogen fuel is burned.

Other thermonuclear processes start. The first is the helium burning when the temperature reaches 10^8 K and the density becomes 10^6 g.cm^{-3}. Helium burning starts with the triple capture reaction

$$3 \left({}^4_2\text{He} \right) \longrightarrow {}^{12}_6\text{C} + 7.65 \text{ MeV}, \tag{1.7}$$

followed by the formation of oxygen via the reaction

$$ {}^{12}_6\text{C} + {}^4_2\text{He} \longrightarrow {}^{16}_8\text{O} + \gamma. \tag{1.8}$$
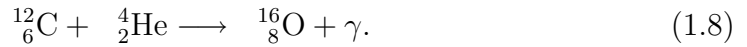
For a star with the Sun mass, helium burning occurs in about 10^7 y. For a much heavier star the temperature can reach 10^9 K. The compression process followed by the burning of heavier elements can lead to the formation of iron. After that the thermonuclear reactions are no more energetic and the star stops producing nuclear energy.

1.2 Thermonuclear cross sections and reaction rates

The nuclear cross section for a reaction between target j and projectile k is defined by

$$\sigma = \frac{\text{number of reactions target}^{-1}\text{sec}^{-1}}{\text{flux of incoming projectiles}} = \frac{r/n_j}{n_k v}. \tag{1.9}$$

where the target number density is given by n_j, the projectile number density is given by n_k , and v is the relative velocity between target and projectile nuclei.
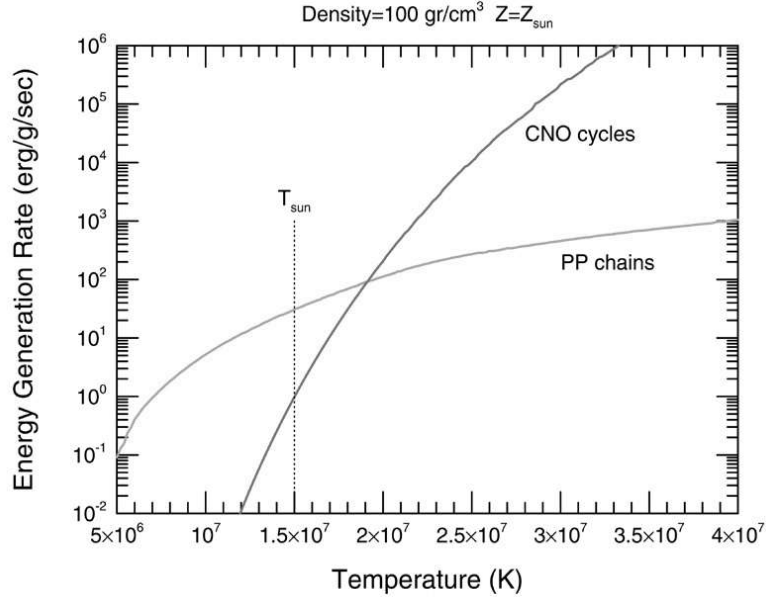
Figure 1.3: Comparison of the energy production in the pp and in the CNO cycle as a function of the star temperature [2].

Then r, the number of reactions per cm^3 and sec, can be expressed as $r = \sigma v n_j n_k$, or, more generally,

$$r_{j,k} = \int \sigma |v_j - v_k| d^3 n_j d^3 n_k. \tag{1.10}$$

The evaluation of this integral depends on the type of particles and distributions which are involved. For nuclei j and k in an astrophysical plasma, obeying a Maxwell-Boltzmann distribution (MB),

$$d^3 n_j = n_j \left(\frac{m_j}{2\pi kT}\right)^{3/2} \exp\left(-\frac{m_j v_j^2}{2kT}\right) d^3 v_j, \tag{1.11}$$

eq. (1.10) simplifies to $r_{j,k} = <\sigma v> n_j n_k$, where $<\sigma v>$ is the average of σv over the temperature distribution in (1.11). More specifically,

$$r_{j,k} = <\sigma \mathrm{v}>_{j,k} n_j n_k \tag{1.12}$$

$$<j,k> \equiv <\sigma \mathrm{v}>_{j,k} = \left(\frac{8}{\mu\pi}\right)^{1/2}(kT)^{-3/2}\int_0^\infty E\sigma(E)\exp(-E/kT)dE. \tag{1.13}$$

Here μ denotes the reduced mass of the target-projectile system. In astrophysical plasmas with high densities and/or low temperatures, effects of electron screening become highly important. This means that the reacting nuclei, due to the background of electrons and nuclei, feel a different Coulomb repulsion than in the case of bare nuclei. Under most conditions (with non-vanishing temperatures) the generalized reaction rate integral can be separated into the traditional expression without screening (1.12) and a screening factor [3]

$$<j,k>^* = f_{scr}(Z_j, Z_k, \rho, T, Y_i) <j,k> . \tag{1.14}$$

This screening factor is dependent on the charge of the involved particles, the density, temperature, and the composition of the plasma. Here Y_i denotes the abundance of nucleus i defined by $Y_i = n_i/(\rho N_A)$, where n_i is the number density of nuclei per unit volume and N_A Avogadro's number. At high densities and low temperatures screening factors can enhance reactions by many orders of magnitude and lead to pycnonuclear ignition.

When in eq. (1.10) particle k is a photon, the relative velocity is always c and quantities in the integral are not dependent on $d^3 n_j$. Thus it simplifies to $r_j = \lambda_{j,\gamma} n_j$ and $\lambda_{j,\gamma}$ results from an integration of the photodisintegration cross section over a Planck distribution for photons of temperature T

$$d^3 n_\gamma = \frac{1}{\pi^2 (c\hbar)^3} \frac{E_\gamma^2}{\exp(E_\gamma/kT) - 1} dE_\gamma \qquad (1.15)$$

$$r_j = \lambda_{j,\gamma}(T) n_j = \frac{1}{\pi^2 (c\hbar)^3} \int d^3 n_j \int_0^\infty \frac{c\sigma(E_\gamma) E_\gamma^2}{\exp(E_\gamma/kT) - 1} dE_\gamma. \qquad (1.16)$$

There is, however, no direct need to evaluate photodisintegration cross sections, because, due to detailed balance, they can be expressed by the capture cross sections for the inverse reaction $l + m \rightarrow j + \gamma$ [4]

$$\lambda_{j,\gamma}(T) = \left(\frac{G_l G_m}{G_j}\right)\left(\frac{A_l A_m}{A_j}\right)^{3/2}\left(\frac{m_u kT}{2\pi\hbar^2}\right)^{3/2} <l, m> \exp(-Q_{lm}/kT). \qquad (1.17)$$

This expression depends on the reaction Q-value Q_{lm}, the temperature T, the inverse reaction rate $< l, m >$, the partition functions $G(T) = \sum_i (2J_i+1) \exp(-E_i/kT)$ and the mass numbers A of the participating nuclei in a thermal bath of temperature T.

A procedure similar to eq. (1.16) is used for electron captures by nuclei. Because the electron is about 2000 times less massive than a nucleon, the velocity of the nucleus j is negligible in the center of mass system in comparison to the electron velocity ($|v_j - v_e| \approx |v_e|$). The electron capture cross section has to be integrated over a Boltzmann, partially degenerate, or Fermi distribution of electrons, dependent on the astrophysical conditions. The electron capture rates are a function of T and $n_e = Y_e \rho N_A$, the electron number density [5]. In a neutral, completely ionized plasma, the electron abundance is equal to the total proton abundance in nuclei $Y_e = \sum_i Z_i Y_i$ and

$$r_j = \lambda_{j,e}(T, \rho Y_e) n_j. \qquad (1.18)$$

This treatment can be generalized for the capture of positrons, which are in a thermal equilibrium with photons, electrons, and nuclei. At high densities ($\rho > 10^{12}$ g.cm^{-3}) the size of the neutrino scattering cross section on nuclei and electrons ensures that enough scattering events occur to thermalize a neutrino distribution. Then also the inverse process to electron capture (neutrino capture) can occur and the neutrino capture rate can be expressed similarly to Eqs. (1.16) or (1.18), integrating over the neutrino distribution. Also inelastic neutrino scattering on nuclei can be expressed in this form. Finally, for normal decays, like beta or alpha
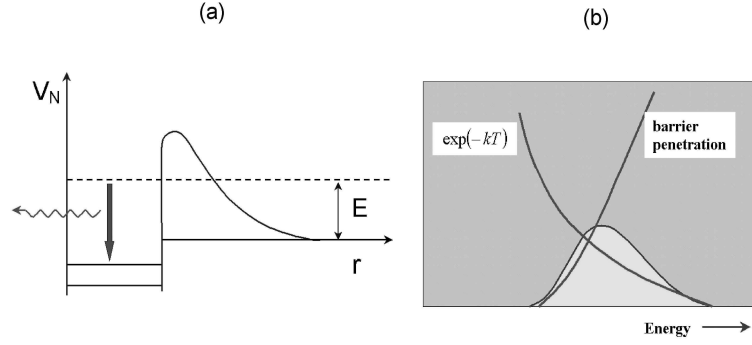
Figure 1.4: (a) Schematic representation of the nuclear+Coulomb potential for fusion of charged particles. (b) The integrand of eq. (1.13) is the product of an exponentially falling distribution with a fastly growing cross section in energy.

decays with half-life $\tau_{1/2}$, we obtain an equation similar to Eqs. (1.16) or (1.18) with a decay constant $\lambda_j = \ln 2/\tau_{1/2}$ and

$$r_j = \lambda_j n_j. \tag{1.19}$$

The nuclear cross section for charged particles is strongly suppressed at low energies due to the Coulomb barrier. For particles having energies less than the height of the Coulomb barrier, the product of the penetration factor and the MB distribution function at a given temperature results in the so-called Gamow peak, in which most of the reactions will take place. Location and width of the Gamow peak depend on the charges of projectile and target, and on the temperature of the interacting plasma (see fig. 1.4).

Experimentally, it is more convenient to work with the astrophysical S factor

$$S(E) = \sigma(E) \ E \ \exp(2\pi\eta), \tag{1.20}$$

with η being the Sommerfeld parameter, describing the s-wave barrier penetration $\eta = Z_1 Z_2 e^2/\hbar v$. In this case, the steep increase of the cross section is transformed in a rather flat energy dependent function (see fig. 1.5). One can easily see the two contributions of the velocity distribution and the penetrability in the integral

$$< \sigma v > = \left(\frac{8}{\pi\mu}\right)^{1/2} \frac{1}{(kT)^{3/2}} \int_0^\infty S(E) \exp\left[-\frac{E}{kT} - \frac{b}{E^{1/2}}\right], \tag{1.21}$$

where the quantity $b = 2\pi\eta E^{1/2} = (2\mu)^{1/2}\pi e^2 Z_j Z_k/\hbar$ arises from the barrier penetrability. Experimentally it is very difficult to take direct measurements of fusion reactions involving charged particles at very small energies. The experimental data can be guided by a theoretical model for the cross section, which can then be extrapolated to the Gamow energy, as displayed in fig. 1.5(b). The dots symbolize the experimental data points. The solid curve is a theoretical prediction, which supposedly describes the data at high energies. Its extrapolation to lower energies yields the desired value of the S-factor (and of σ) at the energy E_0. The extrapolation can be inadequate due to the presence of resonances and of subthreshold resonances, as shown schematically in figure 1.5.
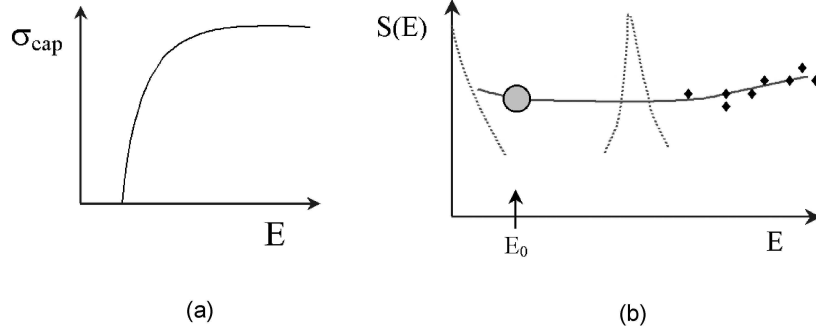
Figure 1.5: (a) Schematic representation of the energy dependence of a fusion reaction involving charged particles. (b) The astrophysical S-factor as defined by eq. (1.20).

Taking the first derivative of the integrand in eq. (1.21) yields the location E_0 of the Gamow peak, and the effective width Δ of the energy window can be derived accordingly

$$E_0 = \left(\frac{bkT}{2}\right)^{2/3} = 1.22(Z_j^2 Z_k^2 A T_6^2)^{1/3}\,\text{keV},$$

$$\Delta = \frac{16E_0 kT^{1/2}}{3} = 0.749(Z_j^2 Z_k^2 A T_6^5)^{1/6}\,\text{keV}, \qquad (1.22)$$

as shown in [6], carrying the dependence on the charges Z_j, Z_k, the reduced mass A of the involved nuclei in units of m_u, and the temperature T_6 given in 10^6 K.

In the case of neutron-induced reactions the effective energy window has to be derived in a slightly different way. For s-wave neutrons ($l = 0$) the energy window is simply given by the location and width of the peak of the MB distribution function. For higher partial waves the penetrability of the centrifugal barrier shifts the effective energy E_0 to higher energies. For neutrons with energies less than the height of the centrifugal barrier this was approximated by [7]

$$E_0 \approx 0.172 T_9 \left(l + \frac{1}{2}\right)\quad\text{MeV}, \qquad \Delta \approx 0.194 T_9 \left(l + \frac{1}{2}\right)^{1/2}\,\text{MeV}, \qquad (1.23)$$

The energy E_0 will always be comparatively close to the neutron separation energy.

1.3 Reaction networks

The time derivative of the number densities of each of the species in an astrophysical plasma (at constant density) is governed by the different expressions for r, the number of reactions per cm^3 and sec, as discussed above for the different reaction mechanisms which can change nuclear abundances

$$\left(\frac{\partial n_i}{\partial t}\right)_{\rho=const} = \sum_j N_j^i r_j + \sum_{j,k} N_{j,k}^i r_{j,k} + \sum_{j,k,l} N_{j,k,l}^i r_{j,k,l}. \qquad (1.24)$$

The reactions listed on the right hand side of the equation belong to the three categories of reactions: (1) decays, photodisintegrations, electron and positron captures and neutrino induced reactions ($r_j = \lambda_j n_j$), (2) two-particle reactions ($r_{j,k} = <j,k> n_j n_k$), and (3) three-particle reactions ($r_{j,k,l} = <j,k,l> n_j n_k n_l$) like the triple-alpha process ($\alpha + \alpha + \alpha \longrightarrow {}^{12}C + \gamma$), which can be interpreted as successive captures with an intermediate unstable target ($\alpha + {}^8 Be^* \longrightarrow {}^{12} C + \gamma$). The individual N^i's are given by: $N_j^i = N_i$, $N_{j,k}^i = N_i / \prod_{m=1}^{n_m} |N_{j_m}|!$, and $N_{j,k,l}^i = N_i / \prod_{m=1}^{n_m} |N_{j_m}|!$. The $N_i's$ can be positive or negative numbers and specify how many particles of species i are created or destroyed in a reaction. The denominators, including factorials, run over the n_m different species destroyed in the reaction and avoid double counting of the number of reactions when identical particles react with each other (for example in the ${}^{12}C + {}^{12}C$ or the triple-alpha reaction) [4]. In order to exclude changes in the number densities $\dot{n}_i$, which are only due to expansion or contraction of the gas, the nuclear abundances $Y_i = n_i/(\rho N_A)$ were introduced. For a nucleus with atomic weight A_i, $A_i Y_i$ represents the mass fraction of this nucleus, therefore $\sum A_i Y_i = 1$. In terms of nuclear abundances Y_i, a reaction network is described by the following set of differential equations

$$\dot{Y}_i = \sum_j N_j^i \lambda_j Y_j + \sum_{j,k} N_{j,k}^i \rho N_A < j,k > Y_j Y_k$$
$$+ \sum_{j,k,l} N_{j,k,l}^i \rho^2 N_A^2 < j,k,l > Y_j Y_k Y_l. \tag{1.25}$$

Eq. (1.25) derives directly from eq. (1.24) when the definition for the, $Y_i's$ is introduced. This set of differential equations is solved numerically. They can be rewritten as difference equations of the form $\Delta Y_i/\Delta t = f_i(Y_j(t + \Delta t))$, where $Y_i(t + \Delta t) = Y_i(t) + \Delta Y_i$. In this treatment, all quantities on the right hand side are evaluated at time $t + \Delta t$. This results in a set of non-linear equations for the new abundances $Y_i(t + \Delta t)$, which can be solved using a multi-dimensional Newton-Raphson iteration procedure [8]. The total energy generation per gram, due to nuclear reactions in a time step Δt which changed the abundances by ΔY_i, is expressed in terms of the mass excess $M_{ex,i} c^2$ of the participating nuclei

$$\Delta \epsilon = - \sum_i \Delta Y_i N_A M_{ex,i} c^2, \qquad \dot{\epsilon} = - \sum_i \dot{Y}_i N_A M_{ex,i} c^2. \tag{1.26}$$

Therefore, the important ingredients to nucleosynthesis calculations are decay half-lives, electron and positron capture rates, photodisintegrations, neutrino induced reaction rates, and strong interaction cross sections.

The solution of the above group of equations allows to deduce the path for the r-process until reaching the heavier elements (see figure 1.6). The relative abundances of elements are also obtained theoretically by means of these equations using stellar models for the initial conditions, as the neutron density and the temperature.
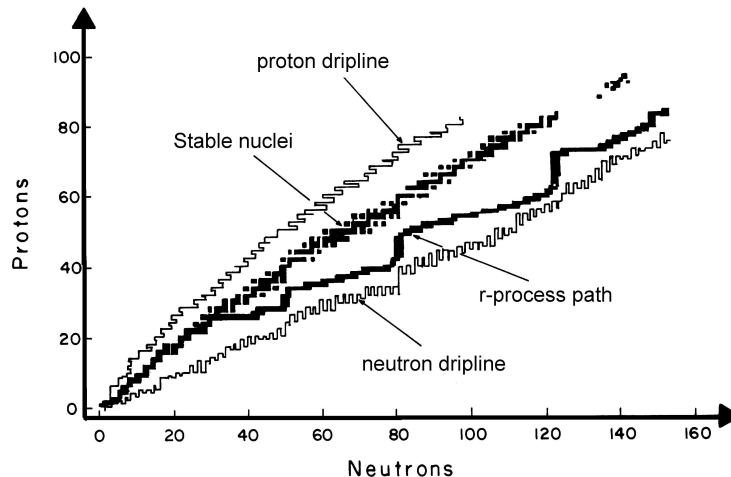
Figure 1.6: Nuclear chart showing the path of the r-process.

1.4 Models for astrophysical nuclear cross sections

Explosive nuclear burning in astrophysical environments produces unstable nuclei, which again can be targets for subsequent reactions. In addition, it involves a very large number of stable nuclei, which are not fully explored by experiments. Thus, it is necessary to be able to predict reaction cross sections and thermonuclear rates with the aid of theoretical models. Especially during the hydrostatic burning stages of stars, charged-particle induced reactions proceed at such low energies that a direct cross-section measurement is often not possible with existing techniques. Hence extrapolations down to the stellar energies of the cross sections measured at the lowest possible energies in the laboratory are the usual procedures to apply. To be trustworthy, such extrapolations should have as strong a theoretical foundation as possible. Theory is even more mandatory when excited nuclei are involved in the entrance channel, or when unstable very neutron-rich or neutron-deficient nuclides (many of them being even impossible to produce with present-day experimental techniques) have to be considered. Such situations are often encountered in the modelling of explosive astrophysical scenarios.

Various models have been developed in order to complement the experimental information.

(a) *Microscopic models.* In this model, the nucleons are grouped into clusters, as was explained in section 3.12. Keeping the internal cluster degrees of freedom fixed, the totally antisymmetrized relative wave functions between the various clusters are determined by solving the Schrödinger equation for a many-body Hamiltonian with an effective nucleon-nucleon interaction. When compared with most others, this approach has the major advantage of providing a consistent, unified and successful description of the bound, resonant, and scattering states of a nuclear system. Various improvements of the model have been made [9].

The microscopic model has been applied to many important reactions involving light systems, and in particular to the various p-p chain reactions [10]. The

available experimental data can generally be well reproduced. The microscopic cluster model or its variant (the microscopic potential model) has also made an important contribution to the understanding of the key $^{12}C(\alpha, \gamma)^{16}O$ reaction rate [11].

(b) The potential models. The potential model has been known for a long time to be a useful tool in the description of radiative capture reactions. It assumes that the physically important degrees of freedom are the relative motion between the (structureless) nuclei in the entrance and exit channels, and by the introduction of spectroscopic factors and strength factors in the optical potential. The associated drawbacks are that the nucleus-nucleus potentials adopted for calculating the initial and final wave functions from the Schrödinger equation cannot be unambiguously defined, and that the spectroscopic factors cannot be derived from first principles. They have instead to be obtained from more or less rough "educated guesses." More details on this model is discussed in the next chapter.

(c) Parameter fits. Reaction rates dominated by the contributions from a few resonant or bound states are often extrapolated in terms of *R-* or *K-matrix* fits, which rely on quite similar strategies. The appeal of these methods rests on the fact that analytical expressions which allow for a rather simple parametrization of the data can be derived from underlying formal reaction theories. However, the link between the parameters of the *R*-matrix model and the experimental data (resonance energies and widths) is only quite indirect. The *K*-matrix formalism solves this problem, but suffers from other drawbacks [12].

The *R*- and *K*-matrix models have been applied to a variety of reactions, and in particular to the analysis of the $^{12}C(\alpha, \gamma)^{16}O$ reaction rate [13].

(d) The statistical models. Many astrophysical scenarios involve a wealth of reactions on intermediate-mass or heavy nuclei. This concerns the non-explosive or explosive burning of C, Ne, O and Si, as well as the s-, r- and p-process nucleosynthesis. Fortunately, a large fraction of the reactions of interest proceed through compound systems that exhibit high enough level densities for statistical methods to provide a reliable description of the reaction mechanism. In this respect, the *Hauser-Feshbach (HF) model* has been widely used with considerable success. Explosive burning in supernovae involves in general intermediate mass and heavy nuclei. Due to a large nucleon number they have intrinsically a high density of excited states. A high level density in the compound nucleus at the appropriate excitation energy allows to make use of the statistical model approach for compound nuclear reactions [14] which averages over resonances.

A high level density in the compound nucleus permits to use averaged transmission coefficients T, which do not reflect a resonance behavior, but rather describe absorption via an imaginary part in the (optical) nucleon-nucleus potential as described in Ref. [15]. This leads to the expression

$$\sigma_i^{\mu\nu}(j, o; E_{ij}) = \frac{\pi \hbar^2/(2\mu_{ij}E_{ij})}{(2J_i^\mu + 1)(2J_j + 1)}$$
$$\times \sum_{J,\pi}(2J + 1)\frac{T_j^\mu(E, J, \pi, E_i^\mu, J_i^\mu, \pi_i^\mu)T_o^\nu(E, J, \pi, E_m^\nu, J_m^\nu, \pi_m^\nu)}{T_{tot}(E, J, \pi)} \tag{1.27}$$

for the reaction $i^\mu(j, o)m^\nu$ from the target state i^μ to the excited state m^ν of the final nucleus, with a center of mass energy E_{ij} and reduced mass μ_{ij}. J denotes the spin, E the corresponding excitation energy in the compound nucleus, and π the parity of excited states. When these properties are used without subscripts they describe the compound nucleus, subscripts refer to states of the participating nuclei in the reaction $i^\mu(j, o)m^\nu$ and superscripts indicate the specific excited states. Experiments measure $\sum_\nu \sigma_i^{0\nu}(j, o; E_{ij})$, summed over all excited states of the final nucleus, with the target in the ground state. Target states μ in an astrophysical plasma are thermally populated and the astrophysical cross section $\sigma_i^*(j, o)$ is given by

$$\sigma_i^*(j, o; E_{ij}) = \frac{\sum_\mu (2J_i^\mu + 1) \exp(-E_i^\mu/kT) \sum_\nu \sigma_i^{\mu\nu}(j, o; E_{ij})}{\sum_\mu (2J_i^\mu + 1) \exp(-E_i^\mu/kT)}. \quad (1.28)$$

The summation over ν replaces $T_o^\nu(E, J, \pi)$ in eq. (1.27) by the total transmission coefficient

$$T_o(E, J, \pi) = \sum_{\nu=0}^{\nu_m} T_o^\nu(E, J, \pi, E_m^\nu, J_m^\nu, \pi_m^\nu)$$
$$+ \int_{E_m^{\nu_m}}^{E-S_{m,o}} \sum_{J_m, \pi_m} T_o(E, J, \pi, E_m, J_m, \pi_m)\rho(E_m, J_m, \pi_m)dE_m. \quad (1.29)$$

Here $S_{m,o}$ is the channel separation energy, and the summation over excited states above the highest experimentally known state ν_m is changed to an integration over the level density ρ. The summation over target states μ in eq. (1.28) has to be generalized accordingly.

The important ingredients of statistical model calculations as indicated in the above equations are the particle and gamma-transmission coefficients T and the level density of excited states ρ. Therefore, the reliability of such calculations is determined by the accuracy with which these components can be evaluated (often for unstable nuclei).

The gamma-transmission coefficients have to include the dominant gamma-transitions (E1 and M1) in the calculation of the total photon width. The smaller, and therefore less important, M1 transitions have usually been treated with the simple single particle approach $T \propto E^3$ of [16]. The E1 transitions are usually calculated on the basis of the Lorentzian representation of the giant dipole resonance. Within this model, the E1 transmission coefficient for the transition emitting a photon of energy E_γ in a nucleus $_N^A Z$ is given by

$$T_{E1}(E_\gamma) = \frac{8}{3} \frac{NZ}{A} \frac{e^2}{\hbar c} \frac{1+\chi}{mc^2} \sum_{i=1}^{2} \frac{i}{3} \frac{\Gamma_{G,i} E_\gamma^4}{(E_\gamma^2 - E_{G,i}^2)^2 + \Gamma_{G,i}^2 E_\gamma^2}. \quad (1.30)$$

Here $\chi(= 0.2)$ accounts for the neutron-proton exchange contribution, and the summation over i includes two terms which correspond to the split of the GDR in statically deformed nuclei, with oscillations along ($i = 1$) and perpendicular ($i = 2$) to the axis of rotational symmetry.

Chapter 2

Radiative capture reactions

2.1 Introduction

Fusion reactions relevant for astrophysics proceed via compound–nucleus forma-
tion, with a very large number of resonances involved, or by direct capture, with
only few or no resonances. To calculate direct capture cross sections one needs
to solve the many body problem for the bound and continuum states of relevance
for the capture process (for a review see, [17]). A much simpler, and popular,
solution is based on a potential model to obtain single-particle energies and wave-
functions [18]. The model assumes two structureless particles interacting via a
potential with a relative coordinate dependence determined by a set of adjusting
parameters. Often, this solution is good enough to yield cross sections within the
accuracy required to reproduce the experiments.

In this chapter I explore the single-particle model to perform a systematic study
of radiative capture reactions for several light nuclei. This study has not yet
been reported in the literature, where one finds its application to isolated cases.
It is also useful to obtain potential parameters for other reaction channels and
predict quantities of interest, such as spectroscopic factors (SF) and asymptotic
normalization coefficients (ANC).

This chapter is organized as follows. In section II I summarize the theoretical
tools used in the single-particle description of direct capture (DC) reactions. I
show how potentials and wavefunctions are built, followed by a description of
how radiative capture cross sections are obtained. Then I discuss the derivation
and interpretation of the asymptotic normalization coefficients. In section III I
present and discuss the results for radiative proton capture, whereas in section IV
I present and discuss the results for radiative neutron capture. The sensitivity of
the S-factors on the potential parameters is discussed in section V. A summary of
the ANCs obtained in this work is described in section VI. Our final conclusions
are given in section VII.

2.2 Direct capture

2.2.1 Potentials and Wavefunctions

In this work we adopt nuclear potentials of the form

$$V(\mathbf{r}) = V_0(r) + V_S(r) \ (\mathbf{l.s}) + V_C(r) \tag{2.1}$$

where $V_0(r)$ and $V_S(r)$ are the central and spin-orbit interactions, respectively, and $V_C(r)$ is the Coulomb potential of a uniform distribution of charges:

$$
\begin{aligned}
V_C(r) &= \frac{Z_a Z_b e^2}{r} \quad \text{for} \quad r > R_C \\
&= \frac{Z_a Z_b e^2}{2R_C} \left(3 - \frac{r^2}{R_C^2} \right) \quad \text{for} \quad r < R_C,
\end{aligned}
\tag{2.2}
$$

where Z_i is the charge number of nucleus $i = a, b$.

Here we use a Woods-Saxon (WS) parameterization to build up the potentials $V_0(r)$ and $V_S(r)$, given by

$$
\begin{aligned}
V_0(r) &= V_0 \ f_0(r), \\
V_S(r) &= - V_{S0} \ \left(\frac{\hbar}{m_\pi c} \right)^2 \frac{1}{r} \frac{d}{dr} f_S(r) \\
\text{with} \quad f_i(r) &= \left[1 + \exp\left(\frac{r - R_i}{a_i} \right) \right]^{-1}.
\end{aligned}
\tag{2.3}
$$

The spin-orbit interaction in Eq. 2.3 is written in terms of the pion Compton wavelength, $\hbar/m_\pi c = 1.414$ fm. The parameters V_0, V_{S0}, R_0, a_0, R_{S0}, and a_{S0} are chosen to reproduce the ground state energy E_B (or the energy of an excited state). For this purpose, we define typical values (Table I) for V_{S0}, R_0, a_0, R_{S0}, and vary only the depth of the central potential, V_0. As we discuss later, a different set of potential depths might be used for continuum states.

For neutron and proton capture reactions, there is no need for using another form for the potentials. The WS set of parameters are well suited to describe any reaction of interest, except perhaps for those cases in which one of the partners is a neutron-rich halo nucleus. Then the extended radial dependence leads to unusual forms for the potentials. Also, for capture reactions in which the light partner is either a deuteron, tritium, α-particle or a heavier nucleus, folding models are more appropriate. Folding models are based on an effective nucleon-nucleon interaction and nuclear densities which are either obtained experimentally (not really, because only charge densities can be accurately determined from electron-scattering), or calculated from some microscopic model (typically Hartree-Fock or relativistic mean field models). The effective interactions as well as the nuclear densities are subject of intensive theoretical studies, which is beyond the scope of this work. We will restrict our studies to neutron and proton radiative capture reactions based on a nucleon-nucleus interaction of the form of Eq. 2.1.

The wavefunctions for the nucleon (n) + nucleus (x) system are calculated by solving the radial Schrödinger equation

$$-\frac{\hbar^2}{2m_{nx}}\left[\frac{d^2}{dr^2} - \frac{l(l+1)}{r^2}\right]u_\alpha(r) + V(r)u_\alpha(r) = E_\alpha u_\alpha(r) \ . \qquad (2.4)$$

The nucleon n, the nucleus x, and the $n+x = a$–system have intrinsic spins labeled by $s = 1/2$, I_x and J, respectively. The orbital angular momentum for the relative motion of $n + x$ is described by l. It is convenient to couple angular momenta as $\mathbf{l} + \mathbf{s} = \mathbf{j}$ and $\mathbf{j} + \mathbf{I}_x = \mathbf{J}$, where $\mathbf{J}$ is called the channel spin. In Eq. 2.1 for V we use $\mathbf{s.l} = [j(j+1) - l(l+1) - 3/4]/2$ and α in Eq. 2.4 denotes the set of quantum numbers, $\alpha_b = \{E_b, l_b, j_b, J_b\}$ for the bound state, and $\alpha_c = \{E_c, l_c, j_c, J_c\}$ for the continuum states.

The bound-state wavefunctions are normalized to unity, $\int dr\,|u_{\alpha_b}(r)|^2 = 1$, whereas the continuum wavefunctions have boundary conditions at infinity given by

$$u_{\alpha_c}(r \to \infty) = i\sqrt{\frac{m_{nx}}{2\pi k\hbar^2}}\left[H_l^{(-)}(r) - S_{\alpha_c}H_l^{(+)}(r)\right]e^{i\sigma_l(E)} \qquad (2.5)$$

where $S_{\alpha_c} = \exp[2i\delta_{\alpha_c}(E)]$, with $\delta_{\alpha_c}(E)$ and $\sigma_l(E)$ being the nuclear and the Coulomb phase-shifts, respectively. In Eq. 2.5, $H_l^{(\pm)}(r) = G_l(r) \pm iF_l(r)$, where F_l and G_l are the regular and irregular Coulomb wavefunctions. For neutrons the Coulomb functions reduce to the usual spherical Bessel functions, $j_l(r)$ and $n_l(r)$. With these definitions, the continuum wavefunctions are normalized as $\langle u_{E_c'}|u_{E_c}\rangle = \delta(E_c' - E_c)\delta_{\alpha\alpha'}$.

2.2.2 Radiative capture cross sections

The radiative capture cross sections for $n+x \to a+\gamma$ and πL ($\pi = E, (M) =$electric (magnetic) L-pole) transitions are calculated with

$$\sigma_{EL,J_b}^{\text{d.c.}} = \frac{(2\pi)^3}{k^2}\left(\frac{E_{nx} + E_b}{\hbar c}\right)^{2L+1}\frac{2(2I_a + 1)}{(2I_n + 1)(2I_x + 1)}$$
$$\times \frac{L+1}{L[(2L+1)!!]^2}\sum_{J_c j_c l_c}(2J_c + 1)$$
$$\times \left\{\begin{matrix} j_c & J_c & I_x \\ J_b & j_b & L \end{matrix}\right\}^2 |\langle l_c j_c \|\mathcal{O}_{\pi L}\| l_b j_b\rangle|^2 , \qquad (2.6)$$

where E_b is the binding energy and $\langle l_c j_c \|\mathcal{O}_{\pi L}\| l_b j_b\rangle$ is the multipole matrix element. For the electric multipole transitions we have

$$\langle l_c j_c \|\mathcal{O}_{EL}\| l_b j_b\rangle = (-1)^{l_b+l_c-j_c+L-1/2}\frac{e_L}{\sqrt{4\pi}}$$
$$\times \sqrt{(2L+1)(2j_b + 1)}\left(\begin{matrix} j_b & L & j_c \\ 1/2 & 0 & -1/2 \end{matrix}\right)$$
$$\times \int_0^\infty dr\, r^L u_b(r)u_c(r), \qquad (2.7)$$

where e_L is the effective charge, which takes into account the displacement of the center-of-mass,

$$e_L = Z_n e \left(-\frac{m_n}{m_a} \right)^L + Z_x e \left(\frac{m_x}{m_a} \right)^L .$$ (2.8)

In comparison with the electric dipole transitions the cross sections for magnetic dipole transitions are reduced by a factor of v^2/c^2, where v is the relative velocity of the $n+x$ system. At very low energies, $v \ll c$, $M1$ transitions will be much smaller than the electric transitions. Only in the case of sharp resonances, the M1 transitions play a significant role, e.g. for the $J = 1^+$ state in ^{8}B at $E_R = 630$ keV above the proton separation threshold [19, 20]. In general, the potential model is not good to reproduce M1 transition amplitudes [21]. We will explore few situations in which the model works well.

The radiative capture cross sections for $n + x \to a + \gamma$ and $M1$ transitions are calculated with

$$\langle l_c j_c \| \mathcal{O}_{M1} \| l_b j_b \rangle = (-1)^{j_c + I_x + J_b + 1} \sqrt{\frac{3}{4\pi}} \mu_N$$

$$\times \left\{ \frac{1}{\tilde{l}_b} e_M \left[\frac{2\tilde{j}_b}{\hat{l}_b} \left(l_b \delta_{j_b,\, l_b+1/2} + (l_b + 1)\, \delta_{j_b,\, l_b-1/2} \right) \right.\right.$$

$$\left. + (-1)^{l_b+1/2-j_c} \frac{\hat{j}_b}{\sqrt{2}} \delta_{j_b,\, l_b\pm1/2} \delta_{j_c,\, l_b\mp1/2} \right]$$

$$+ g_N \frac{1}{\tilde{l}_b^2} \left[(-1)^{l_b+1/2-j_b} \tilde{j}_b \delta_{j_c,\, j_b} \right.$$

$$\left. - (-1)^{l_b+1/2-j_c} \frac{\hat{j}_b}{\sqrt{2}} \delta_{j_b,\, l_b\pm1/2} \delta_{j_c,\, l_b\mp1/2} \right]$$

$$+ g_x (-1)^{I_x+j_b+J_c+1} \hat{J}_b \hat{J}_c \hat{I}_x \tilde{I}_x \left\{ \begin{matrix} I_x & J_c & j_b \\ J_b & I_x & 1 \end{matrix} \right\} \right\}$$

$$\times \int_0^\infty dr\, r\, u_c(r)\, u_b(r),$$ (2.9)

where $\tilde{k} = \sqrt{k(k+1)}$ and $\hat{k} = \sqrt{2k+1}$. The spin g-factor is $g_N = 5.586$ for the proton and $g_N = -3.826$ for the neutron. The magnetic moment of the core nucleus is given by $\mu_x = g_x \mu_N$. If $l_c \neq l_b$ the magnetic dipole matrix element is zero.

The total direct capture cross section is obtained by adding all multipolarities and final spins of the bound state ($E \equiv E_{nx}$),

$$\sigma^{\text{d.c.}}(E) = \sum_{L, J_b} (SF)_{J_b}\, \sigma^{\text{d.c.}}_{L, J_b}(E),$$ (2.10)

where $(SF)_{J_b}$ are spectroscopic factors.

For charged particles the astrophysical S-factor for the direct capture from a continuum state to the bound state is defined as

$$S\left(E\right) = E\ \sigma^{\text{d.c.}}\left(E\right)\ \exp\left[2\pi\eta\left(E\right)\right],$$
$$\text{with} \qquad \eta\left(E\right) = Z_a Z_b e^2/\hbar v, \tag{2.11}$$

where v is the initial relative velocity between n and x.

For some resonances, not reproducible with the single-particle model, we will use a simple Breit-Wigner shape parametrization

$$\sigma_{BW} = \frac{\Gamma}{2\pi}\frac{\sigma_0(E)}{(E - E_R)^2 + \Gamma^2/4}, \tag{2.12}$$

where E_R is the resonance energy. The function $\sigma_0(E)$ is given by

$$\sigma_0(E) = \frac{\pi\hbar^2}{2m_{xn}E}\frac{2J_R + 1}{(2Jx + 1)(2J_n + 1)}\frac{\Gamma_n(E)\Gamma_\gamma(E)}{\Gamma(E)} \tag{2.13}$$

where the total width $\Gamma = \Gamma_n + \Gamma_\gamma$ is the sum of the nucleon-decay and the γ-decay widths. For simplicity, and for the cases treated here, we will assume that the resonances are narrow so that $\sigma_0 = \sigma(E_R)$.

2.2.3 Asymptotic normalization coefficients

Although the potential model works well for many nuclear reactions of interest in astrophysics, it is often necessary to pursue a more microscopic approach [22, 23] to reproduce experimental data. In a microscopic approach, instead of the single-particle wavefunctions one often makes use of overlap integrals, $I_b(\mathbf{r})$, and a many-body wavefunction for the relative motion, $\Psi_c(\mathbf{r})$. Both $I_b(\mathbf{r})$ and $\Psi_c(\mathbf{r})$ might be very complicated to calculate, depending on how elaborated the microscopic model is. The variable $\mathbf{r}$ is the relative coordinate between the nucleon and the nucleus x, with all the intrinsic coordinates of the nucleons in x being integrated out. The direct capture cross sections are obtained from the calculation of $\sigma_{L,J_b}^{\text{d.c.}} \propto |\langle I_b(r)||r^L Y_L||\Psi_c(r)\rangle|^2$.

The imprints of many-body effects will eventually disappear at large distances between the nucleon and the nucleus. One thus expects that the overlap function asymptotically matches the solution of the Schrödinger equation 2.4, with $V = V_C$ for protons and $V = 0$ for neutrons. That is, when $r \to \infty$,

$$I_b(r) = C_1\frac{W_{-\eta,l_b+1/2}(2\kappa r)}{r}, \quad \text{for protons}$$
$$= C_2\sqrt{\frac{2\kappa}{r}}K_{l_b+1/2}(\kappa r), \quad \text{for neutrons} \tag{2.14}$$

where the binding energy of the $n + x$ system is related to κ by means of $E_b = \hbar^2\kappa^2/2m_{nx}$, $W_{p,q}$ is the Whittaker function and K_μ is the modified Bessel function. In Eq. 2.14, C_i is the asymptotic normalization coefficient (ANC).

In the calculation of $\sigma_{L,J_b}^{\text{d.c.}}$ above, one often meets the situation in which only the asymptotic part of $I_b(r)$ and $\Psi_c(r)$ contributes significantly to the integral over

Parameter	Adopted value
$R_0 = R_{S0} = R_C$	$r_0(A+1)^{1/3}$ fm
r_0	1.25
$a_0 = a_{S0}$	0.65 fm
V_{s0}	-10 MeV

Table 2.1: Parameters of the single-particle potentials, except for few cases explicitly mentioned in the text.

r. In these situations, $\Psi_c(r)$ is also well described by a simple two-body scattering wave (e.g. Coulomb waves). Therefore the radial integration in $\sigma^{\text{d.c.}}_{L,J_b}$ can be done accurately and the only remaining information from the many-body physics at short-distances is contained in the asymptotic normalization coefficient C_i, i.e. $\sigma^{\text{d.c.}}_{L,J_b} \propto C_i^2$. We thus run into an effective theory for radiative capture cross sections, in which the constants C_i carry all the information about the short-distance physics, where the many-body aspects are relevant. It is worthwhile to mention that these arguments are reasonable for proton capture at very low energies, because of the Coulomb barrier.

The spectroscopic factors, SF, are usually obtained by adjusting the calculated cross sections to reproduce the experimental ones. Here we try to follow the literature as closely as possible. When experimental data are not available, we use spectroscopic factors taken from the literature. For the cases in which experimental data exist, we also try to use spectroscopic factors published in the literature, and fit the data by varying the depth of the WS potential for the continuum states.

The asymptotic normalization coefficients, C_α, can also be obtained from the analysis of peripheral, transfer and breakup, reactions. As the overlap integral, Eq. 2.14, asymptotically becomes a Whittaker function, so does the single particle bound-state wavefunction u_α, calculated with Eq. 2.4. If we call the single particle ANC by b_i, then the relation between the ANC obtained from experiment, or a microscopic model, with the single particle ANC is given by $(SF)_i b_i^2 = C_i^2$. This becomes clear from Eq. 2.10. The values of $(SF)_i$ and b_i obtained with the simple potential model are useful telltales of the complex short-range many-body physics of radiative capture reactions. One can also invert this argumentation and obtain spectroscopic factors if the C_i are deduced from a many-body model, or from experiment, and the b_i are calculated from a single particle potential model [24].

2.3 Proton capture

Table 2.2 summarizes the potential parameters used in cases where the potential model works reasonably well for radiative proton capture reactions. A discussion is presented case by case in the following subsections. Unless otherwise stated, we use the parameters according to Table 2.1 for the single-particle potential. The parameters for the continuum potential, V_c, are the same as for the bound state potential, except for few cases discussed explicitly in the text.

Reaction	E_b	V_b	SF	b	$> R_0$	$S(0)$
d(p, γ)^{3}He	5.49	-44.43	0.7	1.86	0.98	0.14
^{6}Li(p, γ)^{7}Be	5.61	-65.91	0.83 [33]	2.21	1.28	66.8
^{6}Li(p, γ)^{7}Be*	5.18	-64.94	0.84 [34]	2.08	1.19	32.7
^{7}Li(p, γ)^{8}Be	17.26	-75.69	1.0	7.84	1.01	238.
^{7}Be(p, γ)^{8}B	0.14	-41.26	1.0	0.72	1.00	19.4
^{8}B(p, γ)^{9}C	1.30	-41.97	1.0 [56]	1.31	1.08	42.5
^{9}Be(p, γ)^{10}B	6.59	-49.83	1.0 [61]	3.43	1.27	1052
^{11}C(p, γ)^{12}N	0.60	-40.72	0.4 [70]	1.49	1.01	50.8
^{12}C(p, γ)^{13}N	1.94	-41.65	1.0	2.05	1.04	2346
^{13}C(p, γ)^{14}N	7.55	-50.26	0.33	5.31	1.10	6217
^{13}N(p, γ)^{14}O	4.63	-46.02	1.88 [85]	3.97	1.45	5771
^{14}N(p, γ)^{15}O*	0.50	-14.83	1.5	4.24	1.00	1470
^{15}N(p, γ)^{16}O	12.13	-54.81	1.8 [102]	10.16	0.78	$2.21 \cdot 10^4$
^{16}O(p, γ)^{17}F	0.60	-49.69	0.9 [109]	0.96	1.02	304
^{16}O(p, γ)^{17}F*	0.11	-50.70	1.0 [109]	77.21	1.00	9075
^{20}Ne(p, γ)^{21}Na*	0.006	-47.24	0.7	4.02	1.00	$4.28 \cdot 10^4$
^{20}Ne(p, γ)^{21}Na*	2.10	-49.63	0.8	2.43	1.00	2493

Table 2.2: Binding energy (E_b, in MeV), central potential depth of bound state (V_b, in MeV), spectroscopic factor (SF), single-particle asymptotic normalization coefficients (b, in fm$^{-1/2}$), the factor that multiplies S-factor if the integration in Eq. 2.6 starts at $r = R_0$ (nuclear radius) and S-factor at zero energy ($S(0)$, in eV b) for radiative proton capture reactions.

2.3.1   d(p, γ)^{3}He

Understanding of the nature of ^{3}He, the only stable 3-body nucleus, constitutes a major advance towards the solution of the general problem of nuclear forces. In particular, it involves the influence of the third nucleon on the interaction between the other two. This latter interaction has been studied extensively in deuteron and in nucleon-nucleon scattering. These are issues beyond the scope of this work. But we will show that a rather good reproduction of the experimental data for the capture reaction d(p, γ)^{3}He can be obtained with the simple potential model described in the previous sections.

The $J_b = 1/2^+$ ground state of ^{3}He is described as a $j_b = s_{1/2}$ proton coupled to the deuterium core, which has an intrinsic spin $I_x = 1^+$. The gamma-ray transition is dominated by the $E1$ multipolarity and by incoming p waves. Our results require a spectroscopic factor $SF = 0.7$ to fit the experimental data shown in Fig. 2.1. If we add d-waves to the ground-state there is a negligible change in this value. Thus, the contribution of d-waves in the ground state has been neglected. The experimental data are from Ref. [25] (filled squares), Ref. [26] (open squares), Ref. [27] (open circles), Ref. [28] (filled triangles).

In Ref. [29], the ANC for this reaction was found by an analysis of s-wave pd and nd scattering. The ANC for the $l = 0$ channel was found to be 1.97 fm$^{-1/2}$ ($C^2 = 3.9 \pm 0.06$ fm^{-1}) [29]. Our ANC value is $\sqrt{(SF)b^2} = 1.56$ fm$^{-1/2}$, which is in good agreement with the more complicated analysis presented in Ref. [29].
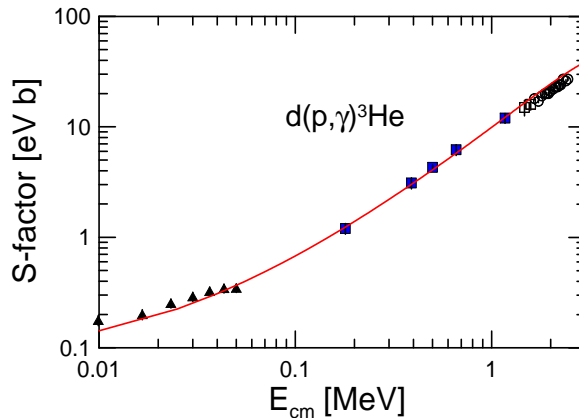
Figure 2.1: Single-particle model calculation for the reaction $d(p,\gamma)^3$He. Experimental data are from Refs. [25, 26, 27, 28]. The parameters calculated according to Table I are used. The potential depth (here $V_b = V_c$) is given in Table II.

2.3.2 ^{6}Li$(p,\gamma)^7$Be

Unlike ^{7}Li, ^{6}Li is predicted to be formed at a very low level in Big Bang nucleosynthesis, ^{6}Li/H $= 10^{-14}$ [30, 31]. Whereas most elements are produced by stellar nucleosynthesis, lithium is mainly destroyed in stellar interiors by thermonuclear reactions with protons. In fact, ^{6}Li is rapidly consumed at stellar temperatures higher than 2×10^6 K. The major source of ^{6}Li has been thought for decades to be the interaction of galactic cosmic rays with the interstellar medium [32]. The low energy capture reaction ^{6}Li$(p,\gamma)^7$Be plays an important role in the consumption of ^{6}Li and formation of ^{7}Be.

The S-factor for this reaction is dominated by captures to the ground state and the 1st excited state of ^{7}Be. Both the ground state ($J_b = 3/2^-$) and the 1st excited state ($J_b = 1/2^-$) of ^{7}Be are described as a $j_b = p_{1/2}$ neutron interacting with the ^{6}Li core, which has an intrinsic spin $I_A = 1^+$. The parameters calculated according to Table I are used. The potential depths which reproduce the ground and excited states are given in Table II.

The continuum state potential depth for transitions to the ground state is set as $V_c = -37.70$ MeV following Ref. [33] and the corresponding one for the 1st excited is adjusted to fit the experimental S-factor for that capture (open circles in Fig. 2.2). In Ref. [33] the potential parameters and the spectroscopic factor for the ground state was obtained from a comparison between a finite-range distorted-wave Born approximation calculation and the experimental differential cross sections for the ^{9}Be$(^8$Li,^{9}Be$)^8$Li elastic-transfer reaction at 27 MeV. The spectroscopic factors so obtained were compared with shell-model calculations and other experimental values. The spectroscopic factor is 0.83 for the ground state following Ref. [33] and 0.84 for the 1st excited state, following Ref. [34].

In Ref. [34], the reaction is also compared with a calculation based on a four-cluster microscopic model. The energy dependence of the astrophysical S-factor for the ^{6}Li $(p,\gamma)^7$Be reaction has been studied in Ref. [35], as well as in Ref. [36] where an analysis of the experimental data of Ref. [37] was done. It was found
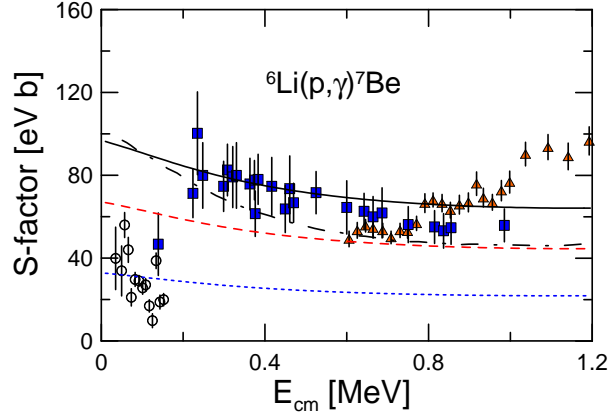
Figure 2.2: Single-particle model calculation for the reaction ^{6}Li(p, γ)^{7}Be. The dotted line is the calculation for the capture to the 1st excited of ^{7}Be and the dashed line for the ground state. The solid line is the total calculated S-factor. Experimental data are from Refs. [38, 39, 34]. The dotted-dashed line is the total S-factor calculated in Ref. [34] using a four-cluster microscopic model.

[36, 35] that the gamma-ray transition is dominated by the $E1$ multipolarity and by incoming s and d waves.

Adopting the spectroscopic values listed above and including s and d incoming waves, we obtain the result shown in Fig. 2.2. Experimental data are from Ref. [38] (filled triangles), Ref. [39] (filled squares) and Ref. [34] (open circles). The agreement with the experimental data is very good and consistent with the previous studies [37, 36, 34, 33]. Based on these results, we obtain an ANC ($\sqrt{(SF)b^2}$) of 2.01 fm$^{-1/2}$ for the ground state and 1.91 fm$^{-1/2}$ for the 1st excited state.

2.3.3 ^{7}Li(p, γ)^{8}Be

The reaction ^{7}Li(p, γ)^{8}Be is part of the pp-chain in the Sun, leading to the formation of ^{8}Be [40]. The unstable ^{8}Be decays into two α-particles in 10^{-16} sec.

For this reaction, we consider only the capture to the ground state of ^{8}Be ($J_b = 0^+$), which is described as a $j_b = p_{3/2}$ proton coupled to the $I_x = 3/2^-$ ^{7}Li core. The gamma-ray transition is dominated by the $E1$ multipolarity and by incoming s and d waves. In order to reproduce the resonance at 0.386 MeV (in the c.m.), we choose a spectroscopic factor equal to 0.15. For the other resonance at 0.901 keV (in the c.m.), we chose $SF = 0.05$.

The result for both M1 resonances are shown in Figure 2.3, by dashed-dotted curves. The potential depth for the continuum state, chosen as to reproduce the resonances, are $V_c = -46.35$ MeV and $V_c = -44.55$ MeV, respectively. The non-resonant component (dashed-line) of the S-factor is obtained with $V_c = -56.69$ MeV and $SF = 1.0$. The experimental data are from Ref. [41] (open circles). This reaction was also studied in Ref. [42]. They have obtained an spectroscopic factor of 0.4 for the first M1 resonance at 0.386 MeV and $SF = 1.0$ for the non-resonant capture. Their analysis is extended to angular distributions for the capture cross-section and analyzing power at $E_{p,lab} = 80$ keV which shows a strong E1-M1
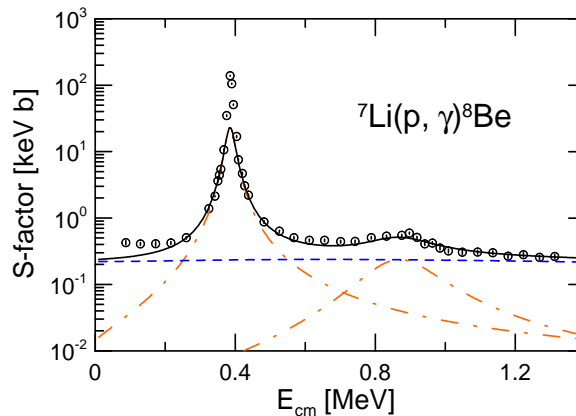
Figure 2.3: Potential model calculation for the reaction ^{7}Li$(p, \gamma)^8$Be. Experimental data are from Ref. [41].

interference, which helps to estimate the spectroscopic amplitudes.

If we only consider the fit to the non-resonant capture, our ANC ($\sqrt{(SF)b^2}$) is 7.84 fm$^{-1/2}$. If we choose spectroscopic factors which reproduce the M1 resonances, the ANC-value evidently changes. This shows that the ANC extracted from radiative capture reactions with the use of a potential model are strongly dependent on the presence of resonances, specially those involving M1 transitions.

2.3.4 ^{7}Be$(\mathbf{p}, \gamma)^8$B

The creation destruction of ^{7}Be in astrophysical environments is essential for understanding several stellar and cosmological processes and is not well understood. ^{8}B also plays an essential role in understanding our Sun. High energy ν_e neutrinos produced by ^{8}B decay in the Sun oscillate into other active species on their way to earth [43]. Precise predictions of the production rate of ^{8}B solar neutrinos are important for testing solar models, and for limiting the allowed neutrino mixing parameters. The most uncertain reaction leading to ^{8}B formation in the Sun is the ^{7}Be$(p, \gamma)^8$B radiative capture reaction [44].

The $J_b = 2^+$ ground state of ^{8}B is described as a $j_b = p_{3/2}$ neutron coupled to the ^{7}Be core, which has an intrinsic spin $I_x = 3/2^-$. In this case, instead of the values in Table I, we take $a = 0.52$ fm and $V_{so} = -9.8$ MeV. This is the same set of values adopted in Ref. [18]. The gamma-ray transition is dominated by the $E1$ multipolarity and by incoming s and d waves. The spectroscopic factor for non-resonant transitions is set to 1.0, which seems to reproduce best the S-factor for this reaction at low energies. Our results are shown in Fig. 2.4. The experimental data are from Ref. [45] (open square), Ref. [46] (open circles), Ref. [47, 44, 48, 49] (solid triangle, open triangle, solid square, solid circle, solid diamond and open diamond).

In Ref. [44], the experimental data is reproduced with the cluster model calculation of Ref. [50] together with two incoherent Breit-Wigner resonances: a 1^+ M1 resonance at 0.63 MeV fitted with $\Gamma_p = 35.7 \pm 0.6$ keV and $\Gamma_\gamma = 25.3 \pm 1.2$
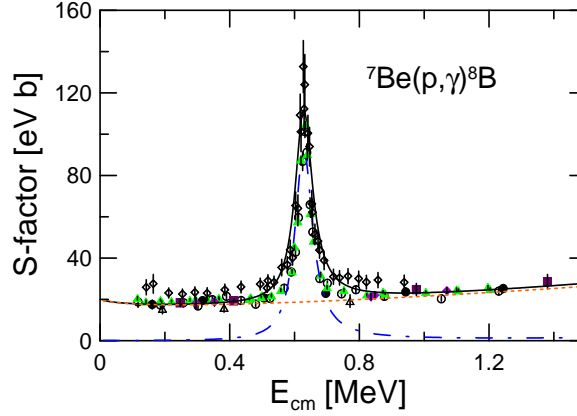
Figure 2.4: Single-particle model calculations for the reaction $^7\text{Be}(\text{p},\gamma)^8\text{B}$. The dashed-dotted line is the calculation for the M1 resonance at $E_{cm} = 0.63$ MeV and the dotted line is for the non-resonant capture. Experimental data are from Refs. [45, 46, 47, 44, 48, 49]. The total S factor is shown as a solid line.

MeV, and a 3^+ resonance at 2.2 MeV fitted with $\Gamma_p = 350$ keV and $\Gamma_\gamma = 150 \pm 30$ MeV. Our calculated M1 resonance (dashed-dotted line) also reproduces well the data if we use $V_c = -38.14$ MeV, and $SF = 0.7$, with the other parameters according to Table I. For the non-resonant E1 transitions we use $V_c = -41.26$ MeV and $SF = 1.0$. The S-factor at $E = 0$, $S_{17}(0)$, is equal to 19.41 eV.b, which is 10% smaller than that from the most recent experimental and theoretical analysis [44, 52].

A different experimental approach was used in Ref. [51], which extracted the ^8B ANC from ^8B breakup reactions at several energies and different targets. In that reference a slightly lower value of $S_{17}(0) = 16.9 \pm 1.7$ eV.b was inferred. That work also quotes an ANC of 0.67 fm$^{-1/2}$ ($C^2 = 0.450(30)$ fm^{-1}). Our ANC, extracted from our fit to the radiative capture reaction, is $\sqrt{(SF)b^2} = 0.72$ fm$^{-1/2}$, not much different from Ref. [51].

2.3.5 $^8\text{B}(\text{p},\gamma)^9\text{C}$

Nucleosynthesis of light nuclei is hindered by the gaps at $A = 5$ and $A = 8$. The gap at $A = 8$ may be bridged by reactions involving the unstable nuclei ^8Li ($T_{1/2} = 5840$ ms) and ^8B ($T_{1/2} = 5770$ ms). The $^8\text{B}(\text{p},\gamma)^9\text{C}$ reaction breaks out to a hot part of the pp chain at temperatures such that this reaction becomes faster than the competing β^+ decay. This reaction is especially relevant in low-metallicity stars with high masses where it can be faster than the triple-α process. It is also important under nova conditions. In both astrophysical scenarios this happens at temperatures several times larger than 10^8 K, corresponding to Gamow window energies around $E = 50 - 300$ keV [68, 54, 55].

The capture process for this reaction is dominated by E1 transitions from incoming s waves to bound p states [56] and the present work is restricted to an analysis of the capture to the ground state of ^9C ($J_b = 3/2^-$), which is described as a $j_b = p_{3/2}$ proton coupled to the ^9C core, which has an intrinsic spin $I_x = 2^+$. The
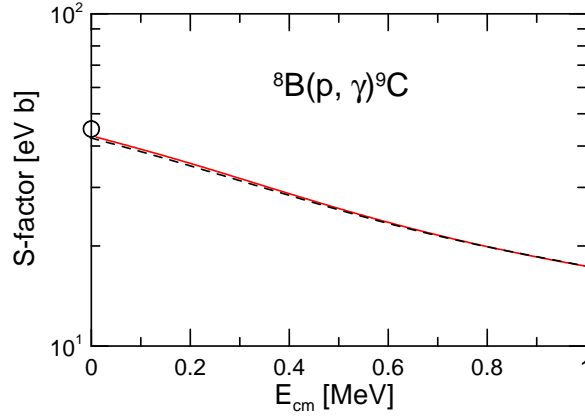
Figure 2.5: Single-particle model calculations for the reaction ^{8}B(p, γ)^{9}C (solid line). The open circle at $E = 0$ is from Refs. [57, 58]. The result from Ref. [56] ($\lambda_{scatt} = 0.55$ fm) is shown as a dashed line.

spectroscopic factor has been set to 1.0 as in Ref. [56], where several spectroscopic factor values are compared.

A renormalized folding potential for the continuum state is used in Ref. [56], while in our calculation V_c is adjusted to -22.55 MeV to yield a similar result. This is done because there are no experimental data for this reaction. The results of both calculations are shown in Fig. 2.5. The open circle at $E = 0$ is from Refs. [57, 58], which is an extrapolated value from a potential model using an ANC deduced from a breakup experiment. Ref. [56] also generates resonances by changing parameters of the folding potential. The ANC found in Ref. [59] is 1.15 fm$^{-1/2}$ ($C^2 = 1.33 \pm 0.33$ fm^{-1}), whereas our ANC ($\sqrt{(SF)b^2}$) = 1.31 fm$^{-1/2}$.

2.3.6 ^{9}Be(p, γ)^{10}B

The reaction ^{9}Be(p,γ)^{10}B plays an important role in primordial and stellar nucleosynthesis of light elements in the p-shell [17, 60]. Hydrogen burning in second generation stars occurs via the proton-proton (pp) chain and CNO-cycle, with the ^{9}Be(p,γ)^{10}B reaction serving as an intermediate link between these cycles.

The $J_b = 3^+$ ground state of ^{10}B is described as a $j_b = p_{3/2}$ proton coupled to the ^{9}Be core, which has an intrinsic spin $I_A = 3/2^-$. The gamma-ray transition for the DC is dominated the $E1$ multipolarity and by incoming s waves. A spectroscopic factor $SF = 1.0$ is used, which is the same value adopted in Ref. [61]. This value reproduces ^{9}Be(d,n)^{10}B and ^{9}Be(^{3}He,d)^{10}B reactions at incident energies of $10 - 20$ MeV, and ^{9}Be(α,t)^{10}B at 65 MeV. It is also in accordance with the theoretical predictions of Refs. [62, 63].

The potential depth for the continuum state $V_c = -31.82$ MeV has been adjusted so that we can reproduce the direct capture measurements reported in Refs. [64]. It also reproduces the results of Ref. [65] where a reanalysis of the existing experimental data on ^{9}Be(p, γ)^{10}B was done within the framework of the R-matrix method. The direct capture part of the S-factor was calculated using the experimentally measured ANC for ^{10}B $\to^9$ Be + p. The results are shown in Fig. 2.6.
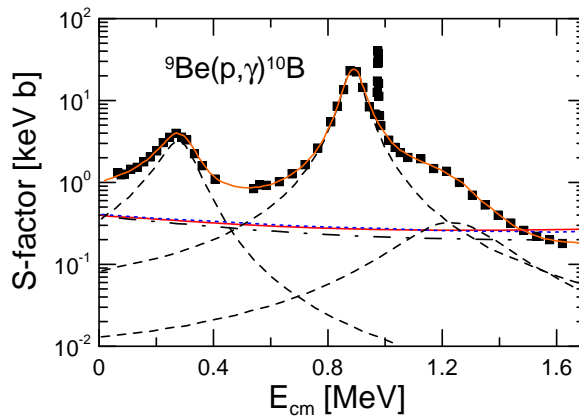
Figure 2.6: Single-particle model calculations for the reaction $^9\text{Be}(p,\gamma)^{10}\text{B}$ (solid line). The experimental data are from Ref. [64]. The fits to the resonances, done in Ref. [64], are shown as dashed lines. DC results from Ref. [65] and Ref. [64] are shown as a dotted-dashed line and a dotted line, respectively. The curve passing through the experimental data points is the sum of our DC calculation and the resonance fits, given by the dashed lines.

The experimental data are from Ref. [64] (filled squares). These data have also been fitted in Ref. [66] using R-matrix formulae that include channel contributions where appropriate. The curve passing through the experimental data points is the sum of our DC calculation and the resonance fits, given by the dashed lines.

In Ref. [67], the differential cross sections for the reactions $^9\text{Be}(^{10}\text{B},^{10}\text{B})^9\text{Be}$ and $^9\text{Be}(^{10}\text{B},^9\text{Be})^{10}\text{B}$ have been measured at an incident energy of 100 MeV. By normalizing the theoretical cross sections to the experimental data, the ANC for $^{10}\text{B} \rightarrow ^9\text{Be} + \text{p}$ was extracted and found to be 2.22 fm$^{-1/2}$ ($C^2 = 4.91$ fm^{-1}), whereas the ANC, $(\sqrt{(SF)b^2})$, obtained from our fit to the previous analysis of Refs. [61, 66] is 3.43 fm$^{-1/2}$.

2.3.7 $^{11}\text{C}(\text{p},\gamma)^{12}\text{N}$

For first generation stars (those composed entirely of nuclei produced in the Big Bang) can only undergo nucleosynthesis via the pp chains or the triple-alpha process until heavier nuclei are produced to initiate the CNO cycle. For supermassive first generation stars, such processes generate too little energy and the triple-alpha reaction turns on too late to cause an explosion. Rather, such stars could simply collapse to black holes. However, hot pp chains provide a path for supermassive first generation stars to produce CNO nuclei at a lower temperature than required by the triple-alpha reaction [68]. These CNO nuclei then serve as seeds for further energy generation, stablizing the star against collapse long enough to permit an explosion to occur. Both the $^8\text{B}(\text{p},\gamma)^9\text{C}$ and $^{11}\text{C}(\text{p},\gamma)^{12}\text{N}$ reactions are important in the hot pp chains.

For the ^{11}C (p, $\gamma)^{12}\text{N}$ reaction, non-resonant capture into the ground state of ^{12}N and resonant capture into the first and second excited states is thought to dominate the reaction rate at stellar energies [69]. There are no experimental data for this reaction, except for indirect determination of the astrophysical S-
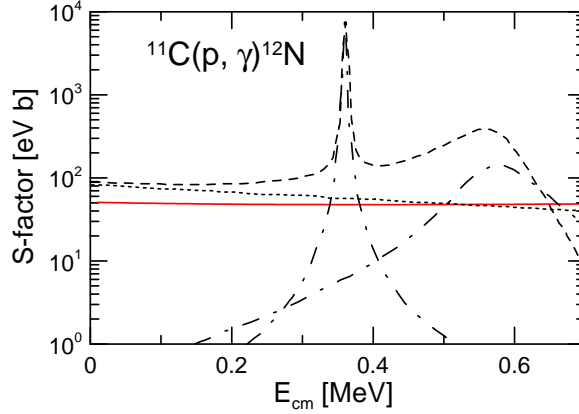
Figure 2.7: Single-particle model calculations for the reaction ^{11}C(p,γ)^{12}N (solid line). R-matrix results from Ref. [69] are also shown by dashed lines (resonances) and a dotted line (non-resonant).

factors, e.g. by using the ANC for ^{12}N $\rightarrow$^{11}C + p from the ^{14}N(^{11}C, ^{12}N)^{13}C peripheral transfer reaction. Another indirect measurement for the astrophysical rate of the ^{11}C + p reaction was obtained from from the Coulomb break-up of a ^{12}N radioactive beam in Ref. [70].

The ground state of ^{12}N ($J_b = 1^+$) is described as a $j_b = p_{1/2}$ proton coupled to the ^{11}C core, which has an intrinsic spin $I_x = 3/2^-$. The direct capture gamma-ray transition is dominated by the $E1$ multipolarity and by incoming s waves. The spectroscopic factor has been set to 0.4, the same value used in Ref. [70] (0.4 ± 0.25).

The result for our DC calculation is shown in Fig. 2.7. Similar results have also been reported in Refs. [69, 70, 71], and in Ref. [72] which also used the ANC method to extract the low-nergy S-factor via measurement of ^{11}C(d, n)^{12}N reaction. The ANC found in Ref. [69] is 1.32 fm$^{-1/2}$ ($C^2 = 1.73\pm0.25$ fm^{-1}) and in Ref. [72] is 1.69 fm^{-1} ($C^2 = 2.86\pm0.91$ fm^{-1}). Our ANC value is $\sqrt{(SF)b^2} = 0.94$ fm$^{-1/2}$.

2.3.8 ^{12}C(p, γ)^{13}N

The abundance ratio ^{12}C/^{13}C is an important measure of stellar evolution and nucleosynthesis. Changes in ratios of ^{12}C/^{13}C in stars happen as they evolve from the main sequence to the first ascent giant branch. Later, the convection zone grows and penetrates to greater depths where it begins to dredge up material that has been hot enough for the CNO cycle to convert to N. This is when the primordial ^{12}C is converted into ^{13}C and ^{14}N by the reactions ^{12}C(p, γ)^{13}N(β^+)^{13}C and ^{13}C(p,γ)^{14}N, hence reducing the ^{12}C/^{13}C ratio. During the late asymptotic giant branch AGB phase, the stars suffer thermal instabilities in the helium shell where partial helium burning occurs causing the ^{12}C/^{13}C ratio to increase [17].

The ^{12}C(p, γ)^{13}N direct capture to the ground state proceeds primarily through E1 ($s_{1/2} \rightarrow p_{1/2}$) and E1 ($d_{3/2} \rightarrow p_{1/2}$) single-particle transitions [73]. The ground
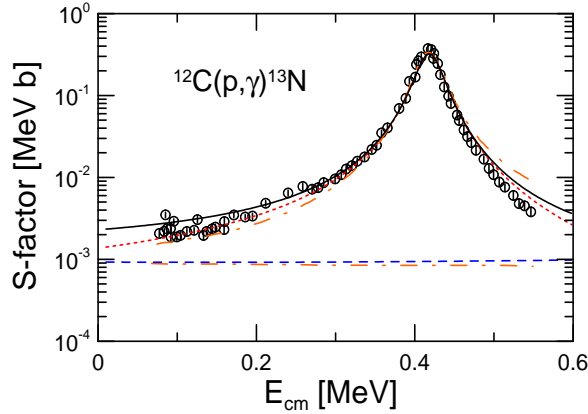
Figure 2.8: Single-particle model calculations for the reaction ^{12}C(p, γ)^{13}N are shown as a dashed line (DC), a dotted line ($E1$ resonance) and a solid line (total). The potential model results from Ref. [73] are shown as dotted-dashed lines.

state of ^{13}N ($J_b = 1/2^-$) is described as a $j_b = p_{1/2}$ proton coupled to the ^{12}C core, which has an intrinsic spin $I_x = 0^+$.

Experimental cross sections for the ^{12}C(p,γ) capture to the ground state of ^{13}N were published in Ref. [74]. Choosing the spectroscopic factor as $SF = 1$, leads to the dashed line shown in Fig. 2.8, if we use the same potential depth as for the bound state. The E1 resonance at 0.422 MeV [73] is generated when we choose $V_c = -53.50$ MeV and a spectroscopic factor equal to 0.35. The result for the resonance is shown as a dotted-line in Fig. 2.8. The total S-factor is shown by a solid line.

The resonance at 0.422 MeV (c.m.) has also been studied experimentally and theoretically in Refs. [77, 76, 75]. The ANC obtained in Refs. [78, 79, 76] is 1.43 ± 0.09 fm$^{-1/2}$, whereas our ANC ($\sqrt{(SF)b^2}$), corresponding to the non-resonant capture, is 2.05 fm$^{-1/2}$.

2.3.9 ^{13}C(p, γ)^{14}N

This reaction is another important reaction in the CNO cycle. It precedes the slowest reaction in the CNO cycle, the ^{14}N(p, γ)^{15}O radiative capture reaction, which defines the rate of energy production in the cycle. The ^{13}C(p, γ)^{14}N radiative capture rate is also important for nucleosynthesis via the slow proton capture process because it depletes the seed nuclei required for the neutron generator reaction ^{13}C(α, n)^{16}O in AGB stars with solar metalicity [80, 81].

Extensive experimental data on this reaction was published in Ref. [82]. One concludes that this capture is dominated by transitions to the ground state. The direct capture to the ground state proceeds primarily through E1 ($s_{1/2} \to p_{1/2}$) and E1 ($d_{3/2} \to p_{1/2}$) single-particle transitions [73]. The ground state of ^{14}N ($J_b = 1^+$) is described as a $j_b = p_{1/2}$ proton coupled to the ^{13}C core, which has an intrinsic spin $I_x = 1/2^-$.

We could not reproduce the E1 resonance at $E_{cm} = 0.518$ MeV using the
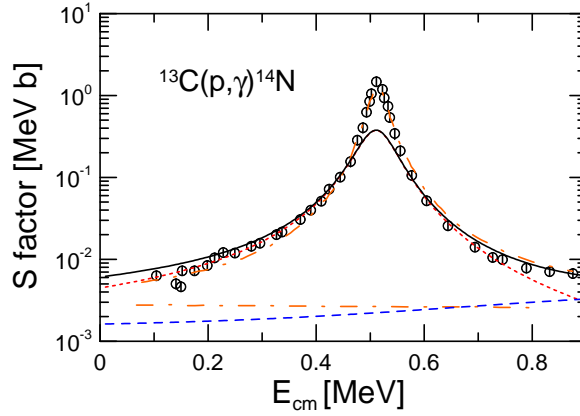
Figure 2.9: Single-particle model calculations for the reaction ^{13}C(p, γ)^{14}N are shown as a dashed line (DC), a dotted line ($E1$ resonance) and a solid line (total). The potential model results from Ref. [73] are shown as dotted-dashed lines.

potential parameters of Ref. [73]. In fact, we notice that figure 5 of Ref. [73] is inconsistent with its caption (center of mass and laboratory systems are swapped). In figure 2.9, the dotted line is our calculation for the resonance, which is obtained with the parameters from Table I and with generated when $V_c = -50.60$ MeV and spectroscopic factor 0.15. For non-resonant capture, the potential depth for the continuum state has been chosen as $V_c = -44.10$ MeV to reproduce the same result as in Ref. [73]. The spectroscopic factor has been set to 0.33 following Ref. [82]. The non-resonant calculation is shown by a dashed line in Fig. 2.9. The total S-factor is shown as a solid line.

In Ref. [83], the ^{13}C(p, γ)^{14}N radiative capture reaction is analyzed within the R-matrix approach. The experimental ANCs induced from the ^{13}C(^{14}N, ^{13}C)^{14}N and ^{13}C(^{3}He, d)^{14}N reactions are used in the analysis. The obtained ANC is 4.3 fm$^{-1/2}$ ($C^2 = 18.2$ fm^{-1}), whereas our ANC value is $\sqrt{(SF)b^2} = 3.05$ fm$^{-1/2}$.

2.3.10 ^{13}N(p, γ)^{14}O

For temperatures up to 10^9 K ($T_9 = 1$), this reaction is vital for understanding hydrogen burning in the hot CNO cycle and the conditions under which break-out into the rp-process might occur.

The ground state of ^{14}O ($J_b = 0^+$) is described as a $j_b = p_{1/2}$ proton coupled to the ^{13}N core, which has an intrinsic spin $I_x = 1/2^-$. The gamma-ray transition for the DC to the ground state is dominated the $E1$ multipolarity and by incoming s waves. For the non-resonant capture (lower curves in figure 2.10), if we choose the potential depth for the continuum state to be the same as that for the bound state ($V_c = V_b$), we obtain S-factors which are up to 3 times larger than the one in Ref. [84] where a theoretical description of this reaction has been reported. We find that $V_c = -25.20$ MeV reproduces rather well the non-resonant capture calculation of Ref. [84]. The spectroscopic factor has been set to 1.88 following Ref. [85], where a DWBA analysis of the ^{13}N(d, n)^{14}O reaction at $E_{cm} = 8.9$
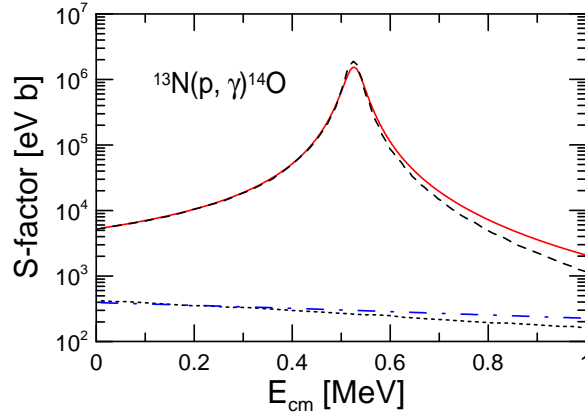
Figure 2.10: Single-particle model calculations for the reaction ^{13}N(p,γ)^{14}O are shown as a dotted-dashed line (non-resonant) and a solid line (E1 resonance). R-matrix results from Ref. [84] are also shown as a dashed line (resonance) and a dotted line (non-resonant).

MeV was used to obtain the ANC for the ground state of ^{14}O$\longrightarrow$^{13}N + p. Our non-resonant DC calculation is shown as a dotted-dashed line in Fig. 2.10.

We reproduce the E1 resonance at 0.528 MeV (s wave capture, according to Ref. [87]) as shown by the solid line in figure 2.10 if we choose $V_c = -52.14$ MeV and $SF = 1.0$. Very similar results were obtained in Refs. [89, 88, 86, 87, 85, 77]. The ANCs reported in there publications are 5.51 fm$^{-1/2}$ ($C^2 = 30.4 \pm 7.1$ fm^{-1}) [84], 5.42 ± 0.48 fm$^{-1/2}$ [85] and 5.39 fm$^{-1/2}$ ($C^2 = 29.0 \pm 4.3$ fm^{-1}) [87]. In Ref. [87] the radiative capture cross section was estimated using an R-matrix approach with the measured ANC from the ^{14}N(^{13}N,^{14}O)^{13}C peripheral transfer reaction at 11.8 MeV/nucleon incident energy. We obtain the ANC value $\sqrt{(SF)b^2} = 5.44$ fm$^{-1/2}$, which is in accordance with these results.

2.3.11 ^{14}N(p, γ)^{15}O

At astrophysical energies, this reaction is the slowest process in the hydrogen burning CNO cycle [17]. It plays a key role in the energy production of more massive main sequence stars and the detailed understanding of the neutrino spectrum of our sun [90, 91] as well as the age determination of globular cluster stars [92].

The main contribution to the S-factor for this reaction is due to the transition to the 6.793 MeV excited state of ^{15}O ($J_b = 3/2^+$) [94, 93], which is described as a $j_b = s_{1/2}$ proton coupled to the ^{14}N core ($I_x = 1^+$). The gamma-ray transition is dominated the E1 multipolarity and by incoming p waves. In this case, instead of the parameters of Table 2.1, we use $r_0 = 1.3$ fm, $r_c = 1.2$, $a = 0.6$ fm and $V_{s0} = -2.0$ MeV, which were also adopted in Ref. [95]. The spectroscopic factor is $SF = 1.5$. The result of our calculation is shown by the dashed line in Fig. 2.11.

Ref. [96] discusses experiments on stripping reactions and theoretical shell-model calculations used to describe the ^{14}N (p, γ)^{15}O radiative capture. These studies indicate that the resonance at 0.259 MeV decays to the 6.793 MeV excited
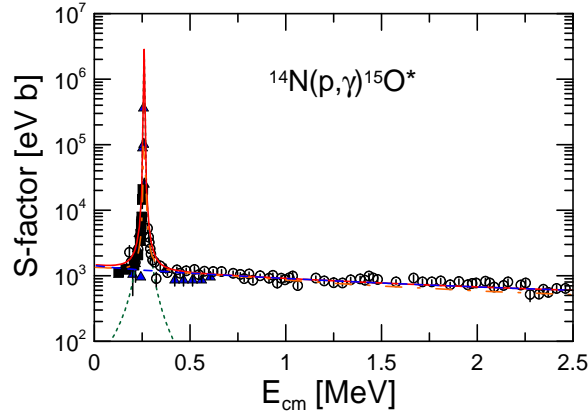
Figure 2.11: Single-particle model calculations for ^{14}N(p, γ)^{15}O capture to the 6.793 MeV excited state of ^{15}O. Dashed line is for the non-resonat capture, dotted line is for the M1 resonance, and the solid line is the total S-factor. The experimental data are from Refs. [94, 98, 99]. The dotted-dashed line is a R-matrix fit obtained in Ref. [94] with the channel radius $a = 5.5$ fm (this curve is almost invisible because it is very close to our results).

state of ^{15}O via a M1 radiation. To describe this resonance, we use the same spectroscopic factor, $SF = 0.51$, as obtained experimentally in Ref. [97] where spectroscopic factors and ANCs have been determined for bound states in ^{15}O using the ^{14}N(^{3}He,d)^{15}O reaction. Several other spectroscopic values from the literature were also discussed in Ref. [97]. We found an optimal value for the potential depth to be $V_c = -49.18$ MeV. Adopting this value, our calculations yield the dotted line shown in the figure.

The total S-factor is shown as a solid line. Experimental data are from Ref. [94] (filled squares), Ref. [98] (filled triangles), Ref. [99] (open circles). The R-matrix method was used to study this reaction in Ref. [94] and Ref. [100]. The ANC found in Ref. [101], deduced from the ^{13}C(^{14}N, ^{13}C)^{14}N and ^{13}C(^{3}He, d)^{14}N reactions, is 4.90 fm$^{-1/2}$ ($C^2 = 24 \pm 5$ fm^{-1}). Ref. [97] adopts the value 4.6 fm$^{-1/2}$ ($C^2 = 21 \pm 5$ fm^{-1}). Our ANC obtained from the DC fitting is $\sqrt{(SF)b^2} = 5.19$ fm$^{-1/2}$.

2.3.12 ^{15}N(p, γ)^{16}O

In second-generation stars with masses larger than the mass of the Sun, hydrogen burning proceeds predominantly through the CNO cycle [17]. The main sequence of reaction leads to an energy release of 25 MeV per cycle. There is a loss of CN catalyst from this cycle through the reaction ^{15}N(p, γ)^{16}O. This is replenished by a sequence of reactions involving oxygen and fluorine, leading to the formation of ^{14}N and ^{15}N. The reaction rate of ^{14}N(p, γ)^{16}O determines the overall abundance of the oxygen isotopes synthesized in the CNO tri-cycle [17] and therefore plays an important role in stellar nucleosynthesis.

This reaction is dominated by the capture into the ground state of ^{16}O ($J_b = 0^+$) [102], which is described as a $j_b = p_{1/2}$ proton coupled to the ^{15}N core ($I_x = 1/2^-$). The reaction is dominated by resonant capture to the ground state through the
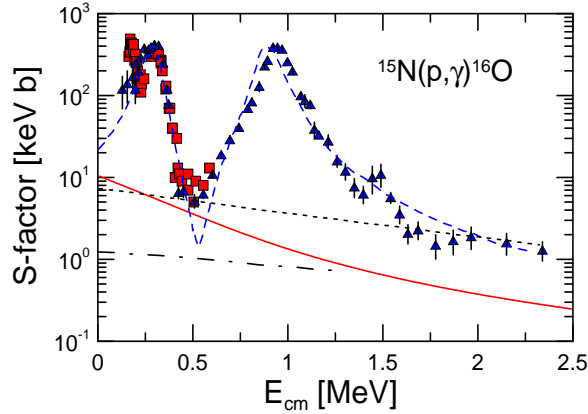
Figure 2.12: Single-particle model calculation for the reaction ^{15}N$(p,\gamma)^{16}$O (solid line). The experimental data are from Refs. [102, 107]. Dashed lines are Breit-Wigner fits to the resonances, as described in Ref. [102]. The dotted line is a non-resonant capture of Ref. [102]. The dotted-dashed line represents the non-resonant capture calculation from Ref. [104].

first two interfering $J^\pi = 1^-$ s-wave resonances at $E_{cm} = 312$ and 964 keV.

We will restrict ourselves to the non-resonant capture to the ground state, as a good reproduction of the resonances is not possible with the simple potential model. The non-resonant capture process proceeds predominantly through an E1 $(s \to p)$ transition [102]. A spectroscopic factor $SF = 1.8$ is used for the ground state of ^{16}O, following Ref. [102] which studied the excitation functions of this reaction at $E_p = 150 - 2500$ keV. This value is also in accordance with Ref. [103].

Our calculation is shown in Fig. 2.12. Experimental data are from Ref. [102] (filled triangles), Ref. [107] (filled squares). Ref. [104] extracted ANCs from the differential cross sections for the ^{15}N$(^3$He,d$)^{16}$O reaction. Using these ANCs and proton and α-resonance widths determined from an R-matrix fit to the data from the ^{15}N$(p, \alpha)^{12}$C reaction, the astrophysical factor for ^{15}N $(p, \gamma)^{16}$O was obtained. The results from Ref. [102] and Ref. [104] are also shown in Fig. 2.12. In Ref. [102], the resonances are described by using a fit with single level Breit-Wigner shapes. The ANC found in Ref. [104] is 13.86 fm$^{-1/2}$ ($C^2 = 192.0 \pm 26.0$ fm^{-1}). Our ANC is very close to this value, i.e., $\sqrt{(SF)b^2} = 13.63$ fm$^{-1/2}$.

2.3.13 ^{16}O$(p, \gamma)^{17}$F

Many stars, including the Sun, will eventually pass through an evolutionary phase that is referred to as the asymptotic giant branch (AGB) [105]. This phase involves a hydrogen and a helium shell that burn alternately surrounding an inactive stellar core. The ^{16}O$(p, \gamma)^{17}$F reaction rate influences sensitively the ^{17}O/^{16}O isotopic ratio predicted by models of massive ($\geq 4M_\odot$) AGB stars, where proton captures occur at the base of the convective envelope (hot bottom burning). A fine-tuning of the ^{16}O$(p, \gamma)^{17}$F reaction rate may account for the measured anomalous ^{17}O/^{16}O abundance ratio in small grains with are formed by the condensation of the material ejected from the surface of AGB stars via strong stellar winds [106].

We calculate the capture to the ground state and to the 1st excited state of
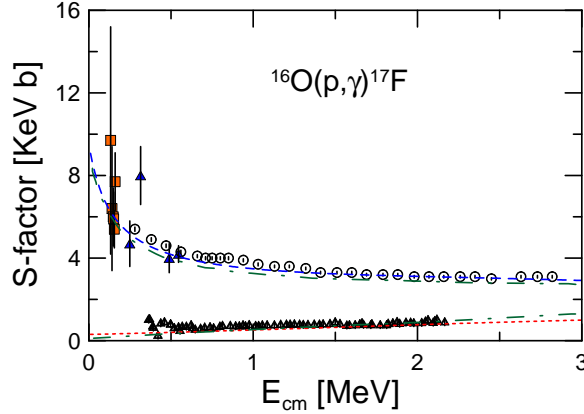
Figure 2.13: Single-particle model calculation for the reaction $^{16}O(p,\gamma)^{17}F$. The dotted line and the dashed line are for the capture to the ground state and to the first excited state respectively. The experimental data are from Refs. [110, 111, 109, 112]. The dotted-dashed lines are the result of shell model calculations published in Ref. [113].

^{17}F. The $J_b = 5/2^+$ ground state ($J_b = 1/2^+$ excited state) ^{17}F is described as a $j_b = d_{5/2}$ neutron ($j_b = s_{1/2}$ neutron) coupled to the ^{16}O core, which has an intrinsic spin $I_x = 0^+$. In this case, the values $a = 0.6$ fm and $R_C = R = 3.27$ fm are adopted, which are the same values used in Ref. [108]. The gamma-ray transitions are dominated by the $E1$ multipolarity and by incoming p waves for both states. The M1 and E2 contributions amount to less than 0.1% of the dominant E1 contribution, as shown in Ref. [109] where a potential model was also used.

We use spectroscopic factors equal to 0.9 and 1.0 for the ground state and the excited state, respectively, following Ref. [109]. Our results are shown in Fig. 2.13. The experimental data are from Ref. [110] (filled squares), Ref. [111] (filled triangles), Ref. [109] (open circles), and Ref. [112] (open triangles).

Ref. [114] reports a study of the $^{16}O(^3He,d)^{17}F$ reaction to determine ANCs for transitions to the ground and first excited states of ^{17}F. The ANCs found in Ref. [114] are 1.04 fm$^{-1/2}$ ($C^2 = 1.08 \pm 0.1$ fm^{-1}) for the ground state, and 80.6 fm$^{-1/2}$ ($C^2 = 6490 \pm 680$ fm^{-1}) for the first excited state of ^{17}F, respectively. Our ANC values are $\sqrt{(SF)b^2} = 0.91$ fm$^{-1/2}$ for the ground state and 77.21 fm$^{-1/2}$ for the 1st excited state.

2.3.14 $^{20}Ne(p,\gamma)^{21}Na$

Along with the p-p chain and the CNO tri-cycle, the Ne-Na cycle [115] is also of importance in hydrogen burning in second-generation stars with masses larger than the mass of the Sun. The $^{20}Ne(p,\gamma)^{21}Na$ reaction is the first reaction of the cycle. The nuclei ^{21}Na, ^{21}Ne, ^{22}Na, ^{22}Ne, and ^{23}Na are gradually created during Ne-Na burning. ^{21}Ne is of additional interest for subsequent He burning in stars. Due to the positive Q-value of 2.56 MeV for the $^{21}Ne(\alpha, n)^{24}Mg$ reaction, ^{21}Ne can act as a source of neutrons. Subsequent capture of these neutrons contributes to the synthesis of the heavier elements [115].
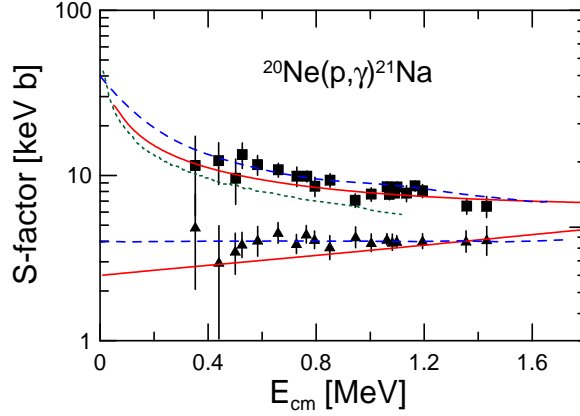
Figure 2.14: Single-particle model calculation for the reaction ^{20}Ne(p, γ)^{21}Na. Upper solid line is for the capture to the 2.425 MeV excited state of ^{20}Ne and lower solid line for the 0.332 MeV excited state. Experimental data are from Ref. [116]. The dashed and dotted lines are theoretical results from Ref. [116] and Ref. [117], respectively

As observed in Ref. [116], the direct capture to the 2.425 MeV ($J^\pi = 1/2^+$) and 0.332 MeV ($J^\pi = 5/2^+$) excited state dominate the total S-factor for this reaction. The $J_b = 1/2^+$ excited state ($J_b = 5/2^+$ excited state) of ^{21}Na is described as a $j_b = s_{1/2}$ proton ($j_b = d_{5/2}$ proton) interacting with the ^{20}Ne core, which has an intrinsic spin $I_x = 0^+$. The gamma-ray transition is dominated by the $E1$ multipolarity and by incoming p waves.

The spectroscopic factor obtained in Ref. [116] is 0.9. More recently, Ref. [117] determined the ANC for ^{21}Na$\rightarrow^{20}$Ne + p from the analysis of ^{20}Ne(^{3}He, d)^{21}Na proton transfer reaction at an incident energy of 25.83 MeV, and obtained the spectroscopic factor of 0.6. We used the spectroscopic factor $SF = 0.7$ for the 2.425 MeV excited state and $SF = 0.8$ for the 0.332 MeV excited state, which are values between those of Refs. [116] and [117]. Our results are shown in Fig. 2.14. Experimental data are from Ref. [116].

For the 2.425 MeV excited stated, the ANC found in Ref. [117] is 8.29×10^{16} fm$^{-1/2}$ ($C^2 = 6.8694 \times 10^{33}$ fm^{-1}), whereas our computed ANC value is $\sqrt{(SF)b^2} = 3.36$ fm$^{-1/2}$. The reason for this large discrepancy is not clear. It might be, as seen from Fig. 2.14, due to the steep slope of the S-factor at low energies. This points to a subthreshold resonance and a possible large sensitivity of the ANC for this state. On the other hand, for the 0.332 MeV excited state, the ANC found in Ref. [117] is 1.55 fm$^{-1/2}$ ($C^2 = 2.41$ fm^{-1}), whereas our computed ANC value is $\sqrt{(SF)b^2} = 2.17$ fm$^{-1/2}$.

2.4 Neutron capture

Table 2.3 summarizes the potential parameters used in the cases where the single-particle model works reasonably well in calculating radiative neutron capture reactions. A discussion is presented case by case in the following subsections. Unless otherwise stated, we use the parameters described in Table 2.1 for the single-

Reaction	E_b	V_b	SF	b	$r > R_0$
^{2}H(n,γ)^{3}H	6.26	-44.63	1.0	1.90	0.97
^{7}Li(n,γ)^{8}Li	2.03	-43.56	0.87 [131]	0.76	1.04
^{7}Li(n,γ)^{8}Li*	1.05	-40.46	0.48 [131]	0.47	1.02
^{8}Li(n,γ)^{9}Li	4.06	-45.29	0.8 [142]	1.25	1.08
^{8}Li(n,γ)^{9}Li*	1.37	-38.57	0.55 [141]	0.54	1.03
^{11}B(n,γ)^{12}B	3.37	-34.33	1.09 [146]	1.35	1.09
^{12}C(n, γ)^{13}C	4.95	-41.35	0.77 [153]	1.85	3.23
^{12}C(n, γ)^{13}C*	1.86	-56.90	0.8 [151]	1.80	1.00
^{12}C(n, γ)^{13}C*	1.27	-28.81	0.14 [153]	0.61	1.23
^{12}C(n, γ)^{13}C*	1.09	-56.85	0.58 [153]	0.15	1.04
^{14}C(n,γ)^{15}C	1.22	-48.63	0.88 [157]	1.44	1.00
^{15}N(n,γ)^{16}N	2.49	-27.06	0.55 [162]	1.14	1.38
^{15}N(n,γ)^{16}N*	2.37	-12.45	0.46 [162]	1.62	1.11
^{15}N(n,γ)^{16}N*	2.19	-49.51	0.54 [162]	0.39	2.77
^{15}N(n,γ)^{16}N*	2.09	-11.90	0.52 [162]	1.50	0.94
^{16}O(n,γ)^{17}O	4.14	-51.77	1.0	0.90	1.17
^{16}O(n,γ)^{17}O*	3.27	51.60	1.0	3.01	0.99
^{18}O(n,γ)^{19}O	3.96	-47.79	0.69 [167]	0.90	1.17
^{18}O(n,γ)^{19}O*	3.86	-55.94	0.013 [167]	0.81	1.14
^{18}O(n,γ)^{19}O*	2.49	-46.33	0.83 [167]	2.48	1.00

Table 2.3: Binding energy (E_b, in MeV), central potential depth of bound state (V_b, in MeV), spectroscopic factor (SF), single-particle asymptotic normalization coefficients (b, in fm$^{-1/2}$) and the factor multiplying the S-factor assuming that the integration in Eq. 2.6 starts at $r = R_0$ (nuclear radius).

particle potential. The parameters for the continuum potential, V_c, are the same as those for the bound state potential, except for the few cases explicitly discussed in the text.

2.4.1 ^{2}H(n, γ)^{3}H

The ^{2}H(p,γ)^{3}He reaction at low energies, followed by d(^{3}He,p)^{4}He, leads to the formation of ^{4}He during the primordial nucleosynthesis era [118, 119, 120]. It also plays a key role during the proto-stars era, in which the energy generated by deuterium burning slowed down the contraction due to the gravitational force [121, 122]. On the other hand, the ^{2}H(n,γ)^{3}H reaction is thought to contribute to inhomogeneous big-bang models [123, 125, 124]. These models assume the existence of neutron-rich and neutron-poor regions resulting from a first-order phase transition from quarks to hadrons as the universe cooled down [123]. In the neutron-rich region, reactions such as ^{2}H(n,γ)^{3}H(d,n)^{4}He(^{3}H,γ)^{7}Li(n,γ)^{8}Li(α,n)^{11}B(n,γ)^{12}B, produce an appreciable amount of intermediate-heavy nuclei.

We consider only the E1 capture to the ground state of ^{3}H ($p \rightarrow s$). The $J_b = 1/2^+$ ground state ^{3}He is described as a $j_b = s_{1/2}$ neutron coupled to the ^{3}H core, which has an intrinsic spin $I_x = 1^+$.

The calculation for this reaction requires a three-body treatment which is beyond the scope of this work. Obviously, the potential model adopted here is
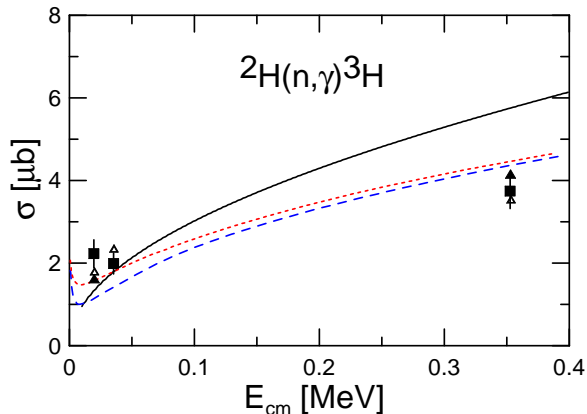
Figure 2.15: Single-particle model calculation for ^{2}H(n,γ)^{3}H (solid line). The experimental data are from Ref. [126]. The phenomenological results (parameter fit) from from Ref. [126] are shown by dashed and dotted lines. Also shown are microscopic calculations with (open trianges) and without (solid triangles) a three-body interaction.

oversimplified for this case. We choose an spectroscopic factor equal to $SF = 1.0$. Our results are shown in Fig. 2.15, where the dashed and dash-dotted curves are the evaluated reaction rates presented in Ref. [126] based on a phenomenological parametrization of the cross section based on evaluated nuclear data tables. The experimental data are from Ref. [126]. In Ref. [126] the neutron-deuteron capture was obtained using time reversal from the two-body photodisintegration amplitude and wavefunctions obtained with the AV18 potential [127] alone or combined with the Urbana IX three-nucleon force [128]. Their results are shown by the open (solid) triangles with (without) the three-body nn interaction. The ANC calculated with our potential model is $\sqrt{(SF)b^2} = 1.90$ fm$^{-1/2}$.

2.4.2 ^{7}Li(n, γ)^{8}Li

The ^{7}Li(n,γ)^{8}Li cross section is often used to extrapolate the capture cross section for the reaction ^{7}Be(p,γ)^{8}B down to the solar energies at $E_{cm} \sim 20$ keV, which is relevant for the production of high energy neutrinos in the Sun [129]. The ^{7}Li(n,γ)^{8}Li reaction is also relevant for the rapid process during primordial nucleosynthesis of nuclei with $A > 12$ in the inhomogeneous big-bang models [124, 130]. In these models, the main reaction chain leading to the synthesis of heavy elements is [124] ^{1}H(n,γ)^{2}H(n,γ)^{3}H(d,n)^{4}He(t, γ)^{7}Li(n, γ)^{8}Li, and then ^{8}Li(α,n)^{11}B (n,γ)^{12}B(β^-)^{12}C(n,γ)^{13}C, etc., for heavier nuclei. The reaction ^{7}Li(n,γ)^{8}Li is thus a crucial input to bridge the gap of mass $A = 8$, leading to the production of heavy elements.

We consider the capture to the ground state and to the first excited state of ^{8}Li. A similar calculation has been done in Ref. [131], where the partial cross sections from neutron capture to the ground and first excited states in ^{8}Li at stellar energies were reported. The gamma-ray transitions are dominated by the $E1$ multipolarity and by incoming s waves and d waves. The $J_b = 2^+$ ground state ($J_b = 1^+$ first excited state) of ^{8}Li is described as a $j_b = p_{3/2}$ neutron interacting
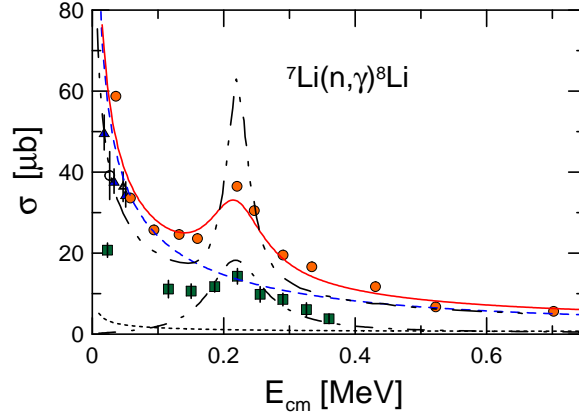
Figure 2.16: Single-particle model calculation for the reaction $^7\text{Li}(n,\gamma)^8\text{Li}$. The dashed and dotted lines are for the capture to the ground state and first excited state, respectively. The dotted-dashed line is the calculated M1 resonance. The total cross section is shown as a solid line. The calculation result from Ref. [131] is shown as a dotted-dotted-dashed line. The experimental data are from refs. [131, 132, 133, 134, 135].

with the ^7Li core, which has an intrinsic spin $I_x = 3/2^-$.

In this particular case, the values $R_0 = R_C = R_{S0} = 2.391$ fm are used. For the continuum state, the potential depth has been adjusted to reproduce the experimental scattering lengths $a_+ = -3.63 \pm 0.05$ fm and $a_- = +0.87 \pm 0.05$ fm for the two components of the channel spin s at thermal energies. The resulting potential depth parameters are $V_c = -56.15$ MeV and $V_c = -46.50$ MeV, for the $s = 2$ and $s = 1$ spin components, respectively. Following Ref. [131], we use the spectroscopic factors $SF(g.s.) = 0.87$ and $SF(1st) = 0.48$, for the ground and first excited states, respectively. The capture to the first excited state contributes to less than 5% of the total cross section. The M1 resonance at $E_R = 0.26$ MeV for capture to the ground state is reproduced with $V_c = -34.93$ MeV and a spectroscopic factor $SF = 1.0$.

The results of this calculation are shown in Fig. 2.16. The dashed and dotted lines are for the capture to the ground state and first excited state, respectively. Adding them together with the dashed-dotted line for the M1 resonance, one gets the total S-factor shown by the solid line. The experimental data are from refs. [132] (filled circles), [131] (filled triangles), [133] (filled squares), [134] (open circles) and [135] (open triangles). Our calculated ANC is $\sqrt{(SF)b^2} = 0.71$ fm$^{-1/2}$ for the ground state and 0.33 fm$^{-1/2}$ for the 1st excited state of ^8Li.

2.4.3 $^8\text{Li}(n,\gamma)^9\text{Li}$

Rapid capture processes (r-processes) might occur in the post-collapse of a type II supernova, leading to the formation of heavy elements. Starting with a He-rich environment the mass-8 gap is bridged by either $\alpha + \alpha + \alpha \rightarrow {}^{12}\text{C}$ or $\alpha + \alpha + n \rightarrow {}^9\text{Be}$ reactions. During this process, a neutron-rich freeze out occurs which triggers the r-process [137]. At this stage, it would also be possible to bridge the $A = 8$ gap through the reaction chain $^4\text{He}(2n,\gamma)^6\text{He}(2n,\gamma)^8\text{He}(\beta^-)^8\text{Li}(n,\gamma)$
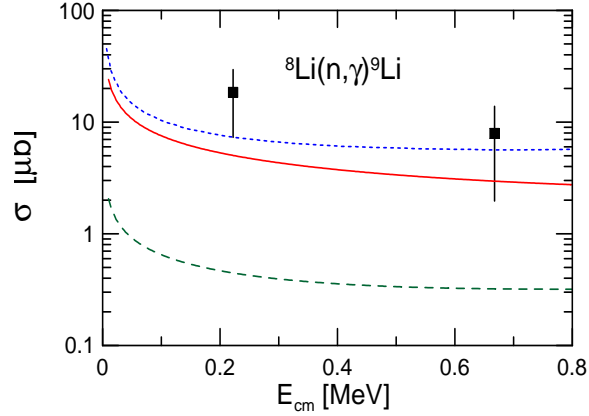
Figure 2.17: Single-particle model calculation for $^8\text{Li}(n,\gamma)^9\text{Li}$. The solid and the dashed lines are the calculations for the capture to the ground and the 1st excited states, respectively. The experimental data are from Ref. [143] using the Coulomb dissociation of ^9Li on Pb targets at 28.5 MeV/A beam energy. The dotted line is the calculation reported in Ref. [144] for the capture to the ground state.

$^9\text{Li}(\beta^-)^9\text{Be}$ [138, 139]. This chain provides an alternative path to proceed along the neutron-rich side of the line of stability towards heavier isotopes. One needs to know to what extent this chain competes with the $^8\text{Li}(\beta^-)^8\text{Be}(2\alpha)$ process. An important clue to the answer depends on an accurate knowledge of the $^8\text{Li}(n,\gamma)^9\text{Li}$ reaction rate.

We consider the E1 s- and d-wave captures to both the ground and the 1st excited state of ^9Li. The $J_b = 3/2^-$ ground state and $J_b = 1/2^-$ 1st excited state in ^9Li are described as a $j_b = p_{3/2}$ neutron coupled to the ^9Li core, which has an intrinsic spin $I_x = 2^+$. Here we use $a = 0.52$ fm, $R = 2.499$ fm and $V_{so} = -9.9$ MeV, which are adopted from Ref. [140]. The spectroscopic factors used in Ref. [141] are 1.65 and 0.55 for the ground and 1st excited state, respectively. However, for the ground state, most of experiments and calculations give $SF \approx 0.8$ (see the summary in Ref. [142]). Thus we use $SF = 0.8$ instead of 1.65 for the ground state. The result is shown in Fig. 2.17. The experimental data are from Ref. [143] using the Coulomb dissociation of ^9Li on Pb targets at 28.5 MeV/A beam energy. From the result one can see the capture to the excited state is much weaker than that to the ground state. Our ANC ($\sqrt{(SF)b^2}$) is 1.12 fm$^{-1/2}$ for the ground state of ^9Li and 0.40 fm$^{-1/2}$ for the 1st excited state of ^9Li.

2.4.4 $^{11}\text{B}(n,\gamma)^{12}\text{B}$

Nucleosynthesis in inhomogeneous big bang models are considerably dependent on neutron capture reactions on light nuclei. Such reactions are also of crucial relevance for the s-process nucleosynthesis in red giant stars. To determine the reaction rates for such different temperature conditions, the neutron capture cross sections need to be known for a wide energy range.

Primordial nucleosynthesis might be affected by spatial variations of both baryon-to-photon and neutron-to-proton ratios, the later being caused by the short diffu-
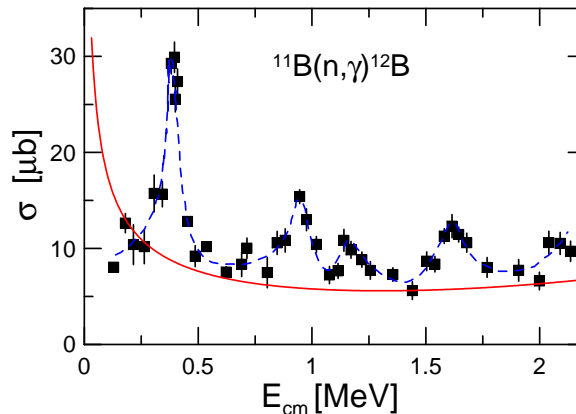
Figure 2.18: Single-particle model calculation for the (non-resonant) capture reaction ^{11}B(n,γ)^{12}B (solid line). The experimental data are from Ref. [147]. The dashed line is a sum of fitted Breit-Wigners superimposed to the non-resonant capture calculation, following Ref. [147].

sion time for neutrons in the primordial plasma. A possible signatures of baryon-number-inhomogeneous big bang is the presence of a high primordial lithium abundance, or a high abundance of beryllium and boron isotopes. As previously mentioned, inhomogeneous big bang models involve chain reactions such as [124] ^{1}H(n,γ)^{2}H(n,γ)^{3}H(d,n)^{4}He(t, γ)^{7}Li(n, γ)^{8}Li, and ^{8}Li(α,n)^{11}B (n,γ)^{12}B(β^{-})^{12}C(n,γ)^{13}C, etc., paving the way to heavier nuclei. Thus, the reaction ^{11}B(n, γ)^{12}B is an important piece of inhomogeneous big bang scenarios [145].

The E1 s- and d-wave captures to the ground state of ^{12}B are calculated. The $J_b = 1^+$ ground state of ^{12}B is described as a $j_b = p_{3/2}$ neutron coupled to the ^{11}B core, which has an intrinsic spin $I_x = 3/2^-$. Ref. [146] extracts the ground state neutron spectroscopic factors for several light by analyzing the previously reported measurements of the angular distributions in (d,p) and (p,d) reactions. We adopt the spectroscopic factor $SF = 1.09$ as in Ref. [146]. Our result for the non-resonant capture (solid line) is shown in Fig. 2.18. The experimental data are from Ref. [147].

Similar to Ref. [147], we describe the total capture cross section by a sum of non-interfering Breit Wigner resonances superimposed on a slowly varying background (non-resonant capture, solid line in the figure) and the radiation widths of the levels are found to be 0.3 eV at 0.36 MeV, 0.3 eV at 0.87 MeV, 0.2 eV at 1.08 MeV, and 0.9 eV at 1.50 MeV, with estimated uncertainties of about 50%.

Without comparison to any experimental data, Ref. [148] describes a calculation using a potential model, where captures to the second and third excited states are considered. Their result is twice as large as the experimental data of Ref. [147].

In Ref. [149] the transfer reactions ^{11}B(d,p)^{12}B and ^{12}C(d,p)^{13}C, at incident energy of 11.8 MeV, have been used to extract the ANC for ^{12}B $\rightarrow$ n + ^{11}B. The ANC found in Ref. [149] is 1.08 fm$^{-1/2}$ ($C^2 = 1.16 \pm 0.10$ fm^{-1}). Our calculated ANC is $\sqrt{(SF)b^2} = 1.41$ fm$^{-1/2}$.
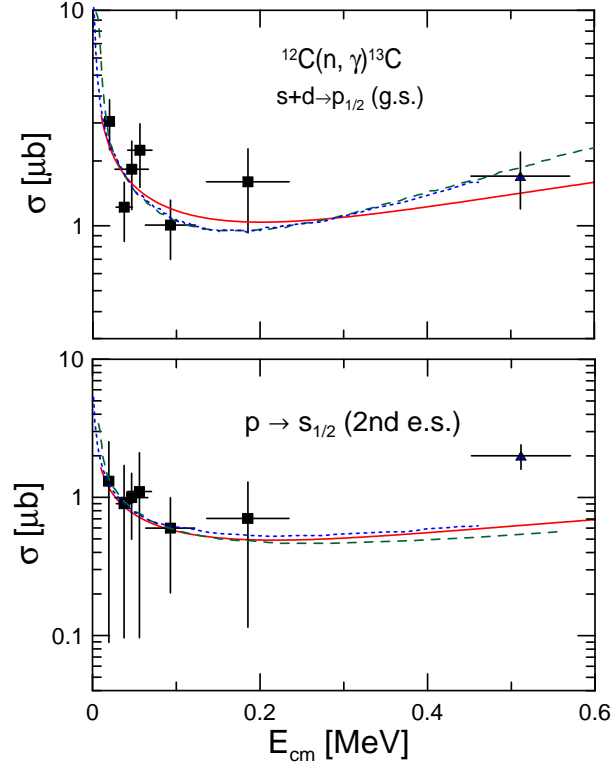
Figure 2.19: Single-particle model calculation for ^{12}C$(n, \gamma)^{13}$C (solid line).The upper panel is for the capture to the ground state whereas the lower one is for capture to the 2nd excited state. The experimental data are from Ref. [150] (filled square) and Ref. [151] (filled triangle). The theoretical results from Ref. [151] and Ref. [152] are shown by the dashed and the dotted lines, respectively.

2.4.5 ^{12}C$(\mathbf{n}, \gamma)^{13}$C

As mentioned above, not only the ^{11}B$(n, \gamma)^{12}$B, but also the ^{12}C$(n, \gamma)^{13}$C radiative capture is an important reaction in stellar nucleosynthesis [124].

We calculated the direct capture to the ground state and the first 3 excited states of ^{13}C and compared with the experimental results of Refs. [150, 151]. The $J_b = 1/2^-$ ground state of ^{13}C ($J_b = 1/2^+$ for the 1st excited state, $J_b = 3/2^-$ for the 2nd excited state and $J_b = 5/2^+$ for the 3rd excited state) is described as a $j_b = p_{1/2}$ proton ($j_b = s_{1/2}$ proton for the 1st excited state, $j_b = p_{3/2}$ proton for the 2nd excited state, $j_b = d_{5/2}$ proton for the 3rd excited state, respectively) coupled to the ^{12}C core, which has an intrinsic spin $I_x = 0^+$. In this particular case, we use $r_0 = 1.236$ fm, $a = 0.62$ fm and $V_{so} = -7$ MeV. These are the same set of parameters adopted in Ref. [152]. The spectroscopic factors published in Ref. [153] are $SF = 0.77$ for the ground state, $SF = 0.65$ for the 1st excited state, $SF = 0.14$ for the 2nd excited state, and $SF = 0.58$ for the 3rd excited state. We adopt these values, except for the 1st excited state. For this state, we use $SF = 0.8$ because it yields a better description of the experimental data in our model. It is also the same value adopted in Ref. [151].

It is also necessary to vary the potential depth for the continuum states for
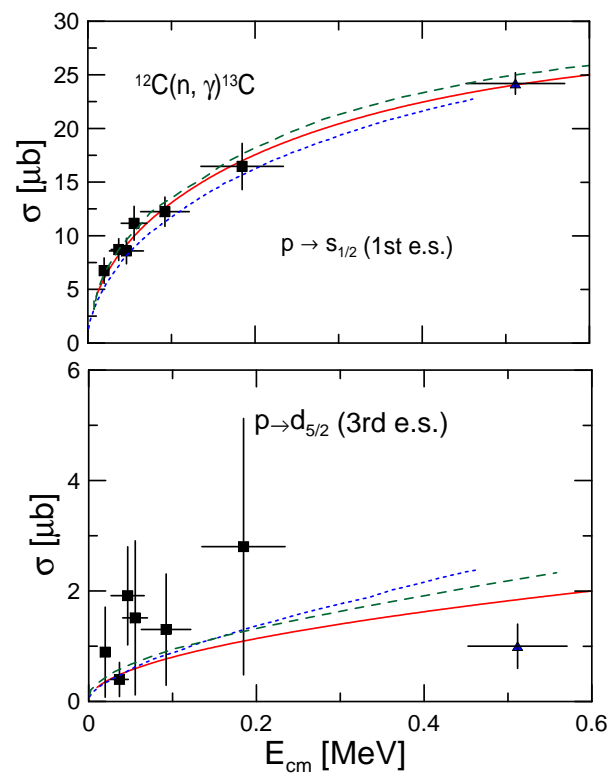
Figure 2.20: The same as Fig. 2.19, but for the transitions to the 1st excited state (upper panel) and to the 3rd excited state (lower panel).

Figure 2.21: Single-particle model calculation for the reaction ^{14}C(n,γ)^{15}C (solid line). The experimental data are from Ref. [158]. The dashed line is the result from Ref. [159] using a similar potential model.

transitions to the different bound states in ^{13}C. For the capture to the 1st and 3rd excited states, we use $V_c = V_b$, where V_b are used to describe the neutron separation energies of the two excited states in ^{13}C (see Table III). For the capture to the ground state we use $V_c = -14.75$ MeV, whereas for the capture to the 2nd excited state, $V_c = -11.50$ MeV is adopted. Our results are shown in Fig. 2.19. This reaction has also been studied in Refs. [152, 151, 154, 148] where a variety of potential models have been used and different spectroscopic factors were adopted.

Our calculated ANC is $\sqrt{(SF)b^2} = 1.62$ fm$^{-1/2}$ for the ground state and 1.61 fm$^{-1/2}$, 0.23 fm$^{-1/2}$, and 0.11 fm$^{-1/2}$ for the 1st, 2nd and 3rd excited states, respectively. In Ref. [149] the transfer reactions ^{11}B(d,p)^{12}B and ^{12}C(d,p)^{13}C, at incident energy of 11.8 MeV, have been used to extract the ANC for ^{13}C $\rightarrow$ n + ^{12}C. The ANC found in Ref. [148] for the 1st excited is 1.84 ± 0.16 fm$^{-1/2}$, in close agreement with our 1.61 fm$^{-1/2}$ value.

2.4.6 ^{14}C(n, γ)^{15}C

As we have discussed previously, inhomogeneous big bang models allow for the synthesis of heavy elements via a chain of neutron capture reactions. This includes the ^{14}C(n,γ)^{15}C reaction. Nucleosynthesis depends on reactions that destroy ^{14}C, the most important of which is ^{14}C(n,γ)^{15}C. This reaction is also a part of the neutron induced CNO cycles in the helium burning layer of AGB stars, in the helium burning core of massive stars, and in subsequent carbon burning [155]. Such cycles may cause a depletion in the CNO abundances. The ^{14}C(n,γ)^{15}C reaction is the slowest of both of these cycles and, therefore the knowledge of its rate is important to predict the ^{14}C abundances.

Due to the weak binding of the ^{15}C ground state, and because there are no low lying resonances, the cross section is mainly determined by an $E1$ non-resonant transition from an initial p-wave scattering state to the ground state [156]. The $J_b = 1/2^+$ ground state of ^{15}C is described as a $j_b = s_{1/2}$ neutron coupled to the ^{14}C core, which has an intrinsic spin $I_x = 0^+$.
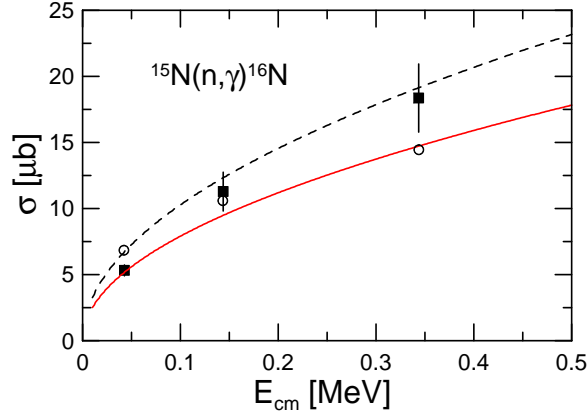
Figure 2.22: Single-particle model calculation results for ^{15}N$(n, \gamma)^{16}$N (solid line). The experimental data are from Ref. [161]. The non-resonant capture calculations of Ref. [161] is shown by open circles. Increasing the values of the spectroscopic values by 30% (compatible with the experimental errors) yields the dashed line.

In Ref. [157] a 14 MeV deuteron beam was used to measure the angular distributions for the ^{14}C(d, p)^{15}C reaction leading to the two bound states and eight of the unbound states of ^{15}C. An spectroscopic factor $SF = 0.88$ for the ground state of ^{14}C has been inferred. Adopting this value, we obtain the DC cross section shown in Fig. 2.21. The experimental data are from Ref. [158].

In Ref. [160] a theoretical analysis of existing experimental data on the Coulomb dissociation of ^{15}C on 208Pb at 68 MeV/nucleon was used to infer the asymptotic normalization coefficient for ^{15}C $\rightarrow$ n + ^{14}C. The ANC value reported in Ref. [160] is 1.13 fm$^{-1/2}$ ($C^2 = 1.28 \pm 0.01$ fm^{-1}). Our ANC value is $\sqrt{(SF)b^2} = 1.35$ fm$^{-1/2}$.

2.4.7 ^{15}N$(\mathbf{n}, \gamma)^{16}$N

The cross section for the reaction ^{15}N$(n,\gamma)^{16}$N is an important input in the reaction network for the production of heavier isotopes in both inhomogeneous big bang and in red giant environments [124].

The direct capture for this reaction is dominated by the $p \rightarrow d$ wave transition to the ground state, $p \rightarrow s$ wave transition to the first excited state of ^{16}N at 0.120 MeV, $p \rightarrow d$ wave transitions to the second excited state at 0.296 MeV and $p \rightarrow s$ wave transitions to the third excited state at 0.397 MeV. These conclusions were made in Ref. [161], where reaction cross sections of ^{15}N$(n, \gamma)^{16}$O was reported and direct capture and shell model calculations were performed to interpret their data. The gamma-ray transitions are all dominated by the $E1$ multipolarity. The $J_b = 2^-$ ground state ($J_b = 0^-$ 1st excited state, $J_b = 3^-$ 2nd excited state, $J_b = 1^-$ 3rd excited state) ^{16}N is described as a $j_b = d_{5/2}$ neutron ($j_b = s_{1/2}$ neutron, $j_b = d_{5/2}$ neutron, $j_b = s_{1/2}$ neutron) coupled to the ^{15}N core, which has an intrinsic spin $I_x = 1/2^-$.

In Ref. [162] (d,n) and (d,p) reactions on ^{15}N were measured and Hauser-Feshbach calculations were used to extract spectroscopic factors with 30% uncer-
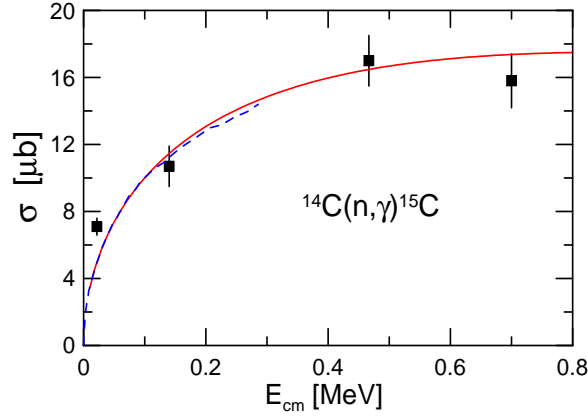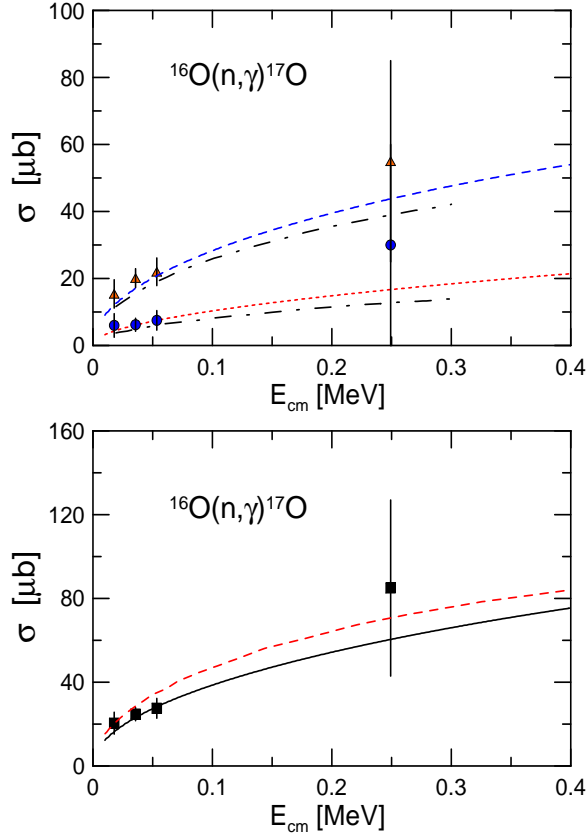
Figure 2.23: Single-particle model calculation for reaction ^{16}O(n, γ)^{17}O (solid lines). The experimental data are from Ref. [164]. Top panel: the capture to the ground state (dotted line, filled circles) and first excited state (dashed line, filled triangles) of ^{17}O are shown separately. The results of a microscopic multicluster model from Ref. [165] are shown by dotted-dashed lines for comparison. Bottom panel: the total cross section of ^{18}O(n, γ)^{19}O (solid line). The result from Ref. [166] is shown as a dashed line.

tainty. Their values are $SF = 0.55$ for the ground state, $SF = 0.46$ for the 2^- state, $SF = 0.54$ for the 3^- state and $SF = 0.52$ for the 1^- state. Our result is shown in Fig. 2.22. The experimental data are from Ref. [161]. Our calculations yield similar results as those of Ref. [161] and Ref. [163], and reproduce the experimental data rather well, considering the $\pm30\%$ error in the spectroscopic factor (see dashed line in Fig. 2.22).

Our calculated ANCs are 0.85 fm$^{-1/2}$ for the ground state of ^{9}Li, 1.10 fm$^{-1/2}$ for the first excited state, 0.29 fm$^{-1/2}$ for the second excited state and 1.08 fm$^{-1/2}$ for the third excited state, respectively.

2.4.8 ^{16}O(n, γ)^{17}O

This reaction is important for s-processes for various metallicity stars and for inhomogeneous big bang models, which, for masses beyond $A > 12$ can proceed via ^{12}C(n,γ)^{13}C(n,γ)^{14}C(n,γ)^{15}N(n,γ)^{16}N(β^-)^{16}O(n,γ)...

The non-resonant, direct capture, to the ground state and to the 1st excited
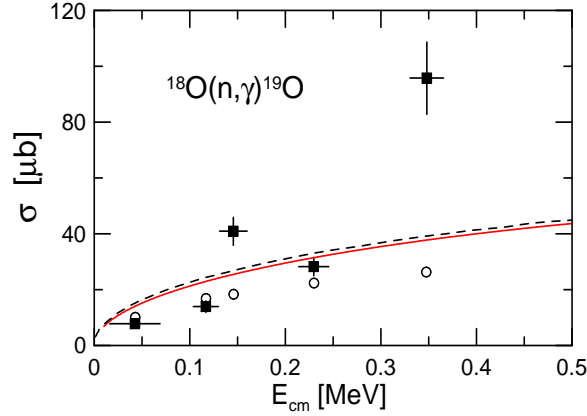
Figure 2.24: Single-particle model calculation for the reaction of ^{18}O(n, γ)^{19}O (solid line). The experimental data are from Ref. [167]. The non-resonant capture calculation from Ref. [167] and [163] are shown as open circles and dashed line, respectively.

state of ^{17}O dominates the cross section in the energy range of $0.02 - 0.28$ MeV [164]. The gamma-ray transitions are dominated by the $E1$ multipolarity and by incoming p-waves. The $J_b = 5/2^+$ ground state ($J_b = 1/2^+$ 1st excited state) of ^{17}O is described as a $j_b = d_{5/2}$ neutron ($j_b = s_{1/2}$ neutron) coupled to the ^{16}O core, which has an intrinsic spin $I_x = 0^+$. We use a spectroscopic factor $SF = 1.0$ for both ground and excited states.

The results of our calculations for these two captures are shown in the top panel of Fig. 2.23 separately. The experimental data are from Ref. [164]. Our potential model calculations yield similar results as the calculations Ref. [165], where a microscopic multicluster model was used. The total cross section is shown in the bottom panel of Fig. 2.23 together with a theoretical result from Ref. [166] where direct and semi-direct components of the neutron capture cross sections were calculated.

Our calculated ANC ($\sqrt{(SF)b^2}$) is 0.90 fm$^{-1/2}$ for the ground state of ^{17}O and 3.01 fm$^{-1/2}$ for the 1st excited state of ^{17}O.

2.4.9 ^{18}O(n, γ)^{19}O

Further nucleosynthesis during inhomogeneous big bang models towards higher masses is controlled by the reaction rate of ^{18}O(n, γ)^{19}O. If this reaction is stronger than the ^{18}O(p,α)^{15}N reaction then material be processed out of the CNO cycle to the region above $A > 20$. This reaction is also of interest for stellar helium burning in AGB stars by means of s-processes.

The direct capture for this reaction is dominated by $p \to d$-wave transitions to the ground state, the first excited state at 0.096 MeV, and the $p \to s$ transition to the second excited state at 1.47 MeV [167]. The gamma-ray transitions are all dominated by the $E1$ multipolarity. The $J_b = 5/2^+$ ground state ($J_b = 3/2^+$ 1st excited state, $J_b = 1/2^+$ 2nd excited state) of ^{17}O is described as a $j_b = d_{5/2}$ neutron ($j_b = d_{3/2}$ neutron, $j_b = s_{1/2}$ neutron) coupled to the ^{18}O core, which has

	V_c (MeV)	44.72	49.69	54.66
^{16}O(p, γ)^{17}F	σ (μb)	4.63×10^{-3}	4.83×10^{-3}	5.05×10^{-3}
	$\Delta\sigma/\sigma$	-4.14%		$+4.55\%$
	V_c (MeV)	46.59	51.77	56.94
^{16}O(n, γ)^{17}O	σ (μb)	14.35	21.41	38.42
	$\Delta\sigma/\sigma$	-32.98%		$+79.45\%$

Table 2.4: Cross sections at 0.4 MeV for the capture to the ground state of the reaction ^{16}O(p, γ)^{17}F with that of ^{16}O(n, γ)^{17}O.

an intrinsic spin $I_x = 0^+$.

We have adopted spectroscopic factors from Ref. [167]. They are $SF = 0.69$ for the ground state, $SF = 0.013$ for the 3/2+ state, and $SF = 0.83$ for the 1/2$^+$ state. Our results are shown in Fig. 2.24. They are close to the calculations reported in Refs. [167, 163]. The experimental data are from Ref. [167]. The data points at 0.138 MeV and 0.331 MeV are much higher than our non-resonant calculation because of the resonances at 0.152 MeV and 0.371 MeV, corresponding to the $3/2^+$ state at 4.109 MeV and to the state at 4.328 ± 003 MeV in ^{19}O, respectively. This has been discussed in details in Ref. [167].

Our calculated ANC ($\sqrt{(SF)b^2}$) is 0.75 fm$^{-1/2}$ for the ground state of ^{19}O, 0.09 fm$^{-1/2}$ for the first excited state and 2.26 fm$^{-1/2}$ for the second excited state.

2.5 Sensitivity on the potential depth parameter

As with any other model, the results obtained with the single-particle model for the cross sections can be very sensitive to the choice of parameters. In order to check this sensitivity, in Table 2.4 we compare the cross sections at 0.4 MeV for the capture to the ground state of the reaction ^{16}O(p, γ)^{17}F with that of ^{16}O(n, γ)^{17}O. The potential depth for continuum state V_c has been varied by $\pm 10\%$ to test the sensitivity of the cross sections on V_c.

The V_c in the third (last) column is 10% smaller (larger) than that of the fourth column, which is used in the calculation for the S-factors or cross sections in sections III and IV. From table 2.4, one can conclude that proton capture is less sensitive to the internal part of the potential, as expected. This is due to the Coulomb barrier. In other words, proton capture reactions tend to be more peripheral than neutron capture reactions. In the proton capture case, the ANC technique is thus expected to work better than in the neutron capture one. But these conclusions obviously change in the presence of potential resonances, when the cross sections can suddenly change by orders of magnitude if the potential depth is slightly varied.

In order to show the large sensitivity of the S-factor, or cross section, on potential parameters close to a resonance, we use the test-case of the ^{15}N(p,γ) reaction. This is shown in figure 2.25 where we plot the ratio between the S-factor at $E = 0$ calculated with a potential depth V_c and the S-factor calculated with a zero potential depth: $S(0, V_c)/S(0, 0)$. The open circle corresponds to the value of V_c used in the calculation presented in figure 2.12.
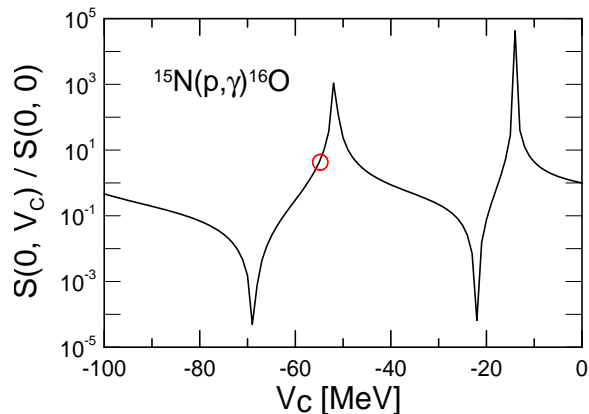
Figure 2.25: Ratio between the S-factor at $E = 0$ calculated with a potential depth V_c and the S-factor calculated with a zero potential depth: $S(0, V_c)/S(0, 0)$. The open circle corresponds to the value of V_c used in the calculation presented in figure 2.12.

As is clearly seen in figure 2.12, a small change (i.e. by 10%) in the value of V_c can cause orders of magnitude change in the corresponding S-factor near a resonance. Thus, although one can indeed reproduce resonant states with the potential model, one has to be very careful with the values of observables obtained with the model, such as the ANCs, or spectroscopic factors. These will also be over-sensitive to the potential fitting parameters.

2.6 ANCs from single-particle models

In figure 2.26 we show the ratio of our calculations of ANCs ($\sqrt{(SF)b^2}$) with the ANCs extracted from the literature and mentioned in this thesis. Not all ANCs are shown because either they have not been indirectly extracted from experiments, or calculated previously. The solid circles are for proton capture whereas the solid triangles are for neutron capture. The dashed line is a guide to the eye and shows the ratio equal to unity. We notice that our ANCs differ up to a factor of 1.6 from previously reported values.

In our calculations, the ANCs are indirectly obtained by adjusting our calculated S-factors or cross sections to the available experimental data. The ANC's from literature are partially obtained by indirectly fitting calculations to experimental data in transfer reactions, or by means of elaborate microscopic models, or else. Evidently, a more consistent comparison between these values deserves a more detailed study.

2.7 Final conclusions

In this chapter, I have explored the single-particle potential model to describe radiative proton and neutron capture reactions of relevance for astrophysics. Using a well defined approach and the same numerical code, I have obtained spectro-
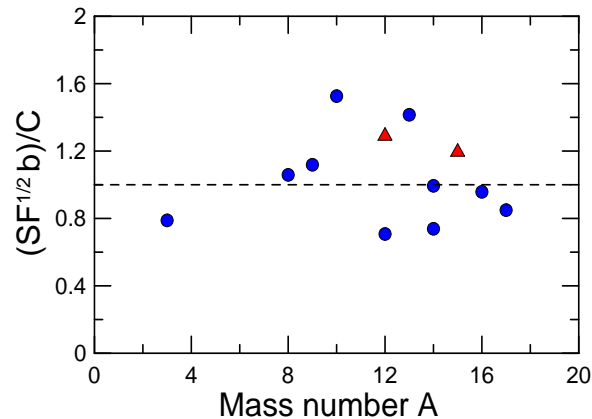
Figure 2.26: Our ANCs ($\sqrt{(SF)b^2}$) divided by the ANCs obtained from references mentioned in the text as function of the mass number A. The solid circles are for proton capture whereas the solid triangles are for neutron capture. The dashed line is equal to unity.

scopic factors and single-particle asymptotic normalization coefficients for several reactions in the mass range $A < 20$.

I have only considered cases for which potential models yields reasonable results. There are several radiative capture reactions which do not fall into this category. They require a more derailed study, with possible adjustments and/or extensions of the model. Evidently, there will be situations for which the potential model will always fail.

Our work has shown minor differences with previously published results. I have demonstrated that there is a reasonable justification for the use of potential model calculations for many reactions which have either been measured experimentally, or calculated theoretically.

A systematic study of asymptotic normalization coefficients and spectroscopic factors based on the single-particle model is very useful to validate other theoretical descriptions of radiative capture reactions. This study is also relevant to correlate spectroscopic observables to other nuclear properties.

Chapter 3

Non-inertial effects in nuclear reactions

3.1 Introduction

Incredibly large accelerations occur when atomic nuclei collide. Two lead nuclei colliding frontally with a center of mass kinetic energy of 500 MeV reach a closest distance of 19.4 fm before they bounce back and move outwardly. At this distance each nucleus accelerates with an intriguing 10^{27} m/s^2. Very few other physical situations in the Universe involve nuclei undergoing such large accelerations, usually having connection to astrophysical objects, as in the vicinity of black holes, neutron stars, where huge gravitational fields exist. In this chapter I explore the effects of large accelerations and large gravitational fields, and their possible influence on nuclear reactions in the laboratory and in astrophysical environments. Nuclear reactions are crucial for the formation of stellar structures and their rates can be affected by various factors. To our knowledge, the effect of large gravitational fields on nuclear reaction rates in stars has not been considered so far.

As mentioned in the previous paragraph, atomic and nuclear systems undergo large accelerations during reactions. The effect of accelerations is observed in terms of excitations followed by decay of these systems. If we consider two-body reactions, there are two systems of reference which are often used to describe the effects of the collision: (a) the center-of-mass (cm) system of the two nuclei and (b) the system of reference of the excited nucleus. System (b) is appropriate to use when the intrinsic properties of the excited nucleus is described in some nuclear model. A typical example is the case of Coulomb excitation. One assumes that the nuclei scatter and their cm wavefunctions are described by Coulomb waves due to the Coulomb repulsion between the nuclei. Then one considers the residual effect of the Coulomb potential on the motion of the nucleons inside the nuclei. This is done by expanding the Coulomb potential in multipoles and using the high order terms (higher than the first one) as source of the excitation process. In this approach one illustrates the privileged role of the cm of the nuclear system: the net effect of the external forces is to (i) accelerate all the particles together, along with the cm of the system, and (ii) to change the intrinsic quantum state of the

system through the spatial variation of the interaction within the system. Thus the theoretical treatment of accelerated many-body systems is well under control in non-relativistic dynamics.

In the non-relativistic case, the separation of variables into intrinsic motion and relative motion between the cm of each nucleus is a simple algebraic procedure. A problem arises when one wants to extend the method to describe intrinsic excitations of relativistic many-body systems. Very few works can be found in the literature addressing this problem. The reason is that for nuclear reactions in the laboratory, the effect is expected to be very small, a common belief which must be tested. Another other reason is that in stellar environments where the gravitational fields are large, huge pressures develop, "crushing" atoms, stripping them from their electrons, and ultimately making nuclei dissolve into their constituents. Effects of nuclear excitation are not relevant in the process. But nuclear reactions are crucial for the formation of stellar structures and their rates can be affected by minor effects.

Nuclei participating in nuclear reactions in a gaseous phase of a star follow inertial trajectories between collisions with other nuclei. Such trajectories are free fall trajectories in which all particles within the nucleus have the same acceleration. That is surely true in the non-relativistic case, but not in the relativistic one because retardation effects lead to corrections due to the nuclear sizes. The central problem here is the question regarding the definition of the center of mass of a relativistic many body system. We have explored the literature of this subject and found few cases in which this problem is discussed. Based on their analysis I show that relativistic effects introduce small corrections in the Lagrangian of a many-body system involving the magnitude of their acceleration. I follow refs. [168, 169, 170], with few modifications, to show that a correction term proportional to the square of the acceleration appears in the frame of reference of the accelerated system. To test the relevance of these corrections, I make a series of applications to nuclear and atomic systems under large accelerations.

3.2   Hamiltonian of an accelerated many-body system

Starting with a Lagrangian of a free particle in an inertial frame and introducing a coordinate transformation into an accelerated frame with acceleration $\mathcal{A}$, a "fictitious force" term appears in the Lagrangian when written in coordinates fixed to the accelerated frame. Thus, in an accelerated system the Lagrangian L for a free particle can be augmented by a (non-relativistic) interaction term of the form $-m\mathcal{A}z$, that is

$$L = -mc^2 + \frac{1}{2}mv^2 - m\mathcal{A}z, \tag{3.1}$$

where z is the particle's coordinate along the direction of acceleration of the reference frame [168].

In the relativistic case, the first step to obtain the Lagrangian of a many body system in an accelerated frame is to setup an appropriate measure of space-time in the accelerated frame, i.e. one needs to find out the proper space-time metric.

The free-particle action $S = -mc \int ds$ requires that $ds = (c - v^2/2c + \mathcal{A}z)dt$, which can be used to obtain ds^2. To lowest order in $1/c^2$ one gets

$$ds^2 = c^2 \left(1 + \frac{\mathcal{A}z}{c^2}\right)^2 dt^2 - dx^2 - dy^2 - dz^2 = g_{\mu\nu}d\xi^\nu d\xi^\mu, \qquad (3.2)$$

where $\mathbf{v}dt = d\mathbf{r}$ was used, with $d\xi^\mu = (cdt, dx, dy, dz)$ and $g_{\mu\nu} = (g_{00}, -1, -1, -1)$, $g_{00} = (1 + \mathcal{A}z/c^2)^2$. The indices μ run from 0 to 3. Eq. (3.2) gives a general form for the metric in an accelerated system. This approach can be found in standard textbooks (see, e.g. ref. [168], § 87).

From the definition for the Hamiltonian, $H = \mathbf{p} \cdot \mathbf{v} - L$, with $\mathbf{p} = \partial L/\partial \mathbf{v} = m\mathbf{v}/\sqrt{g_{00} - v^2/c^2}$, and using the action with the metric of Eq. (3.2), after a straightforward algebra one finds

$$H = \frac{g_{00}mc^2}{\sqrt{g_{00} - \frac{v^2}{c^2}}} = c\sqrt{g_{00}(p^2 + m^2c^2)}. \qquad (3.3)$$

Expanding H in powers of $1/c^2$, one obtains

$$H = \frac{p^2}{2m}\left(1 - \frac{p^2}{4m^2c^2}\right) + m\mathcal{A}z\left(1 + \frac{p^2}{2m^2c^2}\right) + \mathcal{O}\left(\frac{1}{c^4}\right). \qquad (3.4)$$

This Hamiltonian can be applied to describe a system of particles with respect to a system of reference moving with acceleration $\mathcal{A}$, up to order $1/c^2$. For an accelerated nucleus the obvious choice is the cm system of the nucleus. But then the term carrying the acceleration correction averages out to zero in the center of mass, as one has $(\sum_i m_i \mathcal{A}z_i = 0)$. There is an additional small contribution of the acceleration due to the term proportional to p^2. Instead of exploring the physics of this term, one has to account for one more correction before we continue.

The above derivation of the Hamiltonian for particles in accelerated frames does not take into account that the definition of the cm of a collection of particles is also modified by relativity. This is not a simple task as might seem at first look. There is in the literature no consensus about the definition of the cm of a system of relativistic particles. The obvious reason is the role of simultaneity and retardation. Ref. [169] examines several possibilities. For a system of particles it finds convenient to define the coordinates q^μ of the center of mass as the mean of coordinates of all particles weighted with their dynamical masses (energies). The relativistic (covariant) generalization of center of mass is such that the coordinates q^μ must satisfy the relation [169]

$$P^0 q^\mu = \sum_i p_i^0 z_i^\mu, \qquad (3.5)$$

where the coordinates of the ith particle with respect to the center of mass are denoted by z_i^μ and the total momentum vector by $P^\mu = \sum_i p_i^\mu$. Ref. [169] chooses eq. (3.5) as the one that is most qualified to represent the definition of cm of a relativistic system, which also reduces to the non-relativistic definition of the

center of mass. We did not find a better discussion of this in the literature and we could also not find a better way to improve on this definition.

The above definition, Eq. (3.5), leads to the compact form, to order $1/c^2$,

$$\sum_i \frac{m_i \mathbf{r}_i}{\sqrt{g_{00} - \frac{v_i^2}{c^2}}} = \sum_i m_i \mathbf{r}_i \left(1 + \frac{v_i^2}{2c^2} - \frac{z_i \mathcal{A}}{c^2} + \mathcal{O}(\frac{1}{c^4}) \right)$$
$$= 0, \tag{3.6}$$

where $\mathbf{r}_i = (x_i, y_i, z_i)$ is the coordinate and v_i is the velocity of the ith particle with respect to the cm.

For a system of non-interacting particles the condition in Eq. (3.6) implies that, along the direction of motion,

$$\sum_i \mathcal{A} m_i z_i = -\sum_i \mathcal{A} m_i z_i \left(\frac{v_i^2}{2c^2} - \frac{z_i \mathcal{A}}{c^2} \right). \tag{3.7}$$

Hence, the Hamiltonian of Eq. (3.4) for a collection of particles becomes

$$H = \sum_i \frac{p_i^2}{2m_i} \left(1 - \frac{p_i^2}{4m_i^2 c^2} \right) + \frac{\mathcal{A}^2}{c^2} \sum_i m_i z_i^2 + U(r_i) + \mathcal{O}(\frac{1}{c^4}), \tag{3.8}$$

where we have added a scalar potential $U(r_i)$, which would represent a (central) potential within an atom, a nucleus, or any other many-body system.

Notice that the term proportional to $-m\mathcal{A}z$ completely disappears from the Hamiltonian after the relativistic treatment of the cm. This was also shown in ref. [170]. It is important to realize that non-inertial effects will also carry modifications on the interaction between the particles. For example, if the particles are charged, there will be relativistic corrections (magnetic interactions) which need to be added to the scalar potential $U(r_i) = \sum_{j \neq i} Q_i Q_j / |\mathbf{r}_i - \mathbf{r}_j|$. As shown in ref. [170], the full treatment of non-inertial effects together with relativistic corrections will introduce additional terms proportional to $\mathcal{A}$ and $\mathcal{A}^2$ in the Hamiltonian of Eq. (3.8), to order $1/c^2$. Thus, a more detailed account of non-inertial corrections of a many-body system requires the inclusion of $\mathcal{A}$-corrections in the interaction terms, too. We refer the reader to ref. [170] or Appendix A where this is discussed in more details. Here we will only consider the consequences of the acceleration correction term in Eq. (3.8),

$$H_{nin} = \frac{\mathcal{A}^2}{c^2} \sum_i m_i z_i^2. \tag{3.9}$$

3.3 Reactions within stars

Nuclei interacting in a plasma or undergoing pycnonuclear reactions in a lattice can experience different accelerations, allowing an immediate application of eq. 3.9. But in order to use this equation to measure changes induced by the gravitational fields in stars, we assume that one can replace $\mathcal{A}$ by the local gravitational field,

g. This assumption deserves more discussion. If we pick two nuclei participating in a nuclear reaction within a star, they are probably in a gaseous phase following inertial trajectories in between collisions. The effect of gravity is that the two nuclei follow two slightly different inertial trajectories because of the difference in gravitational field between their two positions. Thus the best way to study the reaction problem is to calculate reaction rates in terms of a local metric at a point within the star. This metric can be deduced from General Relativity at the reaction observation point. To first-order one can also use eq. 3.2, which is shown in ref. [168] to describe particles in a gravitational field. Here instead, we will adopt the Hamiltonian of eq. 3.8 as representative of the same problem. Here we will not attempt to prove the equality between the two procedures, and several other issues (e.g. time-dependence of accelerations, modification of interactions in presence of a gravitational field, etc.), leaving this for future studies. Our goal is to make an estimation of where in the Universe one would have gravitational fields strong enough to change appreciably the reaction rates or the internal structure of many body systems.

3.3.1 Nuclear fusion reactions

Nuclear fusion reactions proceed in stars at low energies, e.g., of the order of 10 KeV in our Sun [171, 172]. Due to the Coulomb barrier, it is extremely difficult to measure the cross sections for charged-particle-induced fusion reactions at laboratory conditions. The importance of small effects such as the correction of Eq. (3.9) in treating fusion reactions is thus clear because the Coulomb barrier penetrability depends exponentially on any correction. To calculate the effect of the term given by eq. (3.9) we use, for simplicity, the WKB penetrability factor

$$P(E) = \exp\left[-\frac{2}{\hbar}\int_{R_N}^{R_C} dr\, |p(r)|\right], \tag{3.10}$$

where $p(r)$ is the (imaginary) particle momentum inside the repulsive barrier. The corrected fusion reaction is given by

$$\sigma = \sigma_C \cdot \mathcal{R}, \tag{3.11}$$

where σ_C is the Coulomb repulsion cross section and $\mathcal{R} = P_{corr}(E)/P(E)$ is the correction due to Eq. (3.9). The non-inertial effect is calculated using $|p(r)| = \sqrt{2m\left[V_C(r) - E\right]}$ and

$$|p_{corr}(r)| = \sqrt{2m\left[V_C(r) + \frac{\mathcal{A}^2 m r^2 \langle\cos^2\theta\rangle}{c^2} - E\right]} \tag{3.12}$$

where $\langle\cos^2\theta\rangle = 1/2$ averages over orientation and the Coulomb potential is given by $V_C = Z_1 Z_2 e^2/r$. In order to assess the magnitude of the acceleration $\mathcal{A}$ for which its effect is noticeable, we consider a proton fusion reaction with a $Z = 17$ nucleus (chlorine) at $E = 0.1$ MeV. This is a typical fusion reaction in stellar sites of interest. For this energy, we get $R_C = Z_1 Z_2 e^2/E = 245$ fm and take $R_N = 3.2$ fm.
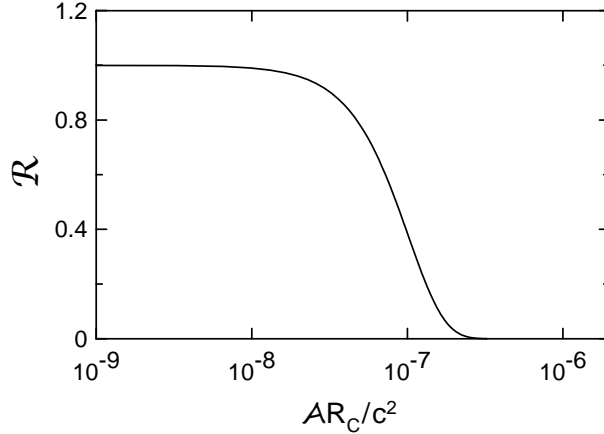
Figure 3.1: Suppression factor due to the non-inertial effects, $\mathcal{R}$, for fusion reactions of protons on chlorine at $E = 0.1$ MeV, and as a function of the gravitational field (in dimensionless units).

As we see in Fig. 3.1 the effect of acceleration becomes visible for accelerations of the order $g = \mathcal{A} = 10^{-7}c^2/R_C \approx 4 \times 10^{27}$ m/s^2, which is about 26 orders of magnitude larger than the acceleration due to gravity on earth's surface and 15 orders of magnitude larger than the one at the surface of a neutron star (assuming $M_{ns} = M_\odot$ and $R_{ns} = 10$ km). It appears that the effect is extremely small in stellar environments of astrophysical interest where nuclear fusion reactions play a role. Such large gravitational fields would only be present in the neighborhood of a black-hole. Under such extreme conditions nuclei are likely to disassembly, as any other structure will.

3.3.2 Atomic transitions

As an example in atomic physics, we consider the energy of the 2p$_{1/2}$ level in hydrogen which plays an important role in the Lamb shift and probes the depths of our understanding of electromagnetic theory. We calculate the energy shift of the 2p$_{1/2}$ level within the first-order perturbation theory and we get

$$\Delta E_{nin}^{2p_{1/2}} = \left\langle 2p_{1/2} \left| H_{nin} \right| 2p_{1/2} \right\rangle = \frac{24a_H^2 \mathcal{A}^2 m_e}{c^2}, \tag{3.13}$$

where $a_H = \hbar^2/m_e e^2 = 0.529$ Å. One should compare this value with the Lamb splitting which makes the 2p$_{1/2}$ state slightly lower than the 2s$_{1/2}$ state by $\Delta E_{Lamb} = 4.372 \times 10^{-6}$ eV. One gets $\Delta E_{nin}^{2p_{1/2}} \simeq \Delta E_{Lamb}$ for $\mathcal{A} \simeq 10^{21}$ m/s^2, which is 9 orders of magnitude larger than gravity at the surface of a neutron star. Thus, even for tiny effects in atomic systems, the effect would only be noticeable for situations in which electrons are bound in atoms.

3.4 Reactions in the laboratory

The apparent conclusion from the last section is that it is very unlikely that non-inertial effects due to gravitational fields are of relevance in stars. Nowhere,

except in the vicinity of a black-hole, accelerations are of order of 10^{20} m/s^2, which would make the effect noticeable. However, there is another way to achieve such large accelerations and that is nothing else than the huge accelerations which occur *during* nuclear reactions. For example, for a nuclear fusion reaction, at the Coulomb radius (distance of closest approach, R_C) the acceleration is given by

$$\mathcal{A}_C = \frac{Z_1 Z_2 e^2}{R_C^2 m_0}, \tag{3.14}$$

where $m_0 = m_N A_1 A_2 / (A_1 + A_2)$ is the reduced mass of the system and m_N is the nucleon mass. For typical values, $E = 1$ MeV, $Z_1 = Z_2 = 10$, and $A_1 = A_2 = 20$, one obtains $R_C = Z_1 Z_2 e^2 / E = 144$ fm and $\mathcal{A}_C = 6.2 \times 10^{25}$ m/s^2. This is the acceleration that the cm of each nucleus would have with respect to the laboratory system.

As we discussed in the introduction, the cm of the excited nucleus is the natural choice for the reference frame. This is because it is easier to adopt a description of atomic and nuclear properties in the cm frame of reference. Instead, one could also chose the cm of the colliding particles. This later (inertial) system makes it harder to access the acceleration effects, as one would have to boost the wave-functions to an accelerated system, after calculating it in the inertial frame. This is a more difficult task. We thus adopt the cm of the excited nucleus, using the Hamiltonian of section II. This Hamiltonian was deduced for a constant acceleration. If the acceleration is time-dependent, the metric of eq. 3.2 also changes. Thus, in the best case scenario, the Hamiltonian of eq. 3.8 can be justified in an adiabatic situation in which the relative velocity between the many-body systems are much smaller than the velocity of their constituent particles with respect to their individual center of masses. If we accept this procedure, we can study the effects of accelerated frames on the energy shift of states close to threshold, as well as on the energy location of low-lying resonances.

3.4.1 Reactions involving halo nuclei

The nuclear wave-function of a (s-wave) loosely-bound, or "halo", state can be conveniently parameterized by

$$\Psi \simeq \sqrt{\frac{\alpha}{2\pi}} \frac{\exp(-\alpha r)}{r}, \tag{3.15}$$

where the variable α is related to the nucleon separation energy through $S = \hbar^2 \alpha^2 / 2m_N$. In first order perturbation theory the energy shift of a halo state will be given by

$$\Delta E_{nin}^N = \langle \Psi | H_{nin} | \Psi \rangle = \frac{1}{8S} \left(\frac{Z_1 Z_2 e^2 \hbar}{R_C^2 m_0 c} \right)^2. \tag{3.16}$$

Assuming a small separation energy $S = 100$ keV, and using the same numbers in the paragraph after eq. 3.14, we get $\Delta E_{nin}^N = 0.024$ eV, which is very small, except for states very close to the nuclear threshold, i.e. for $S \to 0$. But the effect increases with Z^2 for symmetric systems (i.e. $Z_1 = Z_2 = A_1/2$). It is thus of the order of $\Delta E_{nin}^N = 1 - 10$ eV for larger nuclear systems.

There might exist situations where this effect could be manifest. For instance, the triple-alpha reaction which bridges the mass $= 8$ gap and forms carbon nuclei in stars relies on the lifetime of only 10^{-17} s of ^{8}Be nuclei. It is during this time that another alpha-particle meets ^{8}Be nuclei in stars leading to the formation of carbon nuclei. This lifetime corresponds to an energy width of only 5.57 ± 0.25 eV [173]. As the third alpha particle approaches ^{8}Be the effects of linear acceleration will be felt in the reference frame of ^{8}Be. This will likely broaden the width of the ^{8}Be resonance (which peaks at $E_R = 91.84 \pm 0.04$ KeV) and consequently its lifetime. However, this line of thought could be wrong if one assumes that the third alpha particle interacts individually with each of the two alpha particles inside ^{8}Be, and that the effects of acceleration internal to the ^{8}Be nucleus arise from the different distances (and thus accelerations) between the third alpha and each of the first two. To our knowledge, this effect has not been discussed elsewhere and perhaps deserves further investigation, if not for this particular reaction maybe for other reactions of astrophysical interest involving very shallow nuclear states.

3.4.2 Nuclear transitions

Many reactions of astrophysical interest are deduced from experimental data on nucleus-nucleus scattering. Important information on the position and widths of resonances, spectroscopic factors, and numerous other quantities needed as input for reaction network calculations in stellar modelling are obtained by means of nuclear spectroscopy using nuclear collisions in the laboratory. During the collisions the nuclei undergo huge accelerations, of the order of $\mathcal{A} \simeq 10^{28}$ m/s^2. Hence, non-inertial effects will definitely be important.

A simple proof of the statements above can be obtained by studying the Coulomb excitation. The simplest treatment that one can give to the problem is a semi-classical calculation. The probability of exciting the nucleus to a state f from an initial state i is given by

$$a_{if} = -\frac{i}{\hbar} \int V_{if}\, e^{i\omega t} dt, \qquad (3.17)$$

where $\omega = (E_f - E_i)/\hbar$, is the probability amplitude that there will be a transition i→f. The matrix element $V_{if} = \int \Psi_f^* V \Psi_i\, d\tau$ contains a potential V of interaction between the nuclei. The square of a_{if} measures the transition probability from i to f and this probability should be integrated along the trajectory.

A simple estimate can be done in the case of the excitation of a initial, $J = 0$, state of a deformed nucleus to an excited state with $J = 2$ as a result of a frontal collision with scattering angle of $\theta = 180°$. The perturbation V is due to the interaction of the charge $Z_1 e$ of the projectile (one of the two nuclei) with the quadrupole moment of the target (the other) nucleus. This quadrupole moment should work as an operator that acts between the initial and final states. One finds that $V = Z_1 e^2 Q_{if}/2r^3$, with

$$Q_{if} = e_i^2 \left\langle \Psi_f^* \left| 3z^2 - r^2 \right| \Psi_i \right\rangle \simeq e_i^2 \left\langle \Psi_f^* \left| z^2 \right| \Psi_i \right\rangle, \qquad (3.18)$$

where e_i is the effective charge of the transition.

The amplitude is then written

$$a_{if} = \frac{Z_1 e^2 Q_{if}}{2i\hbar} \int \frac{e^{i\omega t}}{r^3}\, dt. \tag{3.19}$$

At $\theta = 180°$ the separation r, the velocity v, the initial velocity v_0 and the distance of closest approach s, are related by $v = dr/dt = \pm_0 v_0 \left(1 - s/r\right)$, which is obtained from energy conservation. Furthermore, if the excitation energy is small, we can assume that the factor $e^{i\omega t}$ in eq. (3.19) does not vary much during the time that the projectile is close to the nucleus. Then the remaining integral is easily solved by substitution and one gets

$$a_{if} = \frac{4Z_1 e^2 Q_{if}}{3i\hbar v_0 s^2}. \tag{3.20}$$

Following the same procedure as above, we can calculate the contribution of the Hamiltonian of eq. 3.9. In this case, $\mathcal{A} = Z_1 Z_2 e^2 / m_0 r^2$ and the equivalent potential V is given by

$$V_{nin} = \left(\frac{Z_1 Z_2 e^2}{m_0}\right)^2 \frac{X m_N}{c^2 r^4}, \tag{3.21}$$

where we assume that X nucleons participates in the transition. One then finds

$$a_{if}^{nin} = \left(\frac{Z_1 Z_2 e^2}{m_0}\right)^2 \frac{32 X m_N Q_{if}}{15 i s^3 \hbar v_0 c^2}. \tag{3.22}$$

The ratio between the two transition probabilities is

$$\left|\frac{a_{if}^{nin}}{a_{if}}\right|^2 = \left(\frac{8 X m_N Z_1 Z_2^2 e^2}{5 s m_0^2 c^2}\right)^2. \tag{3.23}$$

Applying eq. 3.23 to the lead-lead collision at 500 MeV, as mentioned in the introduction, we find $\left|a_{if}^{nin}/a_{if}\right|^2 = (0.0093 X)^2$. This yields very small results for the relative importance of non-inertial effects in single particle transitions ($X \simeq 1$), but can become appreciable for the excitation of collective states such as the giant resonances, for which $X \gg 1$. This result is intriguing to say the least. We think that it deserves more studies, assuming that the physics of non-inertial effects described in section II is right. We have made a preliminary study of theses effects in the excitation of giant resonances in relativistic heavy ion collisions using eq. (3.9) which seem to confirm this statement.

3.4.3 Electron screening of fusion reactions

In laboratory measurements of nuclear fusion reactions one has found enhancements of the cross sections due to the presence of atomic electrons. This screening effect leads to an enhancement in the astrophysical S-factor, or cross section:

$$S_{lab}(E) = f(E) S(E) = \exp\left[\frac{\pi \eta \Delta E}{E}\right] S(E), \tag{3.24}$$

where $\eta(E) = Z_1 Z_2 e^2 / \hbar v$, and v is the relative velocity between the nuclei. The energy ΔE is equal to the difference between the electron binding energies in the $(Z_1 + Z_2)$-system and in the target atom (Z_2). For light nuclei it is of the order of 100 eV, enhancing fusion cross sections even for fusion energies of the order of 100 KeV. For more details we refer the interested reader to Ref. [174].

An intriguing fact is that this simple estimate, which is an upper value for ΔE, fails to reproduce the experimental data for a series of cases. In Ref. [175] several small effects, ranging from vacuum polarization to the emission of radiation, have been considered but they cannot explain the experimental data puzzle. Besides vacuum polarization, atomic polarization is one of the largest effects to be considered (among all other small effects [175]).

Non-inertial corrections contribute to polarization potential

$$V_{pol} = -\sum_{n \neq 0} \frac{|\langle 0 | H_{nin} | n \rangle|^2}{E_n - E_0}. \tag{3.25}$$

An estimate based on hydrogenic wavefunctions for the atom yields

$$V_{pol}(r) \simeq -\frac{1}{E_{n0}} \left(\frac{Z_1 Z_2 e \hbar}{m_0 c} \right)^4 \frac{\exp(-2\alpha r)}{r^4}. \tag{3.26}$$

Assuming $\alpha \cong 1/a_H$, $E_{n0} = E_n - E_0 \cong 10$ eV and using Eqs. (3.10) and (3.11) to calculate the modification of the fusion cross sections due to this effect, we find the cross section for D(d,p)T and $^6\text{Li}(d,\alpha)^4\text{He}$ can increase by up to 10%. This is surprising compared with the smaller values reported on Table 1 of Ref. [175]. It is not a very accurate calculation as it relies on many approximations. But it hints for a possible explanation of the difference between the experimental and theoretical values of ΔE, as discussed in Ref. [174].

In stars, reactions occur within a medium rich in free electrons. The influence of dynamic effects of these electrons was first mentioned in Ref. [176] and studied in Ref. [177]. The underlying assumption is that the Debye-Hueckel approximation, based on a static charged cloud, does not apply for fast moving nuclei. In fact, most of the nuclear fusion reactions occur in the tail of the Maxwell-Boltzmann distribution. For these nuclear velocities Ref. [177] finds that an appreciable modification of the Debye-Hueckel theory is necessary. One has to add to this finding the fact that the nuclei get very strongly accelerated as they approach each other, what will further increase the deformation of the Debye-Hueckel cloud.

3.5 Conclusions

In summary, assuming that the Hamiltonian for a system of particles moving in an accelerated frame is contains a correction term of the form given by eq. 3.9, I have explored the non-inertial effects for a limited set of nuclear reactions in stars and in the laboratory. These results are somewhat surprising and present a challenge to our understanding of accelerated many-body systems.

In the case of stellar environments, I have shown that only in the neighborhood of black-holes would non-inertial effects become relevant. But then the whole

method adopted here is probably wrong, as one might have to use the full machinery of general relativity. Nonetheless, it is very unlikely (and perhaps unimportant, except maybe for science-fiction time-travel) that internal structures of any object is of any relevance when it is so close to a black-hole.

The apparent reason for the appearance of non-inertial effects in many-body systems is that the non-inertial term of Eq. (3.9) only appears when relativistic corrections are included, what has precluded its consideration in previous studies, specially for reactions that are thought to be fully non-relativistic such as fusion reactions in stars. The main question is if the relativistic definition of the center of mass, through eq. (3.5) as proposed by Pryce in ref. [169] contains the right virtue of describing correctly the center of mass frame of relativistic many-body systems.

Even in the case of high energies nuclear collisions the intrinsic structure of the nuclei are sometimes an important part of the process under study. Fictitious forces will appear in this system which might not average out and appreciably influence the structure or transition under consideration. It is surprising that, for a reason not quite understood, this effect has been overseen in the literature.

Bibliography

[1] Bahcall J N 1989 Neutrino Astrophysics (Cambridge: Cambridge University Press)

[2] Iben Jr. I 1965 Astrophys. J41 993

[3] Salpeter E E, van Horn H M 1969 Ap. J. 155 183

[4] Fowler W A, Caughlan G E and Zimmermann B A 1967 Ann. Rev. Astron. Astrophys. 5 525

[5] Fuller G M, Fowler W A and Newman M 1985 Ap. J. 293 1

[6] Rolfs C and Rodney W S 1988 Cauldrons in the Cosmos (Chicago: University of Chicago Press)

[7] Wagoner R V 1969 Ap. J. Suppl. 18 247

[8] Press W H, Flannery B P, Teukolsky S A, and Vetterling W T 1993 Numerical Recipes, (Cambridge University Press)

[9] Descouvemont P 1998 Tours Symposium on Nuclear Physics III [AIP Conf. Proc. 425] p.418 (New York: Amer. Inst. Phys.)

[10] Langanke K and Barnes C A 1996 Advances in Nuclear Physics, Negele J W and Vogt E (eds) 22 173 (New York: Plenum Press)

[11] Descouvemont P 1993 Phys. Rev. C47 210

[12] Barker F C 1994 Nucl. Phys. A575 361

[13] Azuma R E et al. 1995 Proc. ENAM 95, M. de Saint Simon and O. Sorlin (eds) p. 619.(Gif-sur-Yvette: Editions Frontières)

[14] Hauser W and Feshbach H 1952 Phys. Rev. A87 366

[15] Mahaux C, Weidenmüller H A 1979 Ann. Rev. Part. Nucl. Sci. 29 1

[16] Blatt J M and Weisskopf H F 1952 Theoretical Nuclear Physics (New York: Wiley)

[17] "Cauldrons in the Cosmos", Claus E. Rolfs and William S. Rodney, Chicago Press, Chicago 1988.

[18] C.A. Bertulani, Comput. Phys. Commun. 156 (2003) 123.

[19] R.G.H. Robertson, Phys. Rev. C7, 543 (1973).

[20] K.H. Kim, M.H. Park, and B.T. Kim, Phys. Rev. C35, 363 (1987).

[21] F.C. Barker, Phys. Rev. C37, 2920 (1988).

[22] P. Navratil, C.A. Bertulani, and E. Caurier, Phys. Lett. B 634 (2006) 191; P. Navratil, C.A. Bertulani, and E. Caurier, Phys. Rev. C73 (2006) 065801.

[23] Sofia Quaglioni and Petr Navratil, Phys. Rev. Lett. 101, 092501 (2008).

[24] H.M. Xu, C.A. Gagliardi, R.E. Tribble, A.M. Mukhamedzhanov and N.K. Timofeyuk, Phys. Rev. Lett. 73 (1994) 2027.

[25] G.M. Griffiths, E.A. Larson and L.P. Robertson, Can. J. Phys. 40, 402 (1962).

[26] B.L. Berman, L.J. Koester Jr. and J.H. Smith, Phys. Rev. 133, B117 (1964).

[27] W. Wolfli, R. Bosch, J. Lang, R. Muller, and P. Marmier, Helv. Phys. Acta 40, 946 (1967).

[28] G.J. Schmid et al, Phys. Rev. C 52, R1732 (1995).

[29] A. M. Mukhamedzhanov, R. E. Tribble, and N. K. Timofeyuk, Phys. Rev. C 51, 3472 (1995).

[30] D. Thomas, D.N. Schramm, K. A. Olive, B. D. Fields, Ap. J. 406, 569 (1993).

[31] E. Vangioni-Flam, et al., New. Astron. 4, 245 (1999).

[32] Phys. Rev. C 56, 1144 (1997).

[33] O. Camargo et al, Phys. Rev. C 78, 034605 (2008).

[34] K. Arai et al, Nucl. Phys. A 699 (2002) 963.

[35] P. M. Prior et al, Phys. Rev. C 70, 055801 (2004).

[36] F.C. Barker, Aust. J. Phys. 33, 159 (1980).

[37] Z. E. Switkowski, J. C. P. Heggie, D. L. Kennedy, D. G. Sargood, F. C. Barker, and R. H. Spear, Nucl. Phys. A331, 50 (1980).

[38] R. Bruss et al, in: F. Käppeler, K. Wisshak (Eds.), Proc. Nuclei in the Cosmos, Karlsruhe, Germany, 1992, IOP, 1993, p. 169.

[39] Z.E. Switkowski et al, Nucl. Phys. A 331 (1979) 50.

[40] "Neutrino Astrophysics", John N. Bahcall, Cambridge University Press, 1989 ISBN: 9780521379755.

[41] D. Zahnow et al, Z. Phys. A 351 229 (1995).

[42] J. M. Sampaio et al, Nucl. Phys. A 688 (2001) 518c.

[43] Q. R. Ahmad et al, Phys. Rev. Lett. 87, 071301 (2001).

[44] A. R. Junghans et al, Phys. Rev. C 68, 065803 (2003).

[45] F. J. Vaughn, R. A. Chalmers, D. Kohler and L. F. Chase, Phys. Rev. C 2, 1657 (1970).

[46] B. W. Filippone, A. J. Elwyn, C. N. Davids and D. D. Koetke, Phys. Rev.C 28, 2222 (1983).

[47] L. T. Baby et al., Phys. Rev. Lett. 90, 022501 (2003).

[48] N. Iwasa et al., Phys. Rev. Lett. 83, 2910 (1999); B. Davids et al., ibid. 86, 2750 (2001); F. Schumann et al., ibid. 90, 232501 (2003).

[49] R.W. Kavanagh et al., Bull. Am. Phys. Soc. 14, 1209 (1969).

[50] P. Descouvemont and D. Baye, Nucl. Phys. A 567, 341 (1994).

[51] L. Trache et al, Phys. Rev. Lett. 87, 271102 (2001).

[52] P. Navratil, C. A. Bertulani and E. Caurier, Nucl. Phys. A 787, 539c(2007).

[53] M. Wiescher, J. Görres, S. Graff, L. Buchmann, and F.-K. Thielemann, Astrophys. J. 343, 352 (1989).

[54] G.M. Fuller, S.E. Woosley, and T.A. Weaver, Astrophys. J. 307, 675 (1986).

[55] H.M.J. Boffin, G. Paulus, M. Arnould, and N. Mowlavi, Astron. Astrophys. 279, 173 (1993).

[56] P. Mohr, Phys. Rev. C 67, 065802 (2003).

[57] L. Trache et al, Phys. Rev. C 66, 035801 (2002).

[58] D. Beaumel et al, Phys. Lett. B 514, 226 (2001).

[59] B. Guo et al, Nucl. Phys. A 761 (2005) 162.

[60] W.A. Fowler, Rev. Mod. Phys. 56, 149 (1984).

[61] K. Miura et al, Nucl. Phys. A 539, 441 (1992).

[62] S. Cohen and D. Kurath, Nucl. Phys. A101, 1 (1967).

[63] S. Varma and P. Goldhammer, Nucl . Phys. A125, 193 (1969).

[64] D. Zahnow, C. Angulo, M. Junker, C. Rolfs, S. Schmidt, W. H. Schulte and E. Somorjai, Nucl. Phys. A 589, 95 (1995).

[65] A. Sattarov et al, Phys. Rev. C 60, 035801 (1999).

[66] F. C. Barker, Nucl. Phys. A 697 (2002) 915.

[67] A. M. Mukhamedzhanov et al, Phys. Rev. C 56, 1302 (1997).

[68] M. Wiescher et al., Astrophys. J. 343, 352 (1989).

[69] Xiaodong Tang et al, Phys. Rev. C 67 015804 (2003).

[70] A. Lefebvre et al., Nucl. Phys. A 592, 69 (1995).

[71] R.E. Tribble et al, Nucl. Phys. A 718 (2003) 147c.

[72] Weiping Liu et al, Nucl. Phys. A 728 (2003) 275.

[73] C. D. Nesaraja et al, Phys. Rev. C 64, 065804 (2001).

[74] C. Rolfs and R. E. Azuma, Nucl. Phys. A227, 291 (1974).

[75] C. Mahaux, Nucl. Phys. 71 (1965) 241.

[76] N. Burtebaev et al, Phys. Rev. C 78, 035802 (2008).

[77] K. Langanke et al, Nucl. Phys. A 435 (1985) 657.

[78] R. Yarmukhamedov, Yad. Fiz. 60, 1017 (1997).

[79] S. V. Artemov et al, Izv. RAN (Bull. Russ. Acad. Sci.) Ser. Fiz. 66, 60 (2002).

[80] R.K. Ulrich, "Essays in Nuclear Astrophysics", Edited by C.A. Barnes, D.D. Clayton, D.N. Schramm, Cambridge Univ. Press, Cambridge, UK, 1982, p. 301.

[81] M. Lugaro, F. Herwig, J.C. Lattanzio, R. Gallino, O. Straniero, Astrophys. J. 586, 1305 (2003).

[82] J. D. King et al, Nucl. Phys. A567, 354 (1994).

[83] A.M. Mukhamedzhanov et al, Nucl. Phys. A 725 (2003) 279.

[84] Guo Bing, Li Zhi-hong, Chin. Phys. Lett. 24, 65 (2007).

[85] Z. H. Li et al, Phys. Rev. C 74, 035801 (2006).

[86] Th. Delbar et al, Phys. Rev. C 48, 3088 (1993).

[87] Xiaodong Tang et al, Phys. Rev. C 69, 055807 (2004).

[88] P. Decrock et al, Phys. Rev. C 48, 2057 (1993).

[89] P. Descouvemont and D. Baye, Nucl. Phys. A500, 155 (1989).

[90] S. Ahlen et al., Phys. Lett. B249, 149 (1990).

[91] C. Arpesella et al., Phys. Lett. B658, 101 (2008).

[92] G. Imbriani et al., Eur. Phys. J. A 25, 455 (2005).

[93] Schurmann et al, Phys. Rev. C 77, 055803 (2008).

[94] A. Formicola et al, Phys. Lett. B 591 (2004) 61

[95] S. O. Nelson et al, Phys. Rev. C 68, 065804 (2003).

[96] S. Raman et al., Phys. Rev. C 50, 682 (1994).

[97] P. F. Bertone et al, Phys. Rev. C 66, 055804 (2002).

[98] R. E. Pixley. The reaction cross section of nitrogen 14 for protons between 220 keV and 600 keV. Ph. D. Thesis, California Institute of Technology, 1957.

[99] U. Schroeder et al, Nucl. Phys. A467 (1987) 240.

[100] C. Angulo et al, Nucl. Phys. A 758 (2005) 391c.

[101] A. M. Mukhamedzhanov et al, Phys. Rev. C 67, 065804 (2003)

[102] C. Rolfs, W. S. Rodney, Nucl. Phys. A 235 (1974) 450.

[103] H. W. Fulbright, J. A. Robins, M. Blann, D. G. Fleming, and H. S. Plendl, Phys. Rev. 184, 1068 (1969).

[104] A. M. Mukhamedzhanov, P. Bem, V. Burjan et al, Phys. Rev. C 78, 015804 (2008).

[105] F. Herwig, Annu. Rev. Astron. Astrophys. 43, 435 (2005).

[106] "Asymptotic Giant Branch Stars", H. J. Habing and H. Olofsson, (Springer, Heidelberg, 2004).

[107] D. F. Hebbard, Nucl. Phys. 15 (1960) 289.

[108] C.A. Bertulani, P. Danielewicz, Nucl. Phys. A 717 199 (2003).

[109] C. Rolfs, Nucl. Phys. A 217 (1973) 29

[110] R. E. Hester, R. E. Pixley and W. A. Lamb, Phys. Rev. 111 1604 (1958).

[111] N. Tanner, Phys. Rev. 114 1060 (1959).

[112] R. Morlock, R. Kunz, A. Mayer et al, Phys. Rev. Lett. 79 3837 (1997).

[113] K. Bennaceur et al, Phys. Lett. B 488, 75 (2000).

[114] C. A. Gagliardi et al., Phys. Rev. C 59, 1149 (1999).

[115] J. B. Marion and W. A. Fowler, Astrophys. J. 125, 221 (1957).

[116] C. Rolfs, W.S. Rodney, M.H. Shapiro, and H. Winkler, Nucl. Phys. A 241, 460 (1975).

[117] A. M. Mukhamedzhanov et al, Phys. Rev. C 73, 035806 (2006).

[118] P. J. E. Peebles, Phys. Rev. Lett. 16, 410 (1966).

[119] H. Sato, Prog. Theor. Phys. 38, 1083 (1967).

[120] R. V.Wagoner,W. A. Fowler, and F. Hoyle, Astrophys. J. 148, 3 (1967).

[121] S. W. Stahler, Astrophys. J. 332, 804 (1988).

[122] C. Casella et al., Nucl. Phys. A706, 203 (2002).

[123] J. H. Applegate and C. J. Hogan, Phys. Rev. D 31, 3037 (1985).

[124] J. H. Applegate, C. J. Hogan, and R. J. Scherrer, Phys. Rev. D 35, 1151 (1987); Ap. J. 329, 572 (1988).

[125] R. A. Malaney and W. A. Fowler, Astrophys. J. 333, 14 (1988).

[126] Y. Nagai et al, Phys. Rev. C 74, 025804 (2006).

[127] R. B. Wiringa, V. G. J. Stoks, and R. Schiavilla, Phys. Rev. C 51, 38 (1995).

[128] B. S. Pudliner, V. R. Pandharipande, J. Carlson, S. C. Pieper, and R. B. Wiringa, Phys. Rev. C 56, 1720 (1997).

[129] B.W. Filippone et al., Phys. Rev. Lett. 50, 452 (1983).

[130] G.M. Fuller, G.J. Mathews and C.R. Alcock, Phys. Rev. D 37, 1380 (1988).

[131] Y. Nagai, et al., Phys. Rev. C 71, 055803 (2005).

[132] W. L. Imhof et al., Phys. Rev. 114, 1037 (1959).

[133] M.Wiescher, R. Steininger, and F. Kaeppeler, Astrophys. J. 344, 464 (1989).

[134] Y. Nagai et al, Astrophys. J. 381, 444 (1991).

[135] M. Heil, F. Kaeppeler, M.Wiescher, and A. Mengoni, Astrophys. J. 507, 997 (1998).

[136] J.E. Lynn, E.T. Jurney and S. Raman, Phys. Rev. 44, 764 (1991).

[137] S. E. Wooseley, J. R. Wilson, G. J. Mathews, R. D. Hoffman, and B. S. Meyer, Astrophys. J. 433, 229 (1994).

[138] V. D. Efros, W. Balogh, H. Herndl, R. Hofinger, and H. Oberhummer, Z. Phys. A 355, 101 (1996).

[139] S. K. Rosswog, C. Friburghaus, and F.-K. Thielemann, Nucl. Phys. A688, 344 (2001).

[140] C. A. Bertulani, J. Phys. G 25, (1999) 1959.

[141] Z.Q. Mao and A.E. Champagne, Nucl. Phys. A 522 (1991) 568.

[142] R. Kanungo et al, Phys. Lett. B 660 (2008) 26.

[143] P. D. Zecher, A. Galonsky, S. Gaff et al, Phys. Rev. C 57, (1998) 959.

[144] P. Banerjee, R. Chatterjee and R. Shyam, Phys. Rev. C 78, 035804 (2008).

[145] T. Kajino, G .J. Mathews, and G. M. Fuller, Astrophys. J. 364, 7 (1990).

[146] M. B. Tsang, Jenny Lee and W. G. Lynch, Phys. Rev. Lett. 95, 222501 (2005).

[147] W. L. Imhof, R. G. Johnson, F. J. Vaughn, and M. Walt, Phys. Rev. 125, 1334 (1962).

[148] C. J. Lin et al, Phys. Rev. C 68, 047601 (2003).

[149] Z. H. Liu et al, Phys. Rev. C 64, 034312 (2001).

[150] T. Ohsaki, Y. Nagai, M. Igashira, T. Shima, K. Takeda, S. Seino, and T. Irie, Astrophys. J. 422, 912 (1994).

[151] T. Kikuchi et al, Phys. Rev. C 57, 2724 (1998).

[152] A. Mengoni et al, Phys. Rev. C 52, R2334 (1995).

[153] F. Ajzenberg-Selove, Nucl. Phys. A 523, 1 (1991).

[154] D. Baye, Phys. Rev. C 70, 015801 (2004).

[155] M. Wiescher, J. Görres, and H. Schatz, J. Phys. G 25, R133 (1999).

[156] N. K. Timofeyuk et al, Phys. Rev. Lett. 96, 162501 (2006).

[157] J. D. Goss et al., Phys. Rev. C 12, 1730 (1975).

[158] R. Reifarth et al, Phys. Rev. C 77 015804(2008).

[159] M. Wiescher, J. Gorres and F. K. Thielemann, The Astrophysical Journal 363, 340 (1990).

[160] N. C. Summers, F. M. Nunes, Phys. Rev. C 78, 011601(R) (2008).

[161] J. Meissner et al, Phys. Rev. C 53, 977 (1996).

[162] W. Bohne et al, Nucl. Phys. A 196, 41 (1972).

[163] H. Herndl et al, Phys. Rev. C 60, 064614 (1999).

[164] M. Igashira, Y. Nagai, K. Masuda, T. Ohsaki, and H. Kitazawa, Astrophys. J. 441, L89 (1995).

[165] M. Dufour, P. Descouvemont, Nucl. Phys. A 694 (2001) 221.

[166] S. Chiba, H. Koura, T. Hayakawa et al, Phys. Rev. C 77, 015809 (2008)

[167] J. Meissner et al, Phys. Rev. C 53, 459 (1996).

[168] L.D. Landau and E.M. Lifshitz, Classical theory of fields (Second Edition), Pergamon Press, p.286

[169] M. H. L. Pryce, Proc. Roy. Soc. A195, 62 (1948).

[170] M.P. Fewell, Nucl. Phys. **A425** (1984) 373.

[171] D.D. Clayton, Principles of Stellar Evolution and Nucleosynthesis, McGraw-Hill, New York, 1968.

[172] C. Rolfs, W.S. Rodney, Cauldrons in the Cosmos, University of Chicago Press, Chicago, IL, 1988.

[173] D. R. Tilley et al., Nucl. Phys. A745, 155 (2004).

[174] C. Rolfs, Prog. Part. Nucl. Phys. 46, 23 (2001).

[175] A.B. Balantekin, C.A. Bertulani and M.S. Hussein, Nucl. Phys. A 627, 324 (1997).

[176] H.E. Mitler, Ap. J. 212, 513 (1977).

[177] C. Carraro, A. Schäffer and S.E. Koonin, Ap. J. 331, 565 (1988).

[178] J. Crampin, W. H. McCrea and D. McNally, Proc. Roy. Soc. A252(1959) 156

[179] D.G. Ashworth, International Journal of Theoretical Physics 22(1983) 873

Appendix A

Hamiltonian in an accelerated frame

A.1 Metric in Accelerated Frame

A.1.1 Landau

In Landau's classical theory of field [168] one finds a metric in an accelerated frame: Let φ be the potential in gravitional field. The Lagrangian of the the particle can be written as

$$L = -mc^2 + \frac{1}{2}mv^2 - m\varphi. \tag{A.1}$$

The action is

$$S = \int L dt = \int (-mc^2 + \frac{1}{2}mv^2 - m\varphi)dt$$
$$= -mc \int (c - \frac{v^2}{2c} + \frac{\varphi}{c})dt. \tag{A.2}$$

In terms of the proper displacement ds

$$S = -mc \int ds. \tag{A.3}$$

Comparing eq. A.2 and eq. A.3:

$$ds = (c - \frac{v^2}{2c} + \frac{\varphi}{c})dt,$$
$$ds^2 = (c - \frac{v^2}{2c} + \frac{\varphi}{c})^2 dt^2$$
$$= (c^2 - v^2 + 2\varphi + \frac{v^4}{4c^2} - \frac{v^2\varphi}{c^2} + \frac{\varphi}{c^2})dt^2. \tag{A.4}$$

Neglecting terms of order $1/c^2$:

$$ds^2 = (c^2 - v^2 + 2\varphi)dt^2$$
$$= c^2(1 + \frac{2\varphi}{c^2})dt^2 - v^2 dt^2$$
$$\approx c^2(1 + \frac{\varphi}{c^2})^2 dt^2 - d\mathbf{r}^2, \tag{A.5}$$

where $\mathbf{v}dt = d\mathbf{r}$. One can now replace φ as Az, where A is the acceleration of the reference frame, and z is the position with respect to that frame. Here one gets the metric in an accelerated frame

$$ds^2 = c^2(1 + \frac{Az}{c^2})^2 dt^2 - dx^2 - dy^2 - dz^2. \tag{A.6}$$

IMPORTANT NOTE: This metric is correct only when the accelerated frame is momentarily at rest with respect to the inertial frame:

$$V = 0,$$
$$V' = A \neq 0. \tag{A.7}$$

where V and A are the velocity and acceleration of an accelerated frame with respect to an inertial frame, respectively.

A.1.2 Joan Crampin

Joan Crampin gives another metric [178]:

$$ds^2 = (1 + G\xi)^2 c^2 d\tau^2 - d\xi^2, \tag{A.8}$$

where

$$c^2 G = \dot{T}\ddot{X} - \dot{X}\ddot{T} = \left(\dot{T}\right)^2 \frac{d}{d\tau}\left(\frac{\dot{X}}{\dot{T}}\right), \tag{A.9}$$

$$\frac{dT}{d\tau} = \left(1 - v^2/c^2\right)^{-1/2}, \tag{A.10}$$

$$\frac{dX/d\tau}{dT/d\tau} = \frac{dX}{dT} = v, \tag{A.11}$$

$$\frac{dv}{d\tau} = \frac{dv}{dt}\frac{dt}{d\tau} = A\left(1 - v^2/c^2\right)^{-1/2}. \tag{A.12}$$

X, T is the coordinate of the origin of an accelerated frame with respect to an inertial frame and v is the velocity in the inertial frame. The dot on the top means $\frac{d}{d\tau}$. Thus

$$G = \frac{A}{c^2}\left(1 - \frac{v^2}{c^2}\right)^{-\frac{3}{2}}. \tag{A.13}$$

The metric can be written as

$$ds^2 = \left[1 + \frac{A\xi}{c^2}\left(1 - \frac{v^2}{c^2}\right)^{-\frac{3}{2}}\right]^2 c^2 d\tau^2 - d\xi^2. \tag{A.14}$$

This is a general form of the metric. If one sets $v = 0$ (the accelerated frame is momentarily at rest in the inertial frame),

$$ds^2 = c^2(1 + \frac{A\xi}{c^2})^2 dt^2 - d\xi^2. \tag{A.15}$$

This is the same with Landau's result. Or one can get this result by constructing a world line of B

$$X^2 - c^2 T^2 = a^2. \tag{A.16}$$

When $T = 0$, this gives $X = a$, $\frac{dX}{dT} = 0$, $\frac{d^2 X}{dT^2} = \frac{c^2}{a}$. This is, at $T = 0$, the observer B is momentarily at rest in the x, t-system and has acceleration c^2/a. The world line can be written as

$$X = a\cosh(c\tau/a), cT = a\sinh(c\tau/a). \tag{A.17}$$

Using $ds^2 = (1 + G\xi)^2 c^2 d\tau^2 - d\xi^2$, The metric becomes

$$\begin{aligned} ds^2 &= (1 + \xi/a)^2 c^2 d\tau^2 - d\xi^2 \\ &= (1 + \frac{A\xi}{c^2})^2 c^2 d\tau^2 - d\xi^2. \end{aligned} \tag{A.18}$$

But how to get $ds^2 = (1 + G\xi)^2 c^2 d\tau^2 - d\xi^2$?
Step 1: Obtain the transformation:

$$\begin{aligned} x &= X(\tau) + \xi \dot{T}(\tau), \\ t &= T(\tau) + \frac{\xi}{c^2}\dot{X}(\tau). \end{aligned} \tag{A.19}$$

Consider a point B. In the inertial frame S, B has coordinates (X, T). Let S' be another inertial frame that has velocity v relative to S and in which the event B has coordinates $(0, \tau)$ in S'. This is an inertial frame where B is momentarily at rest (in S frame, the velocity of B is $v_B = v$). Let (x, t), (x', t') be the coordinates of a given event referred to S and S', respectively, assuming that the x and x' axis lie along the same direction. Then the Lorentz transformation in this case is

$$\begin{aligned} x &= \gamma\left[x' + t'v\right], \\ t &= \gamma\left[t' + x'v/c^2\right]. \end{aligned} \tag{A.20}$$

Move origins of both S and S' to B, then

$$\begin{aligned} x - X &= \gamma\left[x' + (t' - \tau)v\right], \\ t - T &= \gamma\left[t' - \tau + x'v/c^2\right], \end{aligned} \tag{A.21}$$

where

$$\gamma \equiv \left(1 - v^2/c^2\right)^{-1/2} = \left(c^2\dot{T}^2 - \dot{X}^2\right)^{-1/2} c\dot{T} = \dot{T},$$

$$v = \frac{dX}{dT} = \frac{dX/d\tau}{dT/d\tau} = \frac{\dot{X}}{\dot{T}}, \tag{A.22}$$

and other constants are determined so that $x' = 0, t' = \tau$ when $x = X, t = T$ in agreement with the definition of S. Thus one gets

$$x - X = x'\dot{T} + (t' - \tau)\dot{X},$$

$$t - T = x'\dot{X}/c^2 + (t' - \tau)\dot{T}. \tag{A.23}$$

The transformation from (x, t) to (ξ, τ) is obtained from $x' = \xi, t' = \tau$, yielding

$$x = X(\tau) + \xi\dot{T}(\tau),$$

$$t = T(\tau) + \frac{\xi}{c^2}\dot{X}(\tau), \tag{A.24}$$

where X, T is the coordinate of the origin of the accelerated frame with respect to the inertial frame.

Step 2: Insert the transformation

$$x = X(\tau) + \xi\dot{T}(\tau),$$

$$t = T(\tau) + \frac{\xi}{c^2}\dot{X}(\tau), \tag{A.25}$$

$$dx = \dot{X}d\tau + d\xi\dot{T} + \ddot{T}\xi d\tau = \left(\dot{X} + \xi\ddot{T}\right)d\tau + \dot{T}d\xi,$$

$$dt = \dot{T}d\tau + d\xi\frac{\dot{X}}{c^2} + \frac{\xi}{c^2}\ddot{X}d\tau = \left(\dot{T} + \frac{\xi}{c^2}\ddot{X}\right)d\tau + \frac{\dot{X}}{c^2}d\xi, \tag{A.26}$$

into $ds^2 = c^2dt^2 - dx^2$:

$$ds^2 = c^2\left[\left(\dot{T} + \frac{\xi}{c^2}\ddot{X}\right)d\tau + \frac{\dot{X}}{c^2}d\xi\right]^2 - \left[\left(\dot{X} + \xi\ddot{T}\right)d\tau + \dot{T}d\xi\right]^2$$

$$= \left(c^2\dot{T}^2 + 2\xi\dot{T}\ddot{X} + \xi^2\ddot{X}^2/c^2 - \dot{X}^2 - 2\dot{X}\ddot{T}\xi - \ddot{T}^2\xi^2\right)d\tau^2$$

$$+ \left(\frac{\dot{X}^2}{c^2} - \dot{T}^2\right)d\xi^2 + \left(\frac{2\xi\dot{X}\ddot{X}}{c^2} - 2\xi\dot{T}\ddot{T}\right)d\xi d\tau. \tag{A.27}$$

Using the relation

$$c^2 dT^2 - dX^2 = ds^2 = c^2 d\tau^2,$$
$$c^2 \dot{T}^2 - \dot{X}^2 = c^2,$$
$$\dot{T}\ddot{T} - \frac{1}{c^2}\dot{X}\ddot{X} = 0, \tag{A.28}$$

the metric turns to

$$ds^2 = c^2 \left[1 + \frac{2\xi}{c^2}\left(\dot{T}\ddot{X} - \dot{X}\ddot{T}\right) + \frac{\xi^2}{c^6}\left(c^2\ddot{X}^2 - c^4\ddot{T}^2\right)\right] d\tau^2 - d\xi^2. \tag{A.29}$$

One can prove $\frac{\xi^2}{c^6}\left(c^2\ddot{X}^2 - c^4\ddot{T}^2\right) = \frac{\xi^2}{c^4}\left(\dot{T}\ddot{X} - \dot{X}\ddot{T}\right)^2$, so that

$$ds^2 = c^2\left[1 + \frac{2\xi}{c^2}\left(\dot{T}\ddot{X} - \dot{X}\ddot{T}\right) + \frac{\xi^2}{c^4}\left(\dot{T}\ddot{X} - \dot{X}\ddot{T}\right)^2\right] d\tau^2 - d\xi^2$$
$$= \left[1 + \frac{2\xi}{c^2}\left(\dot{T}\ddot{X} - \dot{X}\ddot{T}\right)\right]^2 c^2 d\tau^2 - d\xi^2$$
$$= (1 + G\xi)^2 c^2 d\tau^2 - d\xi^2, \tag{A.30}$$

where $c^2 G = \dot{T}\ddot{X} - \dot{X}\ddot{T} = \left(\dot{T}\right)^2 \frac{d}{d\tau}\left(\frac{\dot{X}}{\dot{T}}\right)$.

Proof of $\frac{\xi^2}{c^6}\left(c^2\ddot{X}^2 - c^4\ddot{T}^2\right) = \frac{\xi^2}{c^4}\left(\dot{T}\ddot{X} - \dot{X}\ddot{T}\right)^2$:

First of all,

$$\frac{\xi^2}{c^4}\left(\dot{T}\ddot{X} - \dot{X}\ddot{T}\right)^2 = \frac{\xi^2}{c^4}\left(\dot{T}^2\ddot{X}^2 + \dot{X}^2\ddot{T}^2 - 2\dot{T}\ddot{T}\dot{X}\ddot{X}\right), \tag{A.31}$$

On the other hand,

$$c^2\dot{T}\ddot{T} - \dot{X}\ddot{X} = 0,$$
$$\left(c^2\dot{T}\ddot{T} - \dot{X}\ddot{X}\right)^2 = 0,$$
$$2\dot{T}\ddot{T}\dot{X}\ddot{X} = \frac{1}{c^2}\dot{X}^2\ddot{X}^2 + c^2\dot{T}^2\ddot{T}^2, \tag{A.32}$$

Thus,

$$\frac{\xi^2}{c^4}\left(\dot{T}\ddot{X} - \dot{X}\ddot{T}\right)^2 = \frac{\xi^2}{c^4}\left(\dot{T}^2\ddot{X}^2 + \dot{X}^2\ddot{T}^2 - \frac{1}{c^2}\dot{X}^2\ddot{X}^2 - c^2\dot{T}^2\ddot{T}^2\right)$$
$$= \frac{\xi^2}{c^4}\left[c^{-2}\dot{T}^2\left(c^2\ddot{X}^2 - c^4\ddot{T}^2\right)\right.$$
$$\left. - c^{-4}\dot{X}^2\left(c^4\ddot{T}^2 - c^2\ddot{X}^2\right)\right]$$
$$= \frac{\xi^2}{c^4}\left(c^2\ddot{X}^2 - c^4\ddot{T}^2\right)\left(\frac{\dot{T}^2}{c^2} - \frac{\dot{X}^2}{c^4}\right). \tag{A.33}$$

Since $\frac{\dot{T}^2}{c^2} - \frac{\dot{X}^2}{c^4} = \frac{1}{c^2}$, one has

$$\frac{\xi^2}{c^4}\left(\dot{T}\ddot{X} - \dot{X}\ddot{T}\right)^2 = \frac{\xi^2}{c^6}\left(c^2\ddot{X}^2 - c^4\ddot{T}^2\right). \tag{A.34}$$

A.1.3   D. G. Ashworth

Based on several assumptions [179]

$$d\sigma'_x = h\left(x', t'\right)dx',$$
$$dT' = f\left(x', t'\right)dt' + g\left(x', t'\right)dx',$$
$$x' = k(t)\left(x - \int_0^t v dt\right),$$
$$t' = j(t)x + m(t), \tag{A.35}$$

where h, f, g, k, j, m can be solved, the author give the transformation equation:

$$x' = \left(x - \int_0^t v dt\right)\left(1 - \frac{v^2}{c^2}\right)^{-1/2},$$
$$y' = y,$$
$$z' = z,$$
$$t' = \int_0^t \left(1 - \frac{v^2}{c^2}\right)^{1/2} dt - vc^{-2}\left(1 - \frac{v^2}{c^2}\right)^{-1/2}\left(x - \int_0^t v dt\right), \tag{A.36}$$

and the metric becomes

$$\begin{aligned}
ds^2 = {} & c^2 v^2 Z^{-2}\left(1 - Z^2/c^2\right)\left(1 - v^2/c^2\right)^{-1} dt'^2 \\
& - 2v\left(1 - Z^2/c^2\right)\left(1 - v^2/c^2\right)^{-1} dx'dt' \\
& - \left(1 - v^4/c^2 Z^2\right)^{-1}\left(1 - v^2/c^2\right)^{-1} dx'^2 \\
& - dy'^2 - dz'^2,
\end{aligned} \tag{A.37}$$

where $Z = v(1 - Wx')$, $W = ac^{-2}\left(1 - v^2/c^2\right)^{-1/2}$. The result was carefully examined and the conclusion is that it is wrong, because $dT' = f\left(x', t'\right)dt' + g\left(x', t'\right)dx'$ is an incorrect assumption, and it leads to the appearance of the cross term $dx'dt'$. However, if one expands the metric in power of $1/c^2$, and set $v = 0$, the metric still turns into Landau's result.

A.2   Centre of mass (c.m.)[169]

Let the coordinates of the ith particle be denoted by z_i^μ, and total momentum vector, $\sum_i p_i^\mu$, being denoted by P^μ. The indices μ run from 0 to 3.

$$ds^2 = g_{00}c^2 dt^2 - dx^2 - dy^2 - dz^2,$$
$$ds = \sqrt{g_{00}c^2 dt^2 - dx^2 - dy^2 - dz^2}$$
$$= cdt\sqrt{g_{00} - \frac{dx^2 + dy^2 + dz^2}{c^2 dt^2}}$$
$$= cdt\sqrt{g_{00} - \frac{v^2}{c^2}},$$
$$d\tau c = cdt\sqrt{g_{00} - \frac{v^2}{c^2}},$$
$$\frac{d\tau}{dt} = \sqrt{g_{00} - \frac{v^2}{c^2}}. \tag{A.38}$$

Denote $\frac{1}{\sqrt{g_{00} - \frac{v^2}{c^2}}} \equiv \gamma$, then

$$\frac{dt}{d\tau} = \gamma. \tag{A.39}$$

Consider four momentum

$$P^\mu = mU^\mu,$$
$$U^0 = \frac{dx^0}{d\tau} = \frac{d(ct)}{d\tau} = c\gamma,$$
$$U^k = \frac{dx^k}{d\tau} = \frac{dx^k}{dt}\frac{dt}{d\tau} = \gamma v^k, \tag{A.40}$$

then

$$P^0 = mc\gamma = E/c,$$
$$P^k = m\gamma v^k. \tag{A.41}$$

Definition of Mass-Centre: In a particular frame, the co-ordiantes of mass centre is the mean of co-ordinates of several particles weighted with their dynamical masses (energies).

By this definition, mass-centre q^μ is given by

$$P^0 q^\mu = \sum_i p_i^0 z_i^\mu. \tag{A.42}$$

To express this in a way that the form of q^μ keep unchanged in different frame, M. H. L. Pryce did the following things($c \to 1$): Using the energy-momentum tensor of an assembly of free particles

$$T^{\mu\nu} = T^{\nu\mu} = \sum_i \int \delta\left(x^0 - z_i^0\right) \delta\left(x^1 - z_i^1\right)$$
$$\cdot \delta\left(x^2 - z_i^2\right) \delta\left(x^3 - z_i^3\right) p_i^\mu dz_i^\nu, \tag{A.43}$$

mass-centre q^μ becomes

$$
\begin{aligned}
P^0 q^\mu &= \int x^\mu T^{00} dx^1 dx^2 dx^3 \\
&= \sum_i \int p_i^\mu x^\mu \delta \left(x^0 - z_i^0 \right) \delta \left(x^1 - z_i^1 \right) \\
&\quad \cdot \delta \left(x^2 - z_i^2 \right) \delta \left(x^3 - z_i^3 \right) dz_i^\nu dx^1 dx^2 dx^3 \\
&= \sum_i p_i^0 z_i^\mu.
\end{aligned}
\tag{A.44}
$$

Besides

$$
\begin{aligned}
P^\mu &= \int T^{0\mu} dx^1 dx^2 dx^3 \\
&= \sum_i \int p_i^\mu \delta \left(x^0 - z_i^0 \right) \delta \left(x^1 - z_i^1 \right) \\
&\quad \cdot \delta \left(x^2 - z_i^2 \right) \delta \left(x^3 - z_i^3 \right) dz_i^\nu dx^1 dx^2 dx^3 \\
&= \sum_i p_i^\mu,
\end{aligned}
\tag{A.45}
$$

$$
\begin{aligned}
M^{\mu\nu} &= \int \left(x^\mu T^{0\nu} - x^\nu T^{0\mu} \right) dx^1 dx^2 dx^3 \\
&= \sum_i \left(z_i^\mu p_i^\nu - z_i^\nu p_i^\mu \right).
\end{aligned}
\tag{A.46}
$$

These enable one to write the equation for q^μ

$$
\begin{aligned}
q^\mu &= \left(t P^\mu + M^{\mu 0} \right) / P^0 \\
&= \left\{ \sum_i \left[t p_i^\mu - \left(z_i^\mu p_i^0 - z_i^0 p_i^\mu \right) \right] \right\} / P^0 \\
&= \left(\sum_i p_i^0 z_i^\mu \right) / P^0.
\end{aligned}
\tag{A.47}
$$

One can generalize it

$$
\begin{aligned}
q^\mu &= \frac{\left(s P^\mu + M^{\mu\nu} n_\nu \right)}{P^\sigma n_\sigma} \\
&= \frac{\left(s P^\mu + M^{\mu 0} n_0 + M^{\mu 1} n_1 + M^{\mu 2} n_2 + M^{\mu 3} n_3 \right)}{P^0 n_0 + P^1 n_1 + P^2 n_2 + P^3 n_3},
\end{aligned}
\tag{A.48}
$$

where n^μ is the direction of the time-axis of a new frame in old frame(t, μ), s is time of new frame. By eq. A.47, one gets $q^0 = t$. To make sure eq. A.48 reduces to eq. A.47 when n^μ is in the same direction with t ($n^\mu = (1, 0, 0, 0)$),

solve equation $q^0 = t$ for s and replace s above[1], then

$$q^\mu = \frac{tP^\mu}{P^0} + \frac{M^{\mu\nu}P^0 n_\nu - M^{0\nu}P^\mu n_\nu}{P^0 P^\sigma n_\sigma}. \tag{A.49}$$

To make q^μ independent of n^μ, substitute P^μ/m for n^μ (It's some thing like Frenet Frame in differential geometry), noticing that $P^\mu P_\mu = m^2$, one obtains

$$q^\mu = \frac{tP^\mu}{P^0} + \frac{M^{\mu\nu}P_\nu}{m^2} + \frac{M^{0\nu}P^\mu P_\nu}{m^2 P^0}, \tag{A.50}$$

Where t is the time for a specific frame. All variables are four-vectors and tensors so the form keeps unchanged in different inertial frame, so it is relativistically covariant. This can also be used in accelerated frame because the problem of accelerated frame still can be solved in special theory of relativity (See section 1).

In a c.m. frame, the space parts of q^k and P^k are zero identically, by eq. A.47[2]

$$q^k = \left(tP^k + M^{k0}\right)/P^0,$$
$$0 = \left(0 + M^{\mu0}\right)/P^0,$$
$$M^{k0} = 0 \quad (k = 1, 2, 3). \tag{A.51}$$

That is

$$\sum_i \left(z_i^k p_i^0 - z_i^0 p_i^k\right) = \sum_i z_i^k p_i^0 - \sum_i z_i^0 p_i^k = 0. \tag{A.52}$$

By eq. A.42 $\sum_i p_i^0 z_i^k = P^0 q^k = 0$,

$$\sum_i \left(z_i^k p_i^0 - z_i^0 p_i^k\right) = \sum_i z_i^0 p_i^k$$
$$= \sum_i z_i^0 m_i \gamma v_i^k$$
$$= \sum_i \frac{m_i z_i^0 v_i^k}{\sqrt{g_{00} - \frac{v_i^2}{c^2}}}$$
$$= \sum_i \frac{m_i \mathbf{r}_i}{\sqrt{g_{00} - \frac{v_i^2}{c^2}}}$$
$$= 0, \tag{A.53}$$

$$\sum_i \frac{m_i \mathbf{r}_i}{\sqrt{g_{00} - \frac{v_i^2}{c^2}}} = 0. \tag{A.54}$$

---

[1]When $n_\sigma = (1, 0, 0, 0)$, by eq. A.48, $q^0 = s$, this is not compatible with eq. A.47 ($q^0 = t$). To make sure $q^0 = \frac{(sP^0 + M^{0\nu}n_\nu)}{P^\sigma n_\sigma} = t$, $s = \frac{P^\sigma n_\sigma t - M^{0\nu}n_\nu}{P^0}$, then $q^\mu = \frac{tP^\mu}{P^0} + \frac{M^{\mu\nu}P^0 n_\nu - M^{0\nu}P^\mu n_\nu}{P^0 P^\sigma n_\sigma}$. At this time, when $n_\sigma = (1, 0, 0, 0)$, $q^0 = t$.

[2]One cannot get the following relation directly from eq. A.50. But since eq. A.47 is the special case of eq. A.50, the result must satisfy both eq. A.47 and A.50, so one can just use the relation of eq. A.47.

A.3 Hamiltonian with no interaction[170]

A.3.1 One free particle

The metric can be written as

$$ds^2 = g_{00}c^2dt^2 - dx^2 - dy^2 - dz^2, \tag{A.55}$$

where $g_{00} = \left[1 + \frac{Az}{c^2}\left(1 - \frac{V^2}{c^2}\right)^{-\frac{3}{2}}\right]^2$, x, y, z, t are coordinates in the accelerated frame. A and V are the acceleration and velocity of the origin of the accelerated frame with respect to the inertial frame.

$$\begin{aligned} ds &= \sqrt{g_{00}c^2dt^2 - dx^2 - dy^2 - dz^2} \\ &= cdt\sqrt{g_{00} - \frac{dx^2 + dy^2 + dz^2}{c^2dt^2}} \\ &= cdt\sqrt{g_{00} - \frac{v^2}{c^2}}, \end{aligned} \tag{A.56}$$

On the other hand

$$S = -mc\int ds, \tag{A.57}$$

Then

$$S = -mc\int c\sqrt{g_{00} - \frac{v^2}{c^2}}dt = \int\left(-mc^2\sqrt{g_{00} - \frac{v^2}{c^2}}\right)dt. \tag{A.58}$$

Moreover

$$S = \int L dt, \tag{A.59}$$

where L is the Lagrangian. Hence the Lagrangian is found to be

$$L = -mc^2\sqrt{g_{00} - \frac{v^2}{c^2}}. \tag{A.60}$$

The momentum is given by

$$\mathbf{p} = \frac{\partial L}{\partial \mathbf{v}} = \frac{m\mathbf{v}}{\sqrt{g_{00} - \frac{v^2}{c^2}}}. \tag{A.61}$$

According to the definition of Hamiltonian, one has

$$H = \mathbf{p} \cdot \mathbf{v} - L$$

$$= \frac{mv^2}{\sqrt{g_{00} - \frac{v^2}{c^2}}} + mc^2 \sqrt{g_{00} - \frac{v^2}{c^2}}$$

$$= \frac{mv^2 + mc^2 \left(g_{00} - \frac{v^2}{c^2} \right)}{\sqrt{g_{00} - \frac{v^2}{c^2}}}$$

$$= \frac{g_{00} mc^2}{\sqrt{g_{00} - \frac{v^2}{c^2}}}. \tag{A.62}$$

The Hamiltonian can also be expressed as a function of $\mathbf{p}$:

$$H = c\sqrt{g_{00} \left(p^2 + m^2 c^2 \right)},$$

because

$$H = c\sqrt{g_{00} \left(p^2 + m^2 c^2 \right)}$$

$$= c\sqrt{g_{00} \left(\frac{m^2 v^2}{g_{00} - \frac{v^2}{c^2}} + m^2 c^2 \right)}$$

$$= c\sqrt{\frac{g_{00}^2 m^2 c^2}{g_{00} - \frac{v^2}{c^2}}}$$

$$= \frac{g_{00} mc^2}{\sqrt{g_{00} - \frac{v^2}{c^2}}}. \tag{A.63}$$

Noticing that $g_{00} = \left[1 + \frac{Az}{c^2} \left(1 - \frac{V^2}{c^2} \right)^{-\frac{3}{2}} \right]^2$, we expand H in powers of $\frac{1}{c^2}$:

```
Mathematica code:
(*x = 1/c^2*)
g00 = (1 + z * A * x * (1 − V^2 * x)^(−3/2))^2;
H = x^(−1/2) * (g00 * (p^2 + m^2 * x^(−1)))^(1/2);
Series[H, {x, 0, 1}]//Expand//Simplify
```

$$H = \frac{p^2}{2m} \left(1 - \frac{p^2}{4m^2 c^2} \right) + mAz \left(1 + \frac{3V^2}{2c^2} + \frac{p^2}{2m^2 c^2} \right) + O\left(\frac{1}{c^4} \right). \tag{A.64}$$

A.3.2   A collection of free particles

The hamiltonian for a collection of free particles is simply the sum of the hamiltonians for each particle, thus

$$H = \sum_i \frac{p_i^2}{2m_i} \left(1 - \frac{p_i^2}{4m_i^2 c^2} \right) + A \sum_i m_i z_i \left(1 + \frac{3V^2}{2c^2} + \frac{p_i^2}{2m_i^2 c^2} \right). \tag{A.65}$$

Suppose that the origin of the reference frame is at the center of mass of the system, which means

$$\sum_i \frac{m_i \mathbf{r}_i}{\sqrt{g_{00} - \frac{v_i^2}{c^2}}} = 0. \tag{A.66}$$

To the first order in $1/c^2$, this is

```
Mathematica code:
(*x = 1/c^2*)
g00 = (1 + zA * x * (1 − V^2 * x)^(−3/2))^2;
p = (g00 − v^2 * x)^(−1/2);
Series[p, {x, 0, 2}]
```

$$\sum_i m_i \mathbf{r}_i \left(1 + \frac{v_i^2}{2c^2} - \frac{z_i A}{c^2} \right) = 0. \tag{A.67}$$

Only using the z-component

$$\sum_i m_i z_i \left(1 + \frac{v_i^2}{2c^2} - \frac{z_i A}{c^2} \right) = 0,$$

$$A \sum_i m_i z_i \left(1 + \frac{v_i^2}{2c^2} - \frac{z_i A}{c^2} \right) = 0, \tag{A.68}$$

$$\sum_i A m_i z_i = - \sum_i A m_i z_i \left(\frac{v_i^2}{2c^2} - \frac{z_i A}{c^2} \right), \tag{A.69}$$

Inserting[3] eq. A.69 into eq. A.65, Hamiltonian H becomes

$$H = \sum_i \frac{p_i^2}{2m_i} \left(1 - \frac{p_i^2}{4m_i^2 c^2} - \frac{3AV^2 z_i}{2c^4} \right) + \frac{A^2}{c^2} \sum_i m_i z_i^2. \tag{A.70}$$

A.4   Hamiltonian with interactions [170]

A.4.1   One charged particle in electromagnetic field

The action for a charged particle in electromagnetic field is

$$S = -mc \int ds - \frac{q}{c} \int A_\mu dx^\mu, \tag{A.71}$$

where

$$\begin{aligned}
A^\mu &= (\phi, c\mathbf{A}), \\
A_\nu &= g_{\mu\nu} A^\mu = (g_{00}\phi, -\mathbf{A}), \\
dx^\mu &= (ct, \mathbf{x}),
\end{aligned} \tag{A.72}$$

---

[3]The reason for just *inserting*: Since p_i, v_i don't change with the position of the frame (property of vector) and one can set any point as $z = 0$, eq. A.65 actually can be taken as the equation for the frame of c.m.. Here one just expresses hamiltonian H in another way.

so

$$S = -mc \int c\sqrt{g_{00} - \frac{v^2}{c^2}}dt - q \int g_{00}\phi dt + q \int \mathbf{A} \cdot d\mathbf{x}$$

$$= \int \left[-mc^2\sqrt{g_{00} - \frac{v^2}{c^2}} - qg_{00}\phi + q\mathbf{A} \cdot \mathbf{v} \right] dt. \tag{A.73}$$

Hence,

$$L = -mc^2\sqrt{g_{00} - \frac{v^2}{c^2}} - qg_{00}\phi + q\mathbf{A} \cdot \mathbf{v}. \tag{A.74}$$

The generalized momentum is

$$\mathbf{P} = \frac{\partial L}{\partial \mathbf{v}} = \frac{m\mathbf{v}}{\sqrt{g_{00} - \frac{v^2}{c^2}}} + q\mathbf{A}. \tag{A.75}$$

$$H = \mathbf{P} \cdot \mathbf{v} - L$$

$$= \left(\frac{mv^2}{\sqrt{g_{00} - \frac{v^2}{c^2}}} + q\mathbf{A} \cdot \mathbf{v} \right)$$

$$- \left(-mc^2\sqrt{g_{00} - \frac{v^2}{c^2}} - qg_{00}\phi + q\mathbf{A} \cdot \mathbf{v} \right)$$

$$= \frac{g_{00}mc^2}{\sqrt{g_{00} - \frac{v^2}{c^2}}} + qg_{00}\phi. \tag{A.76}$$

Since

$$H - qg_{00}\phi = \frac{g_{00}mc^2}{\sqrt{g_{00} - \frac{v^2}{c^2}}}, \tag{A.77}$$

$$c\left[g_{00}\left(\mathbf{P} - q\mathbf{A}\right) + g_{00}mc^2 \right]^{1/2} = c\left(\frac{g_{00}^2 m^2 c^2}{g_{00} - \frac{v^2}{c^2}} \right)^{1/2}$$

$$= \frac{g_{00}mc^2}{\sqrt{g_{00} - \frac{v^2}{c^2}}}, \tag{A.78}$$

one can see that $H - qg_{00}\phi$ equals $c\left[g_{00}\left(\mathbf{P} - q\mathbf{A}\right) + g_{00}mc^2 \right]^{1/2}$. So[4]

$$H - qg_{00}\phi = c\left[g_{00}\left(\mathbf{P} - q\mathbf{A}\right) + g_{00}mc^2 \right]^{1/2},$$

$$H = c\left[g_{00}\left(\mathbf{P} - q\mathbf{A}\right) + g_{00}mc^2 \right]^{1/2} + qg_{00}\phi. \tag{A.79}$$

---

[4] $P_\mu = \left(\frac{H}{c}, \vec{P} \right)$

A.4.2   A collection of charged particles in electromagnetic field

Expansion H in powers of $\frac{1}{c^2}$ and placement of the origin at the c.m. leads to

```
Mathematica code:
(*x = 1/c^2*)
g00 = (1 + z * A * x * (1 - V^2 * x)^(-3/2))^2;
H = x^(-1/2) * (g00 * p^2 + g00 * m^2 * x^(-1))^(1/2) + g00 * q * φ;
Series[H, {x, 0, 1}]
```

$$H = \sum_i \frac{(\mathbf{P} - q\mathbf{A})^2}{2m_i}\left[1 - \frac{(\mathbf{P} - q\mathbf{A})^2}{4m_i^2 c^2}\right]$$
$$+ \frac{A^2}{c^2}\sum_i m_i z_i^2 + \sum_i q_i \phi_i \left[1 + \frac{2A z_i}{c^2}\right]. \tag{A.80}$$

The H above doesn't keep terms involving $\frac{velocity^2}{c^2}$: $\sum_i \frac{A z_i (\mathbf{P} - q\mathbf{A})^2}{2m_i c^2}$, $\sum_i \frac{3 m_i A z_i V^2}{2c^2}$, $-\sum_i \frac{m_i A z_i v_i^2}{2c^2}$

A.4.3   A collection of charged particles with interactions in electromagnetic field

According to A.74, the Lagrangian is

$$L = -m_i c^2 \sqrt{g_{00}\left(i\right) - \frac{v_i^2}{c^2}} - q_i g_{00}\left(i\right)\phi_i + q_i \mathbf{A}_i \cdot \mathbf{v}_i,$$
$$\phi_i = \sum_{j \neq i} \frac{q_j}{4\pi\varepsilon_0 \left|\mathbf{r}_i - \mathbf{r}_j\right|}. \tag{A.81}$$

For light

$$ds^2 = g_{00}c^2 dt^2 - dx^2 - dy^2 - dz^2 = 0,$$
$$g_{00}c^2 dt^2 = d\mathbf{r}^2,$$
$$\sqrt{g_{00}}c\,dt = \left|d\mathbf{r}\right|,$$
$$c\int_{t_i}^{t_j} dt \approx \left[(g_{00})_i^{-1/2} - (g_{00})_j^{-1/2}\right]\left|\int_{\mathbf{r}_i}^{\mathbf{r}_j} d\mathbf{r}\right|,$$
$$c\left(t_i - t_j\right) = \left[(g_{00})_i^{-1/2} - (g_{00})_j^{-1/2}\right]\left|\mathbf{r}_i - \mathbf{r}_j\right|,$$
$$g_{00}^{-1/2} = \left[1 + \frac{Az}{c^2}\left(1 - \frac{V^2}{c^2}\right)^{-\frac{3}{2}}\right]^{-1}$$
$$g_{00}^{-1/2} \approx 1 - \frac{Az}{c^2}\left(1 - \frac{V^2}{c^2}\right)^{-\frac{3}{2}}. \tag{A.82}$$

so

$$c\left(t_i - t_j\right) = \left[1 - \frac{Az}{c^2}\left(1 - \frac{V^2}{c^2}\right)^{-\frac{3}{2}}(z_i - z_j)\right]|\mathbf{r}_i - \mathbf{r}_j|. \qquad (A.83)$$

The form of Lagrangian is not affected by the curvature of the geodesics to order $1/c^2$. The hamiltonian is found to be

```
Mathematica code:
(*x = 1/c^2, d0 = ri − rj*)
d = d0 ∗ (1 − A ∗ x ∗ (1 − V^2 ∗ x)^(−3/2) ∗ (z − zj));
φ = 1/(4 ∗ Pi ∗ ε ∗ qj/d;
g00 = (1 + z ∗ A ∗ x ∗ (1 − V^2 ∗ x)^(−3/2))^2;
H = x^(−1/2) ∗ (g00 ∗ p^2 + g00 ∗ m^2 ∗ x^(−1))^(1/2) + g00 ∗ q ∗ φ;
H1 = x^(−1/2) ∗ (p^2 + m^2 ∗ x^(−1))^(1/2) + q ∗ φ;
Series[H, {x, 0, 1}] − Series[H1, {x, 0, 1}]
```

$$H = H_1 + A\sum_i m_i z_i \left[1 + \frac{3V^2}{2c^2} + \frac{p_i^2}{2m_i^2 c^2} + \frac{q_i}{2\pi\varepsilon_0 m_i c^2}\sum_{j\neq i}\frac{q_j}{|\mathbf{r}_i - \mathbf{r}_j|}\right], \qquad (A.84)$$

where H_1 is the hamiltonian in an inertial frame of reference ($g_{00} = 1$). The term $\frac{q_i}{2\pi\varepsilon_0 m_i c^2}\sum_{j\neq i}\frac{q_j}{|\mathbf{r}_i - \mathbf{r}_j|}$ is caused by the Coulomb force among the charged particles. Noticing $\sum_i\sum_{j\neq i}$, one counts this effect in eq. A.84 twice, so the right form should be $\frac{q_i}{4\pi\varepsilon_0 m_i c^2}\sum_{j\neq i}\frac{q_j}{|\mathbf{r}_i - \mathbf{r}_j|}$. Hence, the hamiltonian is

$$H = H_1 + A\sum_i m_i z_i \left[1 + \frac{3V^2}{2c^2} + \frac{p_i^2}{2m_i^2 c^2} + \frac{q_i}{4\pi\varepsilon_0 m_i c^2}\sum_{j\neq i}\frac{q_j}{|\mathbf{r}_i - \mathbf{r}_j|}\right]. \qquad (A.85)$$

Because of the energy stored in the field generated by the interacting particles, the angular momentum tensor $M^{\mu\nu}$ is (here c is not 1 anymore)

$$\begin{aligned} M^{\mu\nu} &= M^{\mu\nu} \\ &= \frac{1}{c^2}\int\left(x^\mu T^{0\nu} - x^\nu T^{0\mu}\right)dx^1 dx^2 dx^3 \\ &= \sum_i\left(x_i^\mu p_i^\nu - x_i^\nu p_i^\mu\right) + \frac{1}{c^2}\int\left(x^\mu T^{0\nu} - x^\nu T^{0\mu}\right)d\mathbf{r}, \qquad (A.86) \end{aligned}$$

where the first term is particle part, which can be derived from eq. A.43 [5], and the second term is energy part. $M^{k0} = 0$ means

$$\sum_i \frac{m_i\mathbf{r}_i}{\sqrt{g_{00} - \frac{v_i^2}{c^2}}} + \frac{1}{c^2}\int T^{00}\mathbf{r}d\mathbf{r} = 0, \qquad (A.87)$$

---

[5]NOTICE: In eq. A.43, $c \to 1$, but here $c \not\to 1$. If $c \not\to 1$, eq. A.43 becomes $T^{\mu\nu} = T^{\nu\mu} = c^2\sum_i\int\delta\left(x^0 - z_i^0\right)\delta\left(x^1 - z_i^1\right)\delta\left(x^2 - z_i^2\right)\delta\left(x^3 - z_i^3\right)p_i^\mu dz_i^\nu$.

where T^{00} is energy density, so

$$\frac{1}{c^2} \int T^{00} \mathbf{r} dr = \frac{1}{2} \sum_i \frac{E_i'}{c^2} \mathbf{r}_i$$

$$= \frac{1}{2} \sum_i \frac{\sum\limits_{j \neq i} \frac{1}{4\pi\varepsilon_0} \frac{q_i q_j}{|\mathbf{r}_i - \mathbf{r}_j|}}{c^2} \mathbf{r}_i$$

$$= \sum_i \sum_{j \neq i} \frac{1}{8\pi c^2 \varepsilon_0} \frac{q_i q_j}{|\mathbf{r}_i - \mathbf{r}_j|} \mathbf{r}_i, \tag{A.88}$$

where E_i' is the energy stroed in each particle, and $1/2$ is used to avoid double counting the energy due to $\sum\limits_i \sum\limits_{j \neq i}$. Just using z component, eq. A.87 turns to

$$\sum_i \left(\frac{m_i}{\sqrt{g_{00} - \frac{v_i^2}{c^2}}} + \sum_{j \neq i} \frac{1}{8\pi c^2 \varepsilon_0} \frac{q_i q_j}{|\mathbf{r}_i - \mathbf{r}_j|} \right) z_i = 0. \tag{A.89}$$

To the first order in $1/c^2$,

$$\sum_i m_i z_i \left(1 + \frac{v_i^2}{2c^2} - \frac{z_i A}{c^2} \right) + \sum_i \sum_{j \neq i} \frac{1}{8\pi c^2 \varepsilon_0} \frac{q_i q_j}{|\mathbf{r}_i - \mathbf{r}_j|} z_i = 0, \tag{A.90}$$

$$\sum_i m_i A z_i = -\sum_i m_i A z_i \left[\left(\frac{v_i^2}{2c^2} - \frac{z_i A}{c^2} \right) + \sum_{j \neq i} \frac{1}{8\pi m_i c^2 \varepsilon_0} \frac{q_i q_j}{|\mathbf{r}_i - \mathbf{r}_j|} \right]. \tag{A.91}$$

Inserting this into eq.A.85 and neglecting all terms involving $\frac{velocity^2}{c^2}$, one has

$$H = H_1 + A \sum_i m_i z_i \left[\frac{A z_i}{c^2} + \frac{q_i}{8\pi\varepsilon_0 m_i c^2} \sum_{j \neq i} \frac{q_j}{|\mathbf{r}_i - \mathbf{r}_j|} \right]. \tag{A.92}$$

VITA

Junting Huang was born in Yining, Xinjiang, People's Republic of China on October 6, 1984, the son of Jinxin Huang and Fen Deng. After graduating from the Third High School of Yining, Yining, Xinjiang, China in 2003, he enrolled at Lanzhou University, Lanzhou, Gansu, China. He received the Bachelor of Science degree with major in theoretical physics in June 2007 from Lanzhou University. In August 2007, he enroll in the Graduate School of Texas A&M University-Commerce, Commerce, TX, studying physics.

Permanent address:
549 Jiligelang St.
Yining County, Xinjiang province 835100
People's Republic of China